High Temperature Rotating Heat Pipe Setup

Heat Pipe Assisted Annealing Project

B.O.P. Meltzer



High Temperature Rotating Heat Pipe Setup

for the

Heat Pipe Assisted Annealing Project

by

B.O.P. Meltzer

to obtain the degree of Master of Science at the Delft University of Technology, to be defended publicly on Thursday June 2, 2016 at 11:00 AM.

Student number: 4000951

Project duration: September 1, 2015 – June 2, 2016
Thesis committee: Prof. dr. ir. B.J. Boersma TU Delft

Ir. M. Çelik, TU Delft, daily supervisor

Dr. ir. C.A. Infante Ferreira TU Delft

Dr. ir. W. De Jong, TU Delft, supervisor

Dr. ir. P. Pronk Tata Steel

This thesis is confidential and cannot be made public until June 2, 2019.

An electronic version of this thesis is available at http://repository.tudelft.nl/.



Abstract

The heat pipe assisted annealing project is a collaboration between TU Delft, Tata Steel and Drever International. It is aimed at developing a continuous annealing line where the implementation of rotating heat pipes leads to a 70 % reduction in energy consumption by reusing heat recovered at the cooling step. Rotating heat pipes are closed cylindrical containers, containing merely a working medium operating at its vapor-liquid equilibrium. They are highly effective heat transfer devices, due to evaporation of the medium on one end of the pipe, and condensation on the other. Rotation about the longitudinal (horizontal) axis allows for return of the condensate to the evaporation side and maintaining of the cycle.

For further development of the project, an experimental setup is to be designed that can operate at 423 to 873 K (150 to 600 °C) without exceeding an internal pressure limit of 0.5 MPa. The setup has to facilitate measurements that provide insight about heat and mass transfer phenomena inside the heat pipe while operating conditions are similar to those in a continuous annealing line.

Working fluids capable of operating at the specified temperatures have been identified in view of their vapor pressure, chemical stability and safety aspects. Rotational velocity and dimensions of the heat pipe are based on resemblance of flow regimes expected in the continuous annealing line and comparison of experimental data with other studies. Heating and cooling loads provided by the setup are equal to those caused by steel strips in the annealing process. The equipment required to do so is selected with respect to the uniformity of the heating/cooling profile and ease of implementation in the setup. Essential measurements have been identified to provide temperature (internal and external) and pressure profiles, heat fluxes through the pipe shell and insight about internal flow regimes, velocities and phase change rates. Steady and safe operation is ensured by procedures concerning filling, safety and control and by selection of auxiliary equipment. To combine all the required equipment and instrumentation and arrange for manufacture of the setup, preliminary CAD drawings have been made that illustrate the intended design concepts.

Biphenyl, phenanthrene and cesium, in combination with a 316 stainless steel shell, have been selected to cover the temperature range up to $607\,\mathrm{K}$, $717\,\mathrm{K}$ and $873\,\mathrm{K}$ respectively, while complying with the specified criteria. Nevertheless, the TU Delft test setup is restricted to $717\,\mathrm{K}$ because cesium requires an inert external environment for safe operation. The working fluid study has also revealed how critical purity and cleanliness of the heat pipe is. Accordingly, each fluid will have its own heat pipe and thus the setup should support modularity. The dimensions are established at 500 mm length, 50 mm inner diameter and a 5 mm shell thickness. A maximum rotational velocity of 1000 rpm covers all possible internal flow patterns when the heat pipe is loaded up to $10\,\%$ of its volume. A maximum heat input of $2.27\,\mathrm{kW}$ supplied at the evaporator ensures heat fluxes up to $30\,\mathrm{kW}\,\mathrm{m}^{-2}$ at the condenser. Trace heating and mist cooling can supply the necessary heat flows uniformly without compromising safety nor impeding the replacement of heat pipes. Six pairs of thermocouples in the heat pipe shell, distributed over the length, enable both heat flux and temperature profile measurements. Five thermocouples located inside the heat pipe, and distributed over the length as well, provide an inner temperature profile and indirect pressure measurements. Ultrasonic technology is selected for the measurement of the liquid layer thickness, but requires further investigation.

Arrangements have been made for manufacture of the heat pipe embedded with the thermocouples. Additional equipment with the appropriate specifications and its suppliers have been identified. The design concepts will be finalized for manufacture and thus the high temperature rotating heat pipe setup will be realized.

Preface

This thesis is written to obtain the degree of Master of Science in Mechanical Engineering at the TU Delft. The work described in it, is part of a larger project by TU Delft, Tata Steel and Drever International. On behalf of the TU Delft I have been involved in The Heat Pipe Assisted Annealing Project since September 2015. It has been my task to design an experimental setup that can further prove the feasibility of the concept and provide information necessary for its continued development.

This report is intended for all those who will work with the setup, as well as those who are involved in the project in any other way. It can serve as a reference for the specifications and components and how they were selected. Additionally, it contains theory relevant for the design of high temperature rotating heat pipes, which will be required for development of the annealing line.

Whereas I have been contributing in context of my MSc. Sustainable Processes and Energy Technology, Metin Çelik is deeply involved in the entire project as a PhD researcher. He has been a great mentor on a daily basis and his guidance and time have helped me throughout the entire project. For this I would like to thank him. The same goes for Wiebren de Jong, who has assigned me to this project and continued to provide counseling and feedback as my supervisor. Furthermore, I want to thank Pepijn Pronk, Geert Paulussen and Ferry Frinking from Tata Steel for their useful experience and advice. I would also like to thank Bendiks Jan Boersma and Carlos Infante Ferreira for being part of my graduation committee.

A special word of thanks goes out to my parents, who have always supported me and made my education possible. And finally, to Laura for being there and inspiring me to plan.

B.O.P. Meltzer Delft, May 2016

Contents

	intre	duction	•
	1.1	The heat pipe assisted annealing project	1
		1.1.1 Continuous annealing	
		1.1.2 The rotating heat pipe	
		1.1.3 Rotating heat pipe assisted continuous annealing	
		1.1.4 The Tata Steel test rig	
		1.1.5 Other heat pipe test rigs	
	4.0	1.1.6 Outline of the project	
	1.2	Requirements for the TU Delft test rig	
	1.3	Problem statement	
	1.4	Outline	5
2	Wo.	ring Fluids and Shall Matarial	7
_			•
	2.1	Temperature range and chemical groups	
		2.1.1 Vapor pressure	
		2.1.2 Material groups	
	2.2	Performance	1
	2.3	Lifetime	1
		2.3.1 Thermal stability	3
		2.3.2 Compatibility	3
		2.3.3 Life tests	
	2.4	Safety and environment	
	2.5	Availability	
	2.6	Conclusion	
	2.0	Condusion	U
3	Des	gn Calculations 2	1
	3.1	Detailed specifications and requirements	1
		3.1.1 Specifications of an annealing line	
	32	Dimensioning 2	2
	3.2	Dimensioning	
	3.2	3.2.1 Flow regime based	2
	3.2	3.2.1 Flow regime based	2
	3.2	3.2.1 Flow regime based	2
	3.2	3.2.1 Flow regime based 2 3.2.2 Annealing heat pipe geometry based 2 3.2.3 Literature based 2 3.2.4 Outer diameter 2	2 3 3
		3.2.1 Flow regime based 2 3.2.2 Annealing heat pipe geometry based 2 3.2.3 Literature based 2 3.2.4 Outer diameter 2 3.2.5 Division into sections 2	2 3 4
	3.3	3.2.1 Flow regime based 2 3.2.2 Annealing heat pipe geometry based 2 3.2.3 Literature based 2 3.2.4 Outer diameter 2 3.2.5 Division into sections 2 Rotation 2	2 3 4 4
		3.2.1 Flow regime based 2 3.2.2 Annealing heat pipe geometry based 2 3.2.3 Literature based 2 3.2.4 Outer diameter 2 3.2.5 Division into sections 2 Rotation 2 Heat fluxes 2	2 3 4 4 5
	3.3	3.2.1 Flow regime based 2 3.2.2 Annealing heat pipe geometry based 2 3.2.3 Literature based 2 3.2.4 Outer diameter 2 3.2.5 Division into sections 2 Rotation 2	2 3 4 4 5
	3.3	3.2.1 Flow regime based 2 3.2.2 Annealing heat pipe geometry based 2 3.2.3 Literature based 2 3.2.4 Outer diameter 2 3.2.5 Division into sections 2 Rotation 2 Heat fluxes 2	2 3 4 5 5
	3.3	3.2.1 Flow regime based 2 3.2.2 Annealing heat pipe geometry based 2 3.2.3 Literature based 2 3.2.4 Outer diameter 2 3.2.5 Division into sections 2 Rotation 2 Heat fluxes 2 3.4.1 Operating limits 2 3.4.2 Heat input 2	2 2 3 3 4 4 5 7
	3.3 3.4	3.2.1 Flow regime based 2 3.2.2 Annealing heat pipe geometry based 2 3.2.3 Literature based 2 3.2.4 Outer diameter 2 3.2.5 Division into sections 2 Rotation 2 Heat fluxes 2 3.4.1 Operating limits 2 3.4.2 Heat input 2 Mechanical and thermal loads 2	2 2 3 3 4 4 5 5 7 8
	3.3 3.4	3.2.1 Flow regime based 2 3.2.2 Annealing heat pipe geometry based 2 3.2.3 Literature based 2 3.2.4 Outer diameter 2 3.2.5 Division into sections 2 Rotation 2 Heat fluxes 2 3.4.1 Operating limits 2 3.4.2 Heat input 2 Mechanical and thermal loads 2 3.5.1 Stresses 2	22334455789
	3.3 3.4 3.5	3.2.1 Flow regime based 2 3.2.2 Annealing heat pipe geometry based 2 3.2.3 Literature based 2 3.2.4 Outer diameter 2 3.2.5 Division into sections 2 Rotation 2 Heat fluxes 2 3.4.1 Operating limits 2 3.4.2 Heat input 2 Mechanical and thermal loads 2 3.5.1 Stresses 2 3.5.2 Thermal expansion 3	223344557890
4	3.3 3.4 3.5	3.2.1 Flow regime based 2 3.2.2 Annealing heat pipe geometry based 2 3.2.3 Literature based 2 3.2.4 Outer diameter 2 3.2.5 Division into sections 2 Rotation 2 Heat fluxes 2 3.4.1 Operating limits 2 3.4.2 Heat input 2 Mechanical and thermal loads 2 3.5.1 Stresses 2 3.5.2 Thermal expansion 3 pment and Instrumentation	223344557890 1
4	3.3 3.4 3.5	3.2.1 Flow regime based 2 3.2.2 Annealing heat pipe geometry based 2 3.2.3 Literature based 2 3.2.4 Outer diameter 2 3.2.5 Division into sections 2 Rotation 2 Heat fluxes 2 3.4.1 Operating limits 2 3.4.2 Heat input 2 Mechanical and thermal loads 2 3.5.1 Stresses 2 3.5.2 Thermal expansion 3	223344557890 1
4	3.3 3.4 3.5	3.2.1 Flow regime based 2 3.2.2 Annealing heat pipe geometry based 2 3.2.3 Literature based 2 3.2.4 Outer diameter 2 3.2.5 Division into sections 2 Rotation 2 Heat fluxes 2 3.4.1 Operating limits 2 3.4.2 Heat input 2 Mechanical and thermal loads 2 3.5.1 Stresses 2 3.5.2 Thermal expansion 3 pment and Instrumentation	223344557890 1 1
4	3.3 3.4 3.5	3.2.1 Flow regime based 2 3.2.2 Annealing heat pipe geometry based 2 3.2.3 Literature based 2 3.2.4 Outer diameter 2 3.2.5 Division into sections 2 Rotation 2 Heat fluxes 2 3.4.1 Operating limits 2 3.4.2 Heat input 2 Mechanical and thermal loads 2 3.5.1 Stresses 2 3.5.2 Thermal expansion 3 pment and Instrumentation Measurement techniques 3	223344557890 1 12
4	3.3 3.4 3.5 Equ 4.1	3.2.1 Flow regime based 2 3.2.2 Annealing heat pipe geometry based 2 3.2.3 Literature based 2 3.2.4 Outer diameter 2 3.2.5 Division into sections 2 Rotation 2 Heat fluxes 2 3.4.1 Operating limits 2 3.4.2 Heat input 2 Mechanical and thermal loads 2 3.5.1 Stresses 2 3.5.2 Thermal expansion 3 pment and Instrumentation 3 Measurement techniques 3 4.1.1 Reduction of measurements 3 4.1.2 Instrumentation 3	223344557890 1 123
4	3.3 3.4 3.5 Equ 4.1	3.2.1 Flow regime based 2 3.2.2 Annealing heat pipe geometry based 2 3.2.3 Literature based 2 3.2.4 Outer diameter 2 3.2.5 Division into sections 2 Rotation 2 Heat fluxes 2 3.4.1 Operating limits 2 3.4.2 Heat input 2 Mechanical and thermal loads 2 3.5.1 Stresses 2 3.5.2 Thermal expansion 3 pment and Instrumentation 3 Measurement techniques 3 4.1.1 Reduction of measurements 3 4.1.2 Instrumentation 3 Heating 3	223344557890 11234
4	3.3 3.4 3.5 Equ 4.1	3.2.1 Flow regime based 2 3.2.2 Annealing heat pipe geometry based 2 3.2.3 Literature based 2 3.2.4 Outer diameter 2 3.2.5 Division into sections 2 Rotation 2 Heat fluxes 2 3.4.1 Operating limits 2 3.4.2 Heat input 2 Mechanical and thermal loads 2 3.5.1 Stresses 2 3.5.2 Thermal expansion 3 pment and Instrumentation 3 Measurement techniques 3 4.1.1 Reduction of measurements 3 4.1.2 Instrumentation 3	223344557890 1 12345

viii Contents

	4.3	Coolin	g	
		4.3.1	Liquid cooling	
		4.3.2	Air cooling	
		4.3.3	Mist cooling	
		4.3.4	Pressure drop estimations	
	4 4		onal drive	•
	7.7	4.4.1	Characteristics	
		4.4.2	Type	
		4.4.2	турс	
5	Proc		s and Manufacture 45	
	5.1		osition of equipment	
			Additional equipment	
		5.1.2	Overview	į
	5.2	Safety		j
	5.3	Prepar	ation	•
	5.4	Contro	l	,
		5.4.1	Operation within limits	,
		5.4.2	Safety	,
		5.4.3	Overview	
		5.4.4	Practicals)
	5.5		igs and manufacture	,
	0.0	5.5.1	The heat pipe and its sensors	
		5.5.2	Connection to the shafts	
		5.5.3	Cooling duct	
		5.5.4	Rotation	
		5.5.5	Frame	
		5.5.6		
	F 6		Manufacture	
	5.6	Suppli		
		5.6.1	Induction heaters	
		5.6.2	Band heaters	
		5.6.3	Slip ring	
		5.6.4	Fan	
		5.6.5	DC Motor	
		5.6.6	Ultrasonic transducers	
		5.6.7	Frame	į
6	Con	clusior	57	,
•	6.1		isive summary	
	6.2		sion of requirements	
			mendations	
	0.0	6.3.1	Materials	
		6.3.2	High temperature alkali setup	
		6.3.3	Visual access	
			Ultrasonic technology	
		6.3.5	Additional experiments	
		0.3.3	Additional experiments	,
Re	ferer	nces	61	
^	Mate	erial da	ta 67	,
~			ophysical properties	
	Α. ι	111 C 1111	Uprilysical properties	,
			Empirical property correlations	
			Reference tables	
			position rates	
	A.3		ties of design materials	
		A.3.1	Biphenyl	
			Air	
		A.3.3	Steel	

Contents	ix
----------	----

В	Life test data B.1 Life test results and sources	
С	Drawings	77
D	Supplier Inquiries D.1 Datasheets	81 81
Re	eferences	83
Lis	st of Symbols	89

1

Introduction

1.1. The heat pipe assisted annealing project

The heat pipe assisted annealing project is a collaboration between TU Delft, Tata Steel and Drever International aimed at developing a continuous annealing line where the reuse of heat leads to a significant reduction in energy consumption. The project has been ongoing since 2009 and at Tata Steel in IJmuiden there is a test rig present, proving the feasibility of the concept [46]. The graduation project reported in this thesis is part of the heat pipe assisted annealing project, its main goal being the design of a second test rig, capable of operating at higher temperatures and enabling new measurements. The exact objectives of this thesis and the requirements of the TU Delft test rig are discussed later in this introduction. First, a more detailed description of two important concepts is given: the continuous annealing line and the (rotating) heat pipe.

1.1.1. Continuous annealing

Annealing is a heat treatment applied to cold rolled steel. Cold rolling of steel takes place below its crystallization temperature and produces steel strips holding tighter tolerances than hot rolled steel. However, it also brings about adverse mechanical properties due to the substantial stretching of the steel grains, such as brittleness and internal stresses. By heating the cold rolled steel to the right temperature (about 930 K) for a sufficient amount of time, recrystallization takes place and desired properties, such as ductility, are obtained.

In a continuous annealing line, a cold rolled strip is continuously lead over rolls through a furnace, followed by an over-aging and cooling section. All this takes place under an inert atmosphere to prevent oxidation of the steel. The furnace is of the radiant tube type, and is fired by combustion of natural gas. In the cooling section, gas jet cooling technology is used.

1.1.2. The rotating heat pipe

A heat pipe can be seen as a superconductor for heat. It is a heat transfer device with very high effective thermal conductivity at near isothermal conditions. This is achieved through the combination of evaporation, condensation and mass transfer. The heat pipe is a closed system containing only a limited amount of working medium. Heat is supplied on one side of the pipe (the evaporator), causing this medium to evaporate. As it evaporates, the medium expands, leading it to flow into the colder regions of the pipe where the pressure is lower. At the other end of the pipe (the condenser), the heat is extracted, resulting in condensation of the medium [51]. In order to sustain this heat transfer, a mechanism is needed that returns the condensate liquid to the evaporator section, thus closing the cycle.

Different types of heat pipe have different liquid return mechanisms. The most common type —the kind that is usually referred to when one speaks of 'a heat pipe'— uses a wick, a structure consisting of narrow channels where capillary forces drive the liquid towards the evaporator section. The second kind, also known as a thermosyphon, is oriented under inclination or vertically with the condenser section above the evaporator section. Naturally, gravity causes the liquid to flow back into the evaporator. The type that stands central in this thesis is the horizontally (axially) rotating heat pipe. The return of

2 1. Introduction

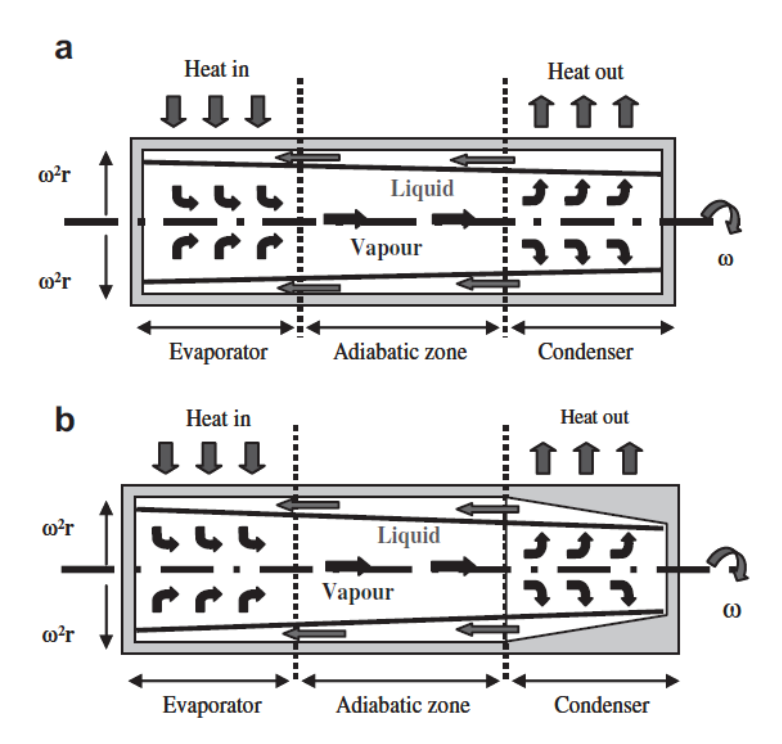


Figure 1.1: A schematic view of the flows inside a rotating heat pipe, with (a) no taper and (b) a taper in the condenser. From: Bertossi et al. [10].

liquid is driven by centrifugal forces resulting from the rotation of the pipe around its longitudinal axis. Commonly, a rotating heat pipe has an internal taper in the condenser but this is not essential for the flow-back mechanism, it just (significantly) enhances it [55]. In Figure 1.1 a schematic cross-section of a rotating heat pipe is depicted.

Since the evaporation and condensation both occur at the boiling point of the working medium, a heat pipe works at a nearly constant temperature and pressure. Only a minor gradient in pressure, and consequentially temperature, is caused by pressure drop over the vapor flow from evaporator to condenser. The working medium determines at which temperature and pressure ranges a heat pipe can operate. Moreover, a heat pipe is self regulating; supplying more heat at the evaporator side leads to the formation of more vapor, resulting in an increase of pressure in the heat pipe. This increase causes the condensation temperature to rise and thus more heat to be expelled [43].

1.1.3. Rotating heat pipe assisted continuous annealing

The rotating heat pipe can be deployed in the continuous annealing process to efficiently transfer heat from the cooling section to the heating section, thus reducing the need to gain heat from the combustion of natural gas. The deployment of rotating heat pipes can therefore lead to 70 % less energy consumption [46]. The rolls over which the strip is wound can be replaced by rotating heat pipes. The part of the strip that is to be cooled provides heat to the evaporator section of the rotating heat pipe, whereas the part of the strip that needs heating extracts heat from the condenser section. At some point, the strip needs to be reversed so that the heated part and the cooled part move counter directional over the same heat pipe.

Figure 1.2 shows a schematic overview of this concept. It was invented at Tata Steel's R&D department and has been patented [44]. Note that, still, some conventional heating and cooling are required to reach the final temperature at the end of the heating and cooling cycle, due to the physical inability to achieve heat transfer without losses. The schematic shows that the rotating heat pipes in the annealing line will operate at a wide range of temperatures. In reality, the full line will likely consist of tens of heat pipes, each operating at a slightly different temperature, so that a gradual heating (and consequentially cooling) profile is achieved.

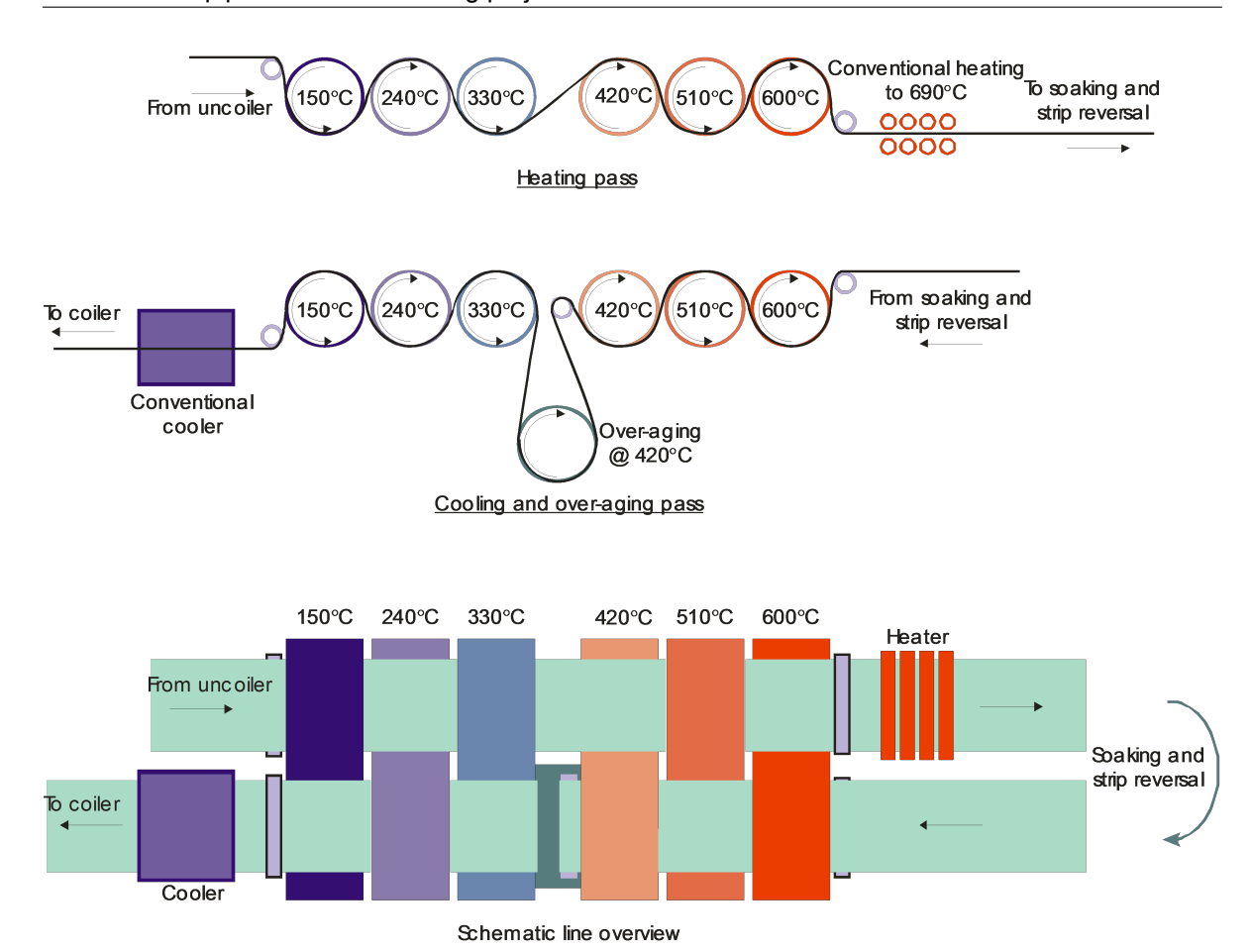


Figure 1.2: A schematic overview of a conceptual rotating heat pipe assisted continuous annealing line. Both a side and top (below) view are depicted.

1.1.4. The Tata Steel test rig

The test rig currently present at Tata Steel is shown in Figure 1.3 and comprises one large rotating heat pipe and two additional rolls to span the strips. The strip at the evaporator side is heated by an induction coil positioned above it, just before the heat pipe so that it supplies heat to it. The strip at the condenser side is not heated, thus representing the cold strip. This way, the test rig resembles a 'cut-out' of one heat pipe out of the complete annealing line.

The temperature of the hot strip is monitored with an infra-red camera and inside the heat pipe three thermocouples measure the temperature at different axial positions. The heat pipe's working medium is water, limiting its working range from 293 to 443 K (20 to 150 °C). At temperatures exceeding this range the internal pressure becomes too high.

1.1.5. Other heat pipe test rigs

The rotating heat pipe was first described by Gray [25] in 1969. Since then the device has found applications in a wide range of fields, e.g. in satellites rotating about their central axis or the cooling of turbine shafts [51]. Nevertheless, other large scale industrial applications of rotating heat pipes, like the one intended in this project, have not been encountered. There are many reports of (rotating) heat pipe test setups however; e.g. for the testing of working fluids [3, 27], validation of theoretical models [16, 55], experiments with high rotational velocity [50] or examining of internal heat transfer conditions [56]. Such studies can provide useful reference material for the design of the TU Delft test rig and at a later stage, for validation of results.

4 1. Introduction

1.1.6. Outline of the project

The design and manufacture of the TU Delft test rig, as well as the high temperature experiments that will follow, are merely part of the much larger project. Experiments are still ongoing at the Tata Steel test rig to assess general performance and stability of the water/stainless steel heat pipe. Heat transfer coefficients between the pipe and the steel strips are derived and the obtained data is also used for validation of numerical models. These models initially comprise only one rotating heat pipe and the strips but will later be expanded into large scale dynamic models of the intended annealing line.

First, the experiments with the TU Delft test rig will have to prove the concept at higher temperatures and provide additional data to improve the models concerning internal phenomena. At the later project stages, a full scale plant can be designed based on the information acquired from the experimental setups, models and literature.

All these tasks have been divided into project work packages. Figure 1.4 shows the content of these packages and how they are related. The design, manufacture and use of the TU Delft test rig are part of work package 3.

1.2. Requirements for the TU Delft test rig

The setup that is to be designed during this graduation project, i.e. the TU Delft test rig, has to cover the rest of the temperature range of a rotating heat pipe assisted annealing line, from 443 to 873 K (150 to 600 °C). In order to be able to do so, the heat pipe has to contain different working fluids than water. Furthermore, the setup has to facilitate a number of observations that can provide insight in the mass and heat transfer phenomena taking place inside the heat pipe. These observations are:

- · Heat flux through the heat pipe shell at every section.
- · The thickness of the condensate layer.
- · The velocity of the condensate.
- · The velocity of the vapor.
- The temperature profile inside the heat pipe.
- The pressure profile inside the heat pipe.

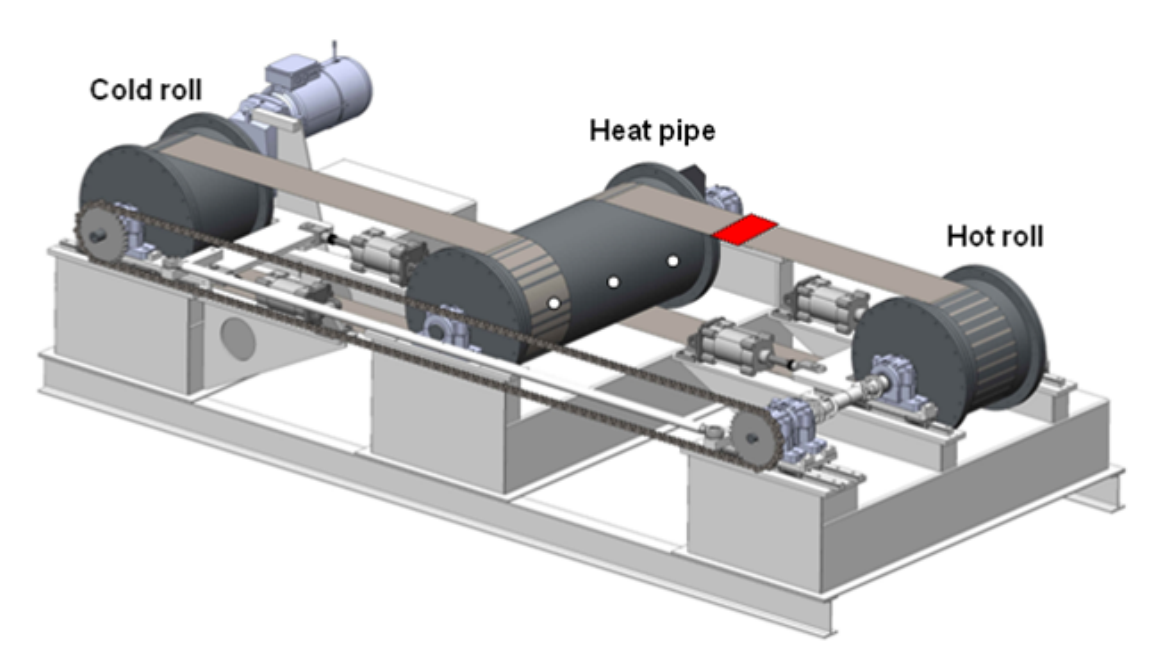


Figure 1.3: A CAD model of the test rig at Tata Steel. The red rectangle indicates where an induction coil is heating the strip. The diameter of the heat pipe is 0.502 m.

1.3. Problem statement 5

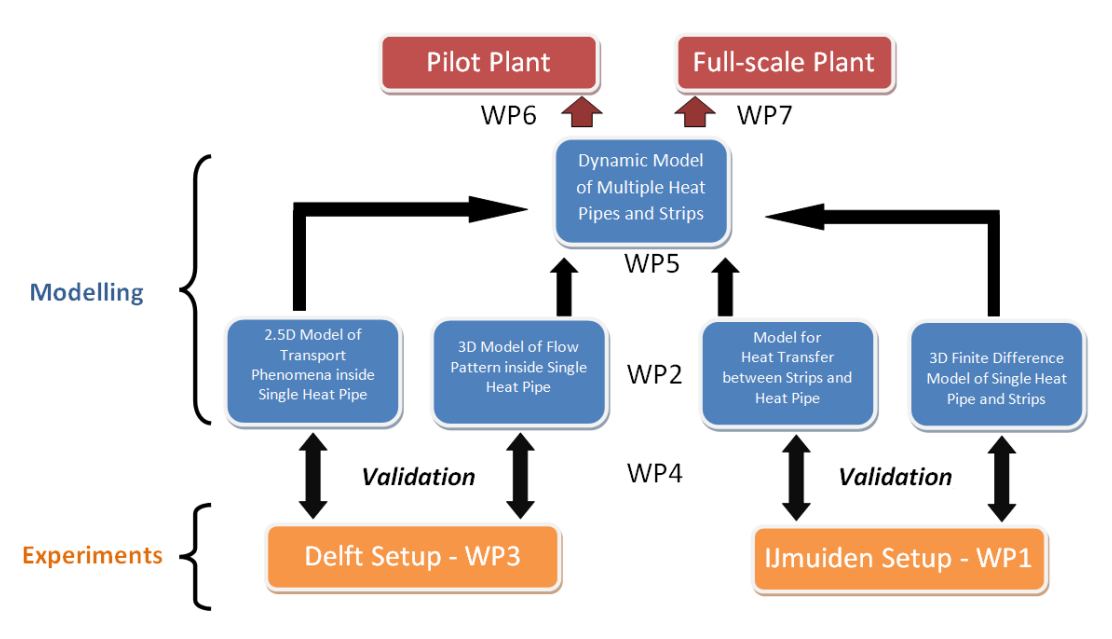


Figure 1.4: The division of the heat pipe assisted annealing project into work packages (WP) and the interaction between them.

- · The temperature profile of the heat pipe shell.
- · The rotational speed of the heat pipe.

In terms of size the setup is supposed to be small-scale and fit a tabletop. Besides serving in the heat pipe assisted annealing project, it should be suitable for student's experiments as well. The setup will be placed at the Process and Energy Laboratory of the 3mE faculty.

1.3. Problem statement

As stated before, the main goal in this thesis is to design a rotating heat pipe test rig that complies to the requirements described above. Therefore the following objectives are formulated:

- Identify which working fluids are applicable in view of their vapor pressure, heat transfer characteristics, stability and health and environment in the temperature range of 443 to 873 K.
- Select the measurement techniques required to enable the desired heat and mass flow observations.
- Design a rotating heat pipe that is compatible with the selected working fluids and facilitates the selected measurement techniques. Furthermore, the conditions of the rotating heat pipe should resemble the operating conditions of a rotating heat pipe in the continuous annealing line.
- Design an experimental setup for both the project and student practicals that accommodates
 the rotating heat pipe and can provide the heating and cooling required for operating conditions
 resembling those of the continuous annealing line.
- Arrange the manufacturing of the setup; select necessary equipment and contact suppliers.

1.4. Outline

First, a selection of suitable working fluids and a shell material is made (Chapter 2), since these form the basis of heat pipe operation and therefore the design. Then in Chapter 3 design calculations are made to determine specifications such as the heat pipe dimensions, heat input, heat removal and rotational velocity. The equipment required to comply with these specifications is then selected in Chapter 4 based on further calculations and research. Important concepts and procedures are treated in Chapter 5. Additionally, design specifics and manufacture methods are discussed. Finally, the thesis in concluded in Chapter 6 and recommendations are made.

Working Fluids and Shell Material

The working fluid inside a heat pipe is a critical component. It determines the temperatures at which the heat pipe can operate, has a major influence on its performance and together with the shell material it restricts lifetime. Finding the optimal working fluid is a process where many different physical and chemical aspects need to be taken into account. In this chapter these aspects; temperature range, performance, lifetime, safety and availability are evaluated and the process of choosing a working fluid and shell combination is described.

2.1. Temperature range and chemical groups

2.1.1. Vapor pressure

The temperature range at which a heat pipe can operate is determined by the vapor pressure of the working fluid. If the vapor pressure in the evaporator is lower than the pressure drop between the evaporator section and the condenser section, the heat pipe cannot function. This phenomenon is described by the viscous (or vapor) limit and is dominant at lower temperatures in the viscous flow regime. In the case of negligible viscous forces, the sonic limit presents itself at lower pressures, caused by choking of the vapor at the evaporator exit.

From a theoretical perspective, the upper limit lies just below the critical point, because a phase change is needed to drive the heat pipe. Practically, it is advised not to go higher than 100 K below the critical point [19]. In some cases the maximum allowable pressure is set by safety restrictions. Another reason to limit the pressure is the stress it induces on the heat pipe shell, resulting in an increased required thickness which leads to reduced conductive heat transfer through the shell.

For the rotating heat pipe assisted annealing project a temperature range from 333 to 873 K has to be covered. The lower part of this range can be covered by a water heat pipe and an experimental setup for this range is already present at Tata Steel. The 423 to 873 K range is to be covered by the setup designed in this thesis. The maximum allowable pressure in the heat pipe is 0.5 MPa, a value established after consulting both the Tata Steel and the P&E laboratory. A minimum operating pressure is not strictly defined because very low vapor pressures are unavoidable when the heat pipe is idle at room temperature. The challenge of identifying materials that have relatively low vapor pressures at temperatures in the 420 to 873 K range and possess the right properties for performance and lifetime, requires that a wide range of material groups is considered.

The first step is to find the vapor pressures of possible working fluids over the temperature range. In the lower temperature band, from roughly 423 to 620 K, there are many applications using fluids at their vapor-liquid equilibrium for heat transfer and many suitable fluids, almost all hydrocarbons and siloxanes, can be found here. The RefProp database covers many of these and contains accurate correlations for their vapor pressures and other properties at saturation [40]. Above roughly 620 K most organics exceed the pressure limit or become unstable, with exception of some aromatic hydrocarbons (more on this in section 2.3.1). Therefore inorganic materials and elements are applied as heat pipe materials in this region [2, 20].

In Figures 2.1(a) to 2.2(c) a selection of possible working fluids is displayed sorted by chemical group and temperature range. Appendix A contains the sources and methods used to obtain the vapor

pressures.

2.1.2. Material groups

In this section an introduction is given to the materials considered for application as a heat pipe working fluid. Their initial selection is mainly based on prior use as heat transfer agents or heat pipe working fluid, suitable vapor pressure regions, availability of thermophysical data and preliminary impressions of their stability. The groups discussed are:

- · Aliphatic (fluorinated)hydrocarbons
- Siloxanes
- Aromatic hydrocarbons
- Halides
- Elements

Simple hydrocarbons and fluorinated hydrocarbons are only applicable in the lowest temperature band as can be seen in Figure 2.1(a). Perfluorocarbons, like PP80 and PP90, are stable and inert due to their shielding by electronegative fluor atoms and therefore applicable at high temperatures but unfortunately their high vapor pressures limit their applicability [62].

Polydimethylsiloxanes (siloxanes) cover a region up to 690 K (Figure 2.1(b)) and possess good stability characteristics, due to the strength of the Si–O-bond (452 kJ mol $^{-1}$ versus 347 to 356 kJ mol $^{-1}$ for C–C) [15]. They have a cyclic or linear structure consisting of SiO(CH $_3$) $_2$ -groups (D), with the linear molecules enclosed by (CH $_3$) $_3$ Si-groups (M). Hence, the cyclic siloxanes are referred to as D $_n$ and the linear ones as MD $_n$ M. Current applications of siloxanes as heat transfer fluids are in organic Rankine cycles [5, 64] .

Aromatic hydrocarbons consist of, or contain, highly stable benzene rings. Figure 2.1(c) shows the vapor pressures of a selection of aromatics. Aromatic hydrocarbons have often been tested and used as heat pipe working fluids and high temperature coolants [24, 27, 41, 54, 63]. Examples of frequently applied aromatic heat transfer fluids are toluene and Dowtherm A. The latter is commercially available as a eutectic mixture of biphenyl (26.5 mol%) and diphenyl oxide (73.5 mol%). Toluene and the xylenes are alkylated benzene derivatives. Naphthalene and phenanthrene are polycyclic aromatic hydrocarbons, meaning that they consist of fused benzene rings. Biphenyl and terphenyl are polyphenyls, i.e. chains of benzene rings connected by C—C-bonds. Perfluorinated aromatics were also considered but it was found that they are less stable than their non-fluorinated counterparts [27].

Figure 2.2(a) and Figure 2.2(b) show the vapor pressures of metal halides. Halides consist of a halogen combined with any other element or organic compound. They have been proposed and tested as possible heat pipe fluids by Saaski and Owzarski [54], and the testing has been continued by others [3, 4]. Similar to other potential fluids, metal halides show good stability and performance characteristics in their working region. Furthermore, they have widely varying vapor pressures and are therefore applicable over the entire temperature range, except for the fluoride halides, whose temperatures generally are too high.

At higher temperatures elements become effective heat pipe fluids. Most of these are alkali metals: cesium, potassium and sodium. Cesium is applied as heat pipe fluid at temperatures exceeding 550 K, whereas potassium and sodium become a viable option above approximately 750 K and 873 K respectively [20]. The alkali metals are the most accepted heat pipe fluids at higher temperatures and for this reason they have been thoroughly tested and are applied in many different situations. Mercury is used in heat pipes because of its favorable vapor pressure and performance characteristics in regions where organics tend to fail but has drawbacks in terms toxicity and low surface tension. The latter is particularly important in wicked heat pipes however, and much less in rotating heat pipes. Sulfur covers a temperature range where little alternatives are present but its viscosity is too high for effective operation. Iodine can be added to reduce viscosity and increase performance, but both materials are highly corrosive [2].

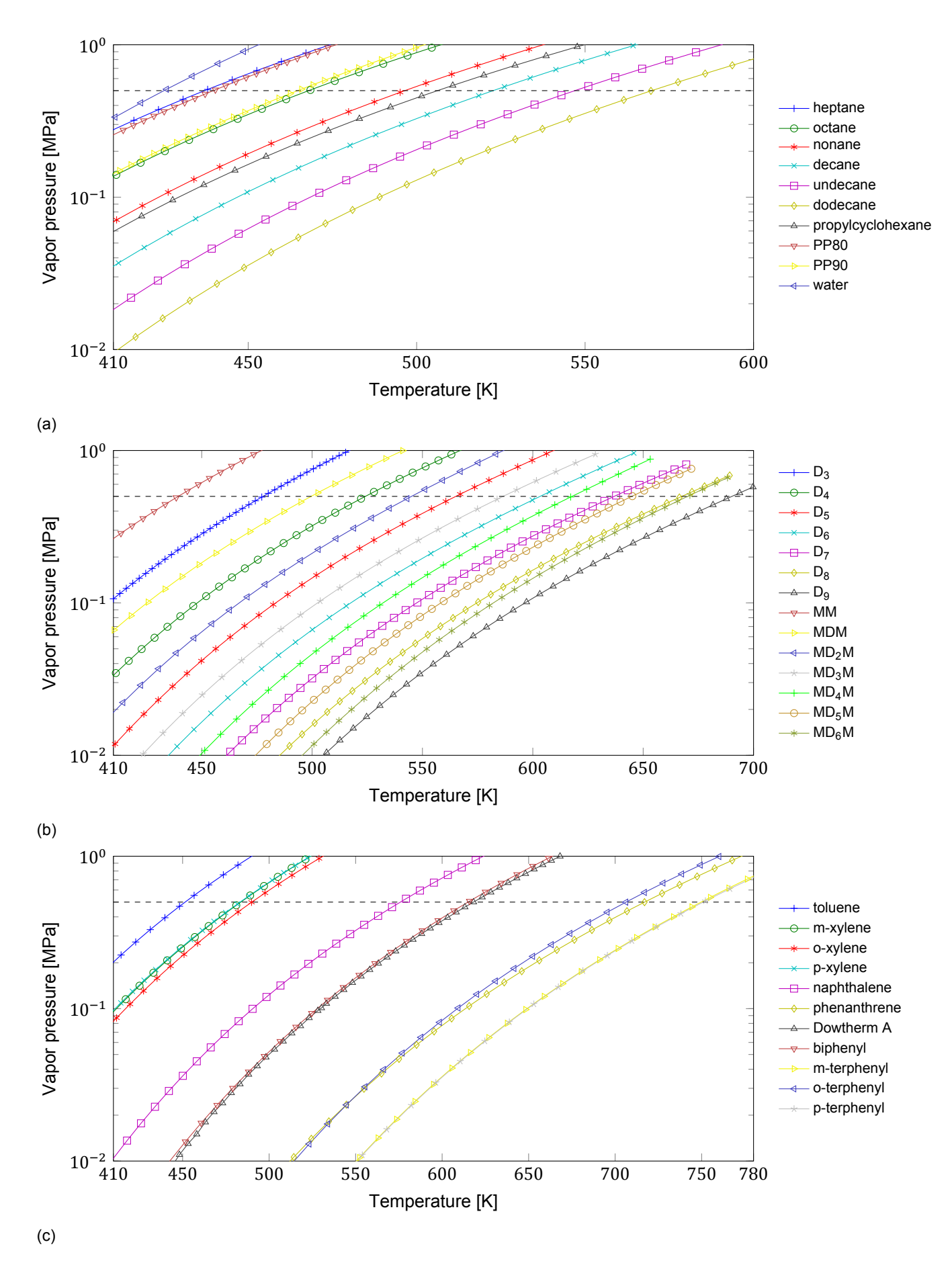


Figure 2.1: The vapor pressures of selected (a) aliphatic hydrocarbons, perfluorocarbons and water, (b) cyclic and linear siloxanes, (c) aromatic hydrocarbons. The dashed line shows the upper pressure limit. The curve for water in (a) is displayed as a reference, its upper temperature limit is where the range for this project starts.

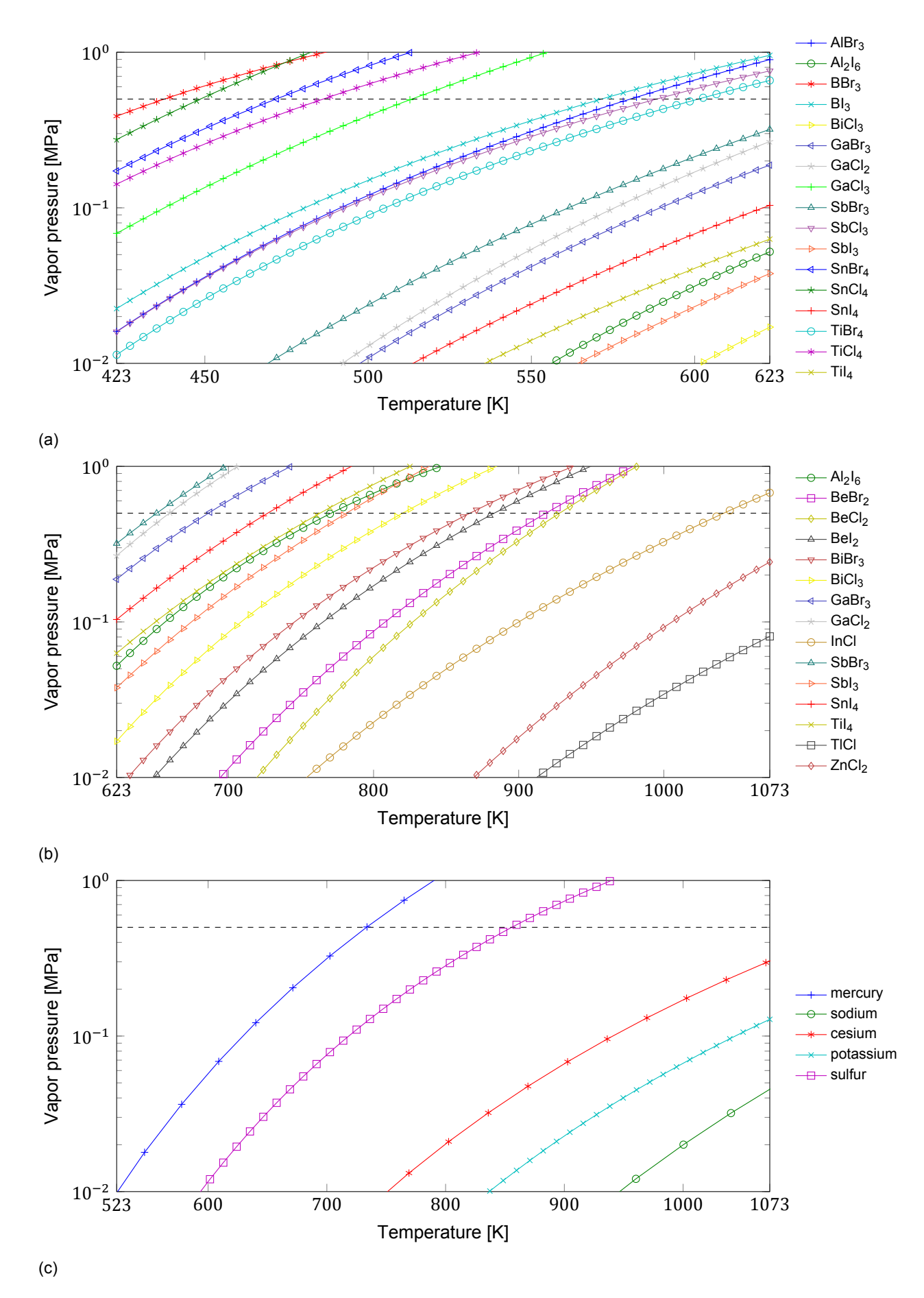


Figure 2.2: The vapor pressures of selected (a) halides in the lower temperature region (b) halides in the upper temperature region, (c) elements. The dashed line shows the upper pressure limit.

2.2. Performance

2.2. Performance

A number of material properties have significant influence on the rotating heat pipe performance, these are:

- Viscosity
- Heat of vaporization
- · Thermal conductivity
- Density

Low vapor and liquid viscosity minimize the resistance in the flows. High latent heat of vaporisation enables good heat transfer while keeping the required vapor flow small, resulting in less pressure drop. The same is true for high density; more heat can be stored in a smaller volume. High thermal conductivity minimizes the radial temperature gradient in the heat pipe and increases heat transfer [51]. A good indication of the working fluid's performance based on its physical properties is the figure of merit M. For rotating heat pipes this is

 $M = \frac{\rho_{\rm l}^2 L \lambda_{\rm l}^3}{\mu_{\rm l}} \tag{2.1}$

where $\rho_{\rm l}$ is the liquid density, L the latent heat of vaporisation, $\lambda_{\rm l}$ the liquid thermal conductivity and $\mu_{\rm l}$ the liquid viscosity. The merit number for rotating heat pipes was derived by Daniels and Al-Jumaily [16] by means of a Nusselt type analysis of the condensate film. According to Daniels and Al-Jumaily the efficiency of the condensation process is a good performance indicator because in a steady-state operating heat pipe the condensation rate is in equilibrium with the evaporation rate and thus indicating heat transfer and temperature. The analysis is used to create an expression for the average heat transfer, where drag effects are neglected, and in which fluid properties are grouped together as the figure of merit.

The figure of merit varies with temperature and therefore a point at which performance is maximal can be established. With further increase in temperature, the heat of vaporization drops and the figure moves towards its minimum at the critical point. For many fluids, the required properties as a function of temperature are very hard to obtain. For the ones available, Figures 2.3(a) and 2.3(b) show the calculated merit number over the relevant temperature region. The sources and methods used to obtain the required properties are described in Appendix A. Some of the correlations were extrapolated beyond the temperature range they were established for, so the calculated values might contain certain errors. This is considered to be acceptable since the figure of merit is merely a performance indicator.

Notable is the pure metal's superior performance compared to the halides and the organics. Water also shows an exceptional performance due to its high enthalpy of vaporization. The hydrocarbons and most of the halides appear to be comparable, whereas the siloxanes lag behind. Unfortunately, for the siloxanes, all the required properties are only available for octamethylcyclotetrasiloxane (D_4) .

Performance seems like an obvious criterion for the selection of a working fluid. It plays a lesser role than expected however, because if the most powerful fluid cannot last a required lifetime, it is useless for the application in the heat pipe assisted annealing project. Or if it is highly toxic or explosive, it cannot be used in a practicum setup for students.

2.3. Lifetime

Two kinds of processes reduce the lifetime and lasting performance of a working fluid: thermal degradation and (electro)chemical reactions with other heat pipe components. In both cases it is the formation of the reaction products that decrease performance or cause direct failure. Non-condensable gases accumulate in the condenser and reduce the heat transfer area. Liquid and solid corrosion products deposit in the evaporator. When impurities and air or moisture are present in the heat pipe other adverse reactions take place and degradation is accelerated. Therefore it is essential that the working fluid is as pure as possible and that no air is permitted to enter the heat pipe. Non-condensable gases can be detected during heat pipe operation by monitoring the temperature difference between different heat pipe sections. Some reaction products may remain in the liquid phase and may even be other potential working fluids. For example, larger linear siloxanes will decompose into smaller cyclic ones

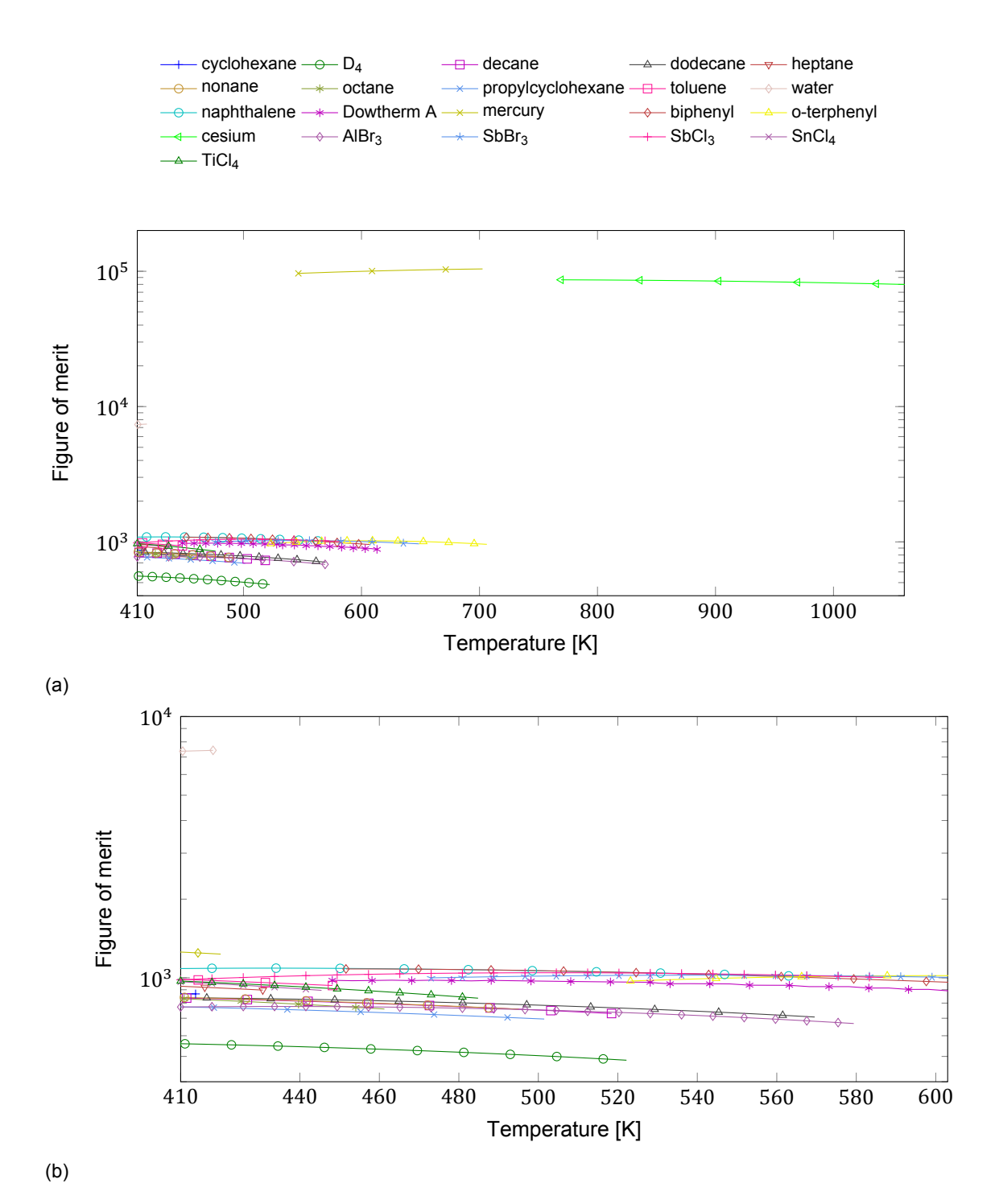


Figure 2.3: (a): The figure of merit for the temperature range 410 to 1060 K. The start and end points of the lines correspond to the temperature range where the fluids can be applied, with the pressure range taken as 0.01 to 0.5 MPa. In (b) a more detailed view of the figure of merit in the 410 to 600 K region is given.

2.3. Lifetime 13

[12, 59]. Nonetheless, these products are still undesirable because their saturation temperature will deviate from the original fluid's.

Understanding the mechanisms behind the adverse reactions provides methods to predict lifetime. Therefore these are discussed in this section. Theoretical predictions only provide a limited view however, because of the complex processes taking place inside the heat pipe, such as evaporation and condensation. Experimental lifetime tests provide more accurate data but have to be available for a specific fluid, temperature range and duration. This is not always the case, but if available, the data is presented here as well and compared to the theory.

2.3.1. Thermal stability

All organic fluids are subject to thermal decomposition, the tendency to isomerize and be converted into smaller molecules. At elevated temperatures the reaction rate increases exponentially but some materials are far more responsive to it than others. The thermal decomposition temperature, often presented in material data sheets as the maximum temperature at which stability is ensured, refers to a certain rate of material decomposition, which might be as high as 1 mole %/h [33]. This means stability predictions cannot be based on the thermal decomposition temperature. Rather needed is the decomposition rate constant k as a function of temperature. This is given by the Arrhenius equation, shown in eq (2.2) [54].

$$k = A \exp\left(-E/RT\right) \tag{2.2}$$

Here A is the pre-exponential factor, E is the activation energy, R is the gas constant and T is the temperature. The values of A and E have been experimentally obtained in multiple studies for most of the organic materials currently under investigation. Decomposition of hydrocarbons can be represented sufficiently well by first order kinetics [6, 18, 35, 47]. The same is true for siloxanes [12, 21, 28, 31]. The first order decay of a material D is

$$\frac{d[\mathsf{D}]}{dt} = -k[\mathsf{D}] \tag{2.3}$$

Solving this differential equation yields an expression for the remaining liquid at time t.

$$[\mathsf{D}] = [\mathsf{D}]_0 \exp(-kt) \tag{2.4}$$

with $[D]_0$ the initial concentration of D.

As a decomposition reaction proceeds, the kinetics might change as a result of reactions with the products. Because only a very small amount of decomposition is allowed in the heat pipe, this is assumed to be insignificant.

Since it is assumed that the heat pipe operates with a pure fluid in vacuum, it is important to review only studies that consider decomposition reactions without presence of water or oxygen. The temperature and pressure range at which the reaction constants were established should be regarded, as well as the container material, due the the influence of surface energy on the activation energy. All these different factors result in occasional inconsistencies between the results of the studies. In Appendix A an overview is given for the sources of A and E used in this thesis and the conditions they were obtained for.

In Figures 2.4(a) to 2.4(c) the decomposition rate as a function of temperature is displayed for the various types of organic working fluids under consideration. Using eq. (2.3) a critical rate can be calculated at which the fluids can operate while having a maximum decomposition of 0.1% per year. The temperatures corresponding to this rate are also indicated. For some fluids this temperature is lower than the upper limit of their working range, i.e. at the maximum allowable vapor pressure. Figures 2.5(a) to 2.5(c) show the fraction of fluid remaining over time when a fluid is operating at this limit. The applicability of some fluids is thus limited when considering thermal stability.

2.3.2. Compatibility

The reaction of organic materials with the heat pipe shell is considered to be negligible, especially when contemplating the fact that most decomposition experiments are carried out in metal (mostly stainless steel) containers and thus all the possible effects are already included in the decomposition rate. Still, the possible presence of catalytic effects should not be ruled out [54]. The Gibbs free energy of formation is higher for many inorganic fluids than for organic fluids, implying more thermal stability. However, salts such as halides can have a strong tendency to electrochemically react with the metal

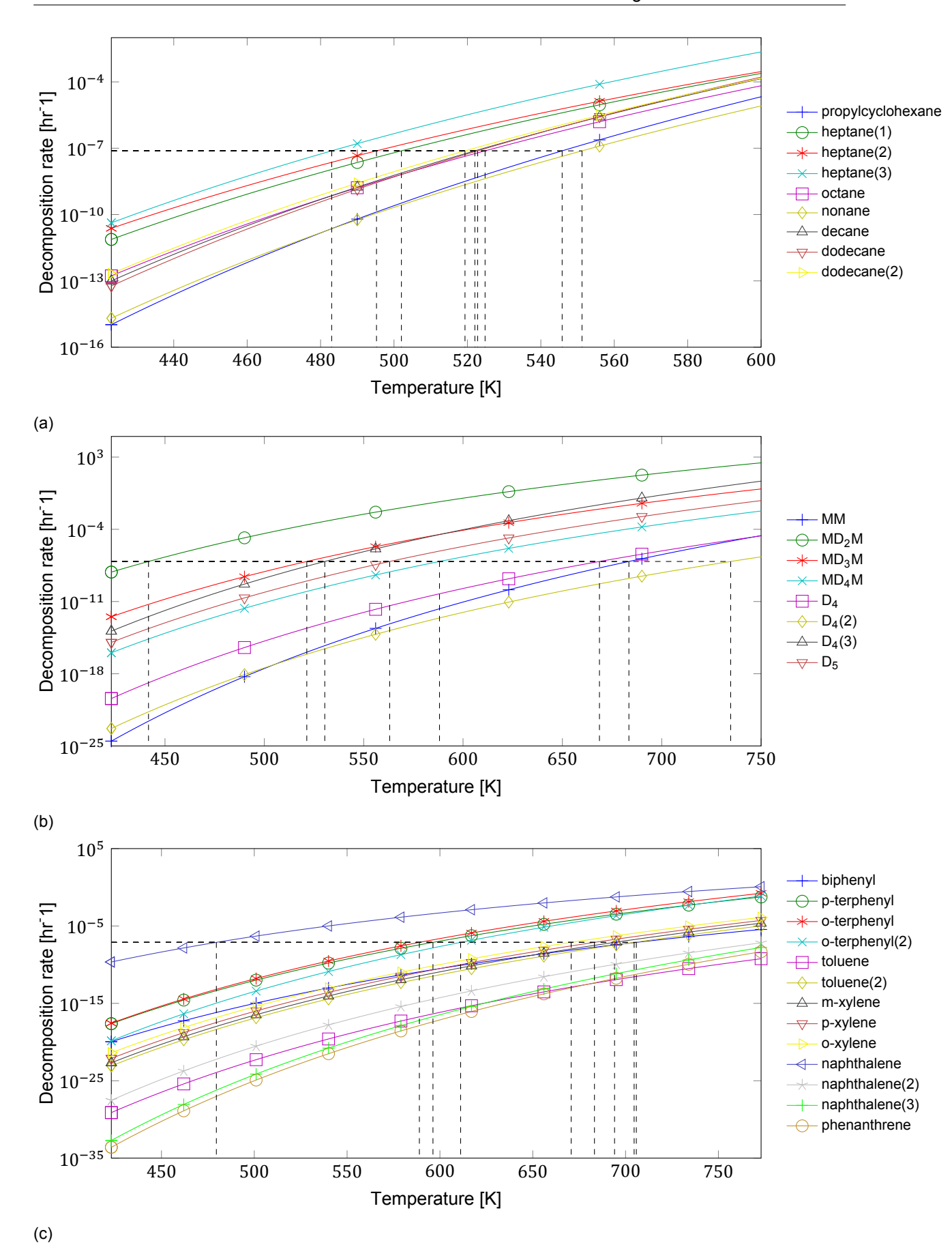


Figure 2.4: The thermal decomposition rate as a function of time for (a) aliphatic hydrocarbons, (b) siloxanes and (c) aromatic hydrocarbons. The horizontal dashed line indicates the critical rate at which there is 0.1 % decomposition per year. The vertical lines indicate the corresponding temperature for each fluid.

2.3. Lifetime

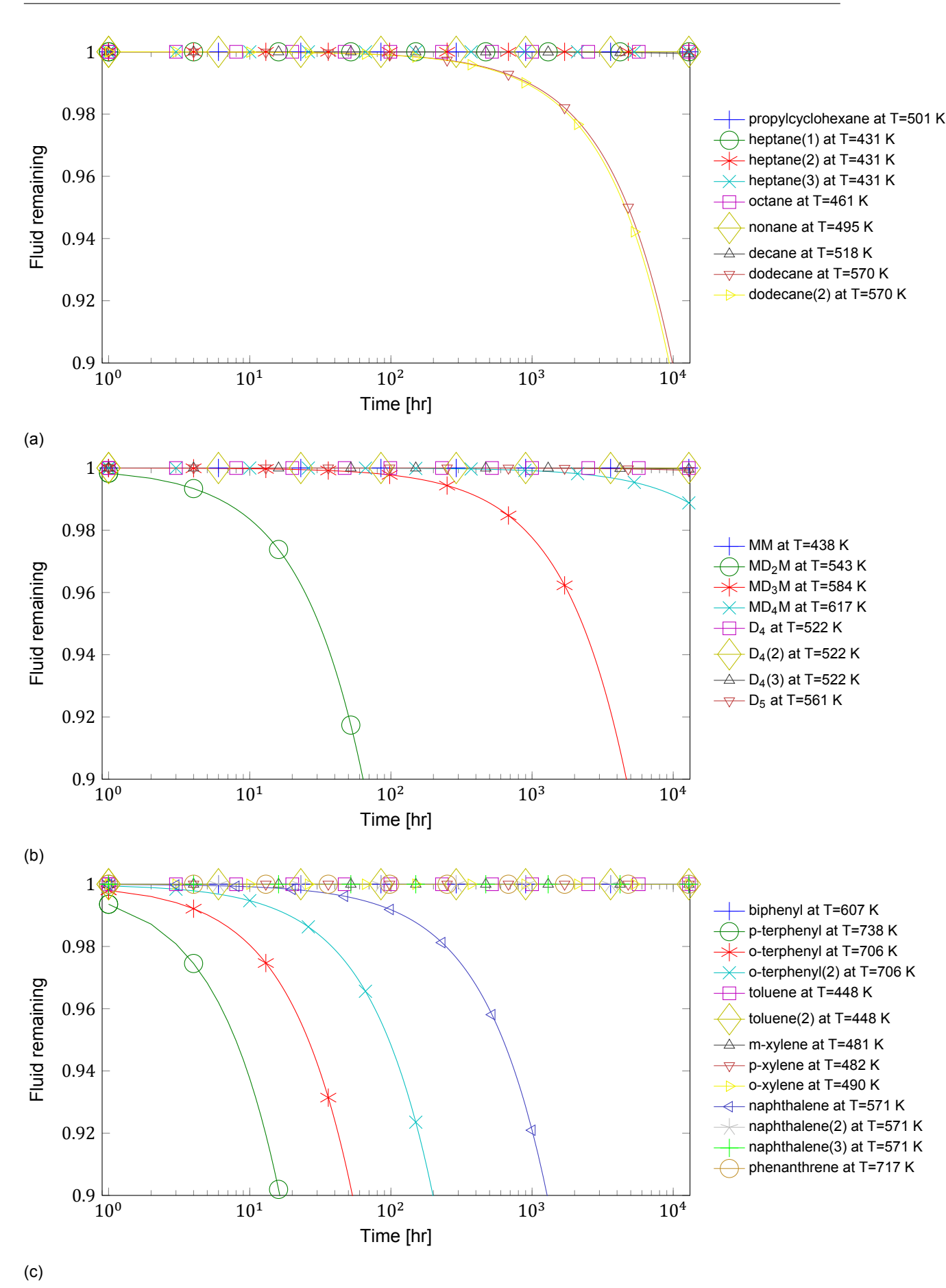


Figure 2.5: The fluid fraction remaining over time at the maximum operating temperature for (a) aliphatic hydrocarbons, (b) siloxanes and (c) aromatic hydrocarbons.

heat pipe shell, resulting in the formation of adverse reaction products. Such a reaction of a shell metal M_s with a metal halide M_fH would be of the form:

$$\alpha M_s + \beta M_f H \longrightarrow \gamma M_s H + \delta M_f$$
 (2.5)

The likelihood of such a reaction taking place can be evaluated by calculating its change in Gibbs free energy:

$$\Delta G = \Delta G^{\circ} + RT \ln \left[\frac{\left(a_{M_{s}H} \right)^{\gamma} \left(a_{M_{f}} \right)^{\delta}}{\left(a_{M_{s}} \right)^{\alpha} \left(a_{M_{f}H} \right)^{\beta}} \right]$$
(2.6)

where a is the activity coefficient and ΔG° is the Gibbs free energy difference at standard conditions. Since the shell and the halide form an electrochemical cell it is useful to determine the electromotive force difference ΔE . It can be written in terms of the free energy:

$$\Delta E = \frac{-\Delta G}{nF} \tag{2.7}$$

with n the number of electrons transferred and F the Faraday constant. Equation (2.7) can be used to create an expression for the electromotive force difference of the reaction (eq. (2.5)), which yields

$$\Delta E = \Delta E^{\circ} + \frac{RT}{nF} \ln \left[\frac{\left(a_{\rm M_s H} \right)^{\gamma} \left(a_{\rm M_f} \right)^{\delta}}{\left(a_{\rm M_s} \right)^{\alpha} \left(a_{\rm M_f H} \right)^{\beta}} \right]$$
(2.8)

Thus to determine the compatibility of a metal halide with a shell, the activity coefficients are needed. Saaski and Owzarski [54] have derived a physical model of an electrochemical cell in which the materials from eq. (2.5) act as components; the electrodes are of the combination M_s , M_sH and M_fH , M_f and the electrolyte is liquid M_fH , i.e. the halide working fluid. The solubilities of M_s and M_fH in M_f and that of M_fH in M_sH are assumed to be negligible, which leads to the approximation that all the activities are equal to unity and therefore $\Delta E = \Delta E^\circ$. This assumption is strengthened by the fact that the reaction will only be in its initial state, as soon as it proceeds too many adverse reaction products will form and the heat pipe fails. Saaski and Owzarski [54] estimated that at 298.15 K the error increases with 5.9 mV for each factor two change in the logarithmic term (containing the activities) of eq. (2.8). This is demonstrated below.

$$\Delta E = \Delta E^{\circ} - \frac{8.314 \cdot 298.15}{3 \cdot 96485.33} \ln(2) = \Delta E^{\circ} - 0.0059 \,\text{V}$$
 (2.9)

Note that the number of electrons transferred in this estimation is three, because the reaction of bismuth(III) chloride with an iron shell was taken as example. The estimated error is very small compared to the electromotive force differences of the possible reaction, yet the reactions will take place at temperatures far higher than 298.15 K and with less electrons transferred, resulting in a larger error. A more conservative estimation of the error could therefore be made at the maximum temperature of 870 K and with two electrons transferred:

$$\Delta E = \Delta E^{\circ} - \frac{8.314 \cdot 870}{2 \cdot 96485.33} \ln(2) = \Delta E^{\circ} - 0.0260 \,\text{V}$$
 (2.10)

An example of the scenario of eq. (2.10) could be the reaction of zinc(II) chloride with an iron shell, taking place in the lower region of its application range (Figure 2.2(b)). The error in such a conservative case is still small enough to use $\Delta E = \Delta E^{\circ}$ as a method to predict compatibility.

The standard electromotive force difference can be expressed as the difference in decomposition potential E_p of the metal shell halide and the working fluid halide:

$$\Delta E^{\circ} = E_{\mathsf{D}}(\mathrm{M_{s}H}) - E_{\mathsf{D}}(\mathrm{M_{f}H}) \tag{2.11}$$

If $\Delta E^{\circ} > 0$, a reaction can occur spontaneously, leading to the decomposition of the halide working fluid. In the case $\Delta E^{\circ} < 0$, the probability of a reaction with the shell is very small and thus the combination is considered stable. Hence, combinations of fluids with high decomposition potentials and shell metal halides with low potential are most stable. Generally, the order of halide decomposition

2.3. Lifetime 17

potential is F > CI > Br > I. For the halides of common shell materials (or alloy constituents) the order of increasing decomposition potential, and thus decreasing stability is Mo < Fe < Ni < Cr < Ti < Al [58]. The decomposition potentials of molten halides are scarcely available and mostly for chlorides, yet some relevant sources have been found [29, 30, 32]. Hamer et al. [29] calculated the values for solid and liquid halides from thermodynamic data for chloride, fluoride, bromide and iodide halides for a temperature range of 298 to 1773 K at 0.1 MPa. Janz [32] provides values for roughly the same halides but only at 773 K and 1073 K. In Figures 2.6(a) to 2.6(c) the electromotive force difference has been plotted for all the halide fluid - shell combinations available. The shell halide reaction product with the highest potential was taken in order to get a conservative number. For example, in case of a titanium shell, titanium(II) halides potentials were taken instead of titanium(III) or (IV). This also explains why in some cases the potential difference between a shell material and a halide fluid containing the same metal is not zero.

Noteworthy is the stability of all the halides in combination with molybdenum. Copper and nickel also show good characteristics, the first seems more stable with chloride and the latter with bromide and iodide. Aluminium and titanium prove to be poor choices when using a halide working fluid. Iron and chromium, the main constituents of stainless steel appear to be stable in many cases but in combination with an iodide, chromium fails.

Some metals would make extremely stable shell materials due to the very low decomposition potential of their halide, but are unsuitable as a construction material (e.g. iridium, platinum and gold). A thin coating containing such metals could increase stability without compromising performance.

2.3.3. Life tests

As mentioned before, the models described in Section 2.3.1 and 2.3.2 only provide estimations and lack incorporation of some complex phenomena occurring in the heat pipe. Therefore, the most solid way to evaluate a working fluid is a life test. The results of these can also be used to evaluate the validity of the models. Fortunately, such tests have been conducted in many studies. However, for some fluid groups, such as siloxanes, only very limited tests have been carried out. Furthermore, the maximum temperature at which the tests have been conducted, is 748 K (and only for a short time at this temperature). The maximum duration of some tests is beyond necessary, nevertheless the duration of many tests falls short. Such tests can still prove to be of value in case the working fluid failed, or provide material for estimations.

Table B.1 (page 73) contains all the available relevant life test results. In every study the temperature differences between the heat pipe sections were monitored in order to detect the formation of adverse reaction products. In most cases a visual and chemical analysis of the heat pipe contents at the end of the experiment was conducted as well. A working fluid - shell combination was labeled compatible when the heat pipe showed steady operation, i.e. constant temperature differences, and when no significant amounts of reaction products were detected upon visual/chemical analysis. In the case of the organics decomposition model (Section 2.3.1), the definition of the theory predicting success was no more than 0.1% decomposition. The halide compatibility model (Section 2.3.2) predicted succes if the electromotive force difference was lower than zero. In both cases these are rather conservative conditions and not based on a correlation between the amount of decomposition and heat pipe failure. Such a correlation would relate the models to an amount of non-condensable gas formed, which could yield the reduction of condenser surface and thus the temperature difference in the condenser.

Often the theory corresponds to the results, yet in some critical situations, failure was not predicted. For organic fluids, this could be due to unaccounted influence of the shell material acting as a catalyst for the decomposition reaction. For example, biphenyl was stable in combination with stainless steel at 623 K, however unstable in combination with mild steel at 598 K for a shorter duration. Similar catalytic effects seem to occur for the o-terphenyl - aluminium combination as well as for naphthalene - copper nickel alloy. A catalytic effect of nickel on benzene pyrolysis has been observed before. In the same study it was reported that stainless steel had no effect on polyphenyls [18]. Generally, stainless steel appears to provide the most stable shell material in combination with organic fluids.

Another conclusion that can be drawn from the data in Table B.1 is the disqualification of o-terphenyl. Based on the vapor pressures, o-terphenyl could be applied up to approximately 700 K, yet it will not last 5520 hours at 598 K. At the temperatures where it is applicable, biphenyl provides a better alternative. The m-terphenyl isomer could perform better than o-terphenyl based on stability predictions but no standalone life tests are available and the tests with terphenyl isomer mixtures do not provide a decisive

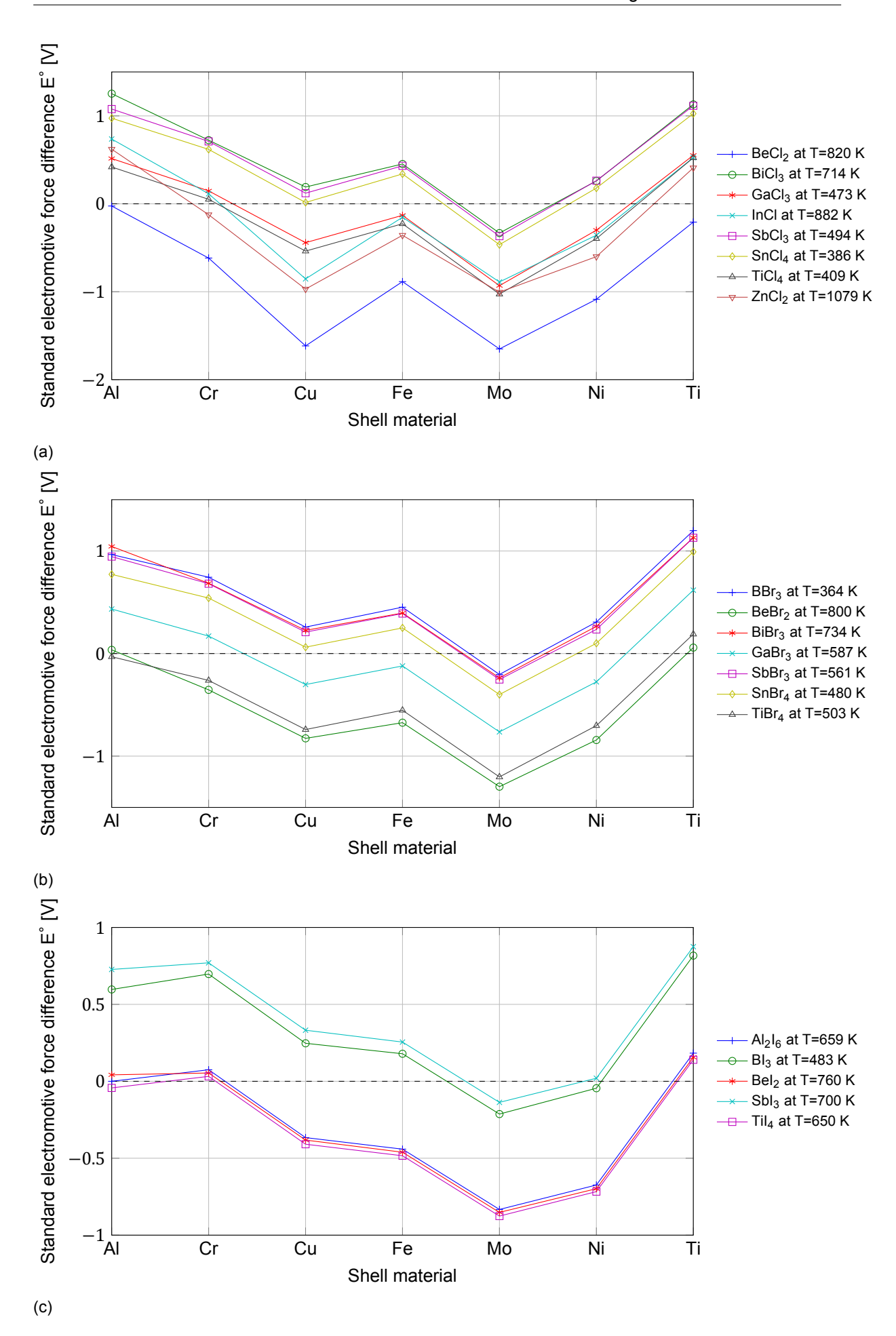


Figure 2.6: The standard electromotive force difference for combinations of liquid halides and materials frequently found in shells. The values are calculated for pressures of 0.1 MPa, because this was the only data available [29, 30]. The corresponding temperatures are displayed in the legend. (a) contains the chlorides, (b) the bromides and (c) the iodides.

answer.

Naphthalene is stable throughout its temperature range for long durations and the life tests agree well to the theory. Based on Figure 2.4(c) it is among the most stable aromatics together with toluene and phenanthrene. The latter is applicable up to approximately 710 K and is supposedly stable according to the model, but no life tests have been conducted.

The siloxane life test have very little value due to the unavailability of the tested fluids' exact composition. In the respective study, it is only disclosed that they consist of either cyclic or linear polydimethyl-siloxanes and that upon postmortem analysis the fluids were converted into jelly-like substances [26].

Like the organics, the halide life tests agree with the theory in most cases. Disagreements only occur when a life test was successful and the theory predicted failure. This can be attributed to the conservative electromotive force calculations where the formation of products with the highest decomposition potential is assumed, and to the 0 V stability threshold. In practice the region just above 0 V is a gray area and a reaction with an electromotive force difference of e.g. 0.1 V is not necessarily significantly unstable [58]. Another limitation of the halide model is the absence of time dependency, meaning that the effect of duration cannot be analyzed with the theory.

The titanium(IV) chloride - nickel chromium life test was successful at the highest temperature, i.e. 573 K, for the halides. This fluid is limited to approximately 485 K by its vapor pressure however. Unfortunately, the halides that are able to cover the higher temperature ranges where organics are inapplicable have not been subjected to life tests.

At such high temperatures, only elements have been tested. With the exception of sulfur, all were stable. Sodium remains stable for a remarkably long time at high temperature. Typically, the stability of alkali metal - shell combinations are interrelated, therefore the life tests with sodium are also a good indicator for the stability of cesium and potassium [20]. Moreover, alkali heat pipes have been in commercial service for many years and steady operation has been confirmed [20, 52].

2.4. Safety and environment

In terms of safety and environment the policies of both Tata Steel and the P&E laboratory need to be taken into account. Although the setup designed in this thesis is only to be placed at the TU Delft, it is wise to comply with the Tata Steel restrictions as well in order to enable application of the same materials. Already, two major design restrictions based on safety were the vapor pressure limit of 0.5 MPa and the exclusion of mercury as a working fluid due to its toxicity.

The Dutch government has published a list with chemicals classified as carcinogenic, mutagenic or reprotoxic (CMR). Tata Steel IJmuiden regulations state that chemicals on this list or chemicals classified as CMR according to REACH 1907/2006 regulations cannot be introduced in new technologies on the company site. This excludes naphthalene and any beryllium compounds as working fluids.

Alkali metals react violently with air and water, and any potential leak of the heat pipe will result in a dangerous situation. For this reason, heat pipes containing alkali metals are best tested and operated under an inert atmosphere. As such an environment is not readily available for the setup at the P&E laboratory, their application as a heat pipe fluid cannot take place here. The continuous annealing line at Tata Steel runs under an inert atmosphere of about 95% nitrogen and 5% hydrogen. Therefore alkali metals can be used for the final application.

2.5. Availability

An inquiry has been executed into the availability of the materials that are most likely to be selected, based on the information in this chapter. Siloxanes are only available as working fluids in mixtures (Syltherm 800) because, as a pure compound, they will isomerize at high temperatures. Unfortunately, such mixtures are non-eutectic and hence evaporation does not take place at a constant temperature, which is undesirable for a heat pipe fluid.

It is suspected that biphenyl is mixed with diphenyloxide for the same reason, i.e. prevention of further isomerization. This mixture is in fact commercially available at eutectic composition, and has been applied as a heat pipe fluid. It is sold per liter as Dowtherm A by Dow Chemical Company or as Therminol VP1 by Eastman Chemical Company.

Pure materials, such as phenanthrene, often become much more expensive when high purity is demanded. Since this is critical for a heat pipe fluid, purification could be done at the P&E laboratory itself.

Cesium is available but at high costs due to its scarcity.

2.6. Conclusion

When all the different aspects described in this chapter are taken into account, a selection of fluids can be made that covers the entire temperature region. Besides the application range, the criteria that weigh the most are stability (test results in particular) and safety.

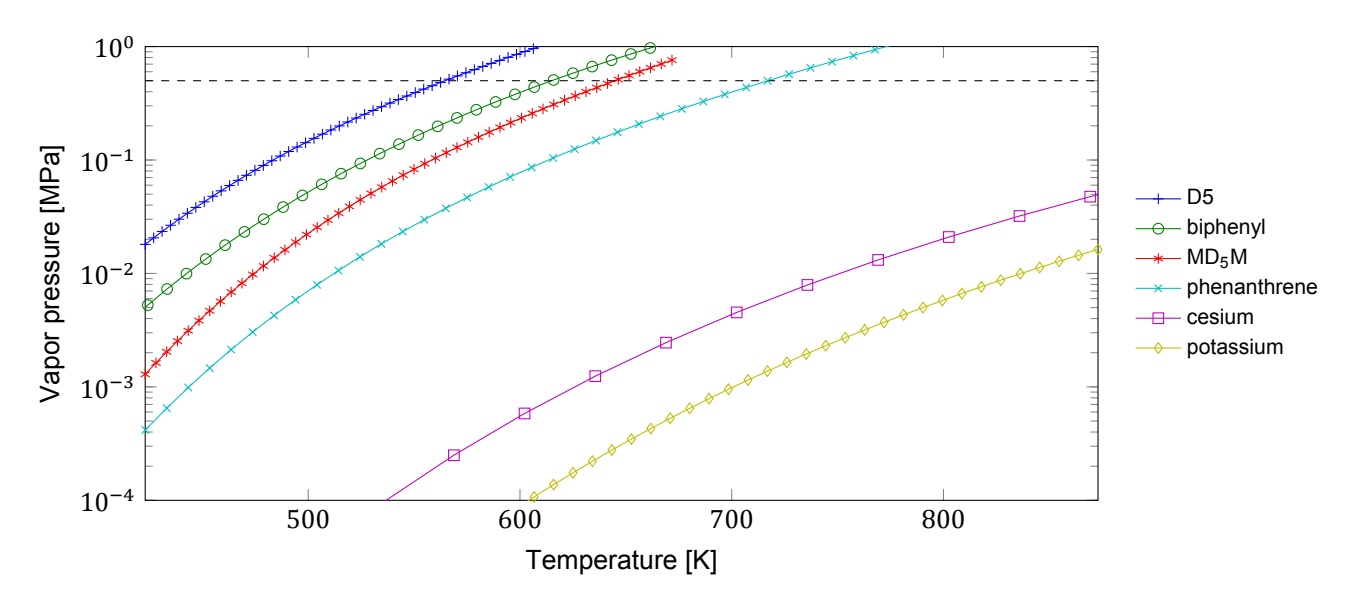


Figure 2.7: The final selection of fluids. Biphenyl, phenanthrene and a siloxane (D_5,MD_5M) can be used in the TU Delft setup. Whereas in the heat pipe assisted continuous annealing line, cesium or another alkali metal like potassium, can be used as well.

Figure 2.7 shows how the full temperature domain is covered with the selected fluids. Biphenyl (or its eutectic mixture with diphenyloxide) can be used up to 607 K. Above this point, there is a serious shortage of potential working fluids; no organics have been tested here for long durations and the applicable halides are either too reactive (bismuth) or unsafe (beryllium). Alkali metals can be used, but only at very low pressures. Although this is done in practice, it is preferred to have an intermediate fluid until the pressures becomes more acceptable. Phenanthrene could provide a solution; the theory suggests it is stable up to its upper limit of 717 K and although it has not been tested, the very similar naphthalene has shown good stability in practice. The latter is not applicable due to the safety criterion but phenanthrene is indeed applicable. It is therefore decided that phenanthrene shall be tested in the TU Delft heat pipe setup.

The alkali metals can cover the upper temperature region. In terms of pressure, cesium is the best option, but since it is a rare metal it might be difficult to obtain enough material for a full annealing line at a reasonable price. If such is the case, the far more abundant potassium or even sodium could be applied. Because of safety, no alkali metals will be used at the TU Delft.

Figure 2.7 also contains two siloxanes, D_5 and MD_5M . Siloxanes are promising as stable heat transfer fluids but no life test results are available. They are among the final selection for the purpose of testing. These tests will not necessarily be conducted with these specific siloxanes and they are primarily in the diagram to illustrate their presence as a group in the final selection.

Finally, it has to be noted that fluids rejected due to stability issues could still be applied in combination with an inert coating (e.g. bismuth halides).

Design Calculations

Now that the working fluids have been specified, the design can proceed with calculation of important figures, concerning dimensions, rotational velocities, heat flows and loads. In the process, some preliminary design choices are made. All this is presented in this chapter accompanied by the backing theory.

One of the design objectives is to create a setup where the operating conditions are the same as in the continuous annealing line. Therefore these conditions, being the basis of the calculations, will be discussed in this chapter as well. In many of the calculations, a reference is made to the properties of biphenyl. How these were obtained is explained in Appendix A. Since the calculations are made in respect of design, they are not primarily aimed at obtaining the most precise values, but rather on determining safe specifications.

3.1. Detailed specifications and requirements

A number of specifications and requirements were already presented in the previous chapters. For convenience, they are again discussed here with more details relevant for the design calculations. Furthermore, the heat pipe materials selection process, described in the previous chapter, has lead to some new insights resulting in an additional requirement. Because the purity of the working fluid is so critical, it is decided to create a separate heat pipe for each medium. This means that the setup now needs to support modularity as well —it should be possible that a heat pipe can be replaced so that multiple types can be tested.

Biphenyl (or Dowtherm A) is the primary fluid that the design calculations will be carried out for. The heat pipe should be suited for phenanthrene and a (possibly eutectic) siloxane mixture as well. Unfortunately not enough of their properties are available to be involved in all the calculations, but the maximum allowable temperature is based on the operating range of phenanthrene. The temperature of phenanthrene corresponding to 0.5 MPa is 717 K, therefore the maximum design temperature, with an addition on account of conservative design, is 773 K. Note that the temperature range has decreased compared to the values presented in the introduction. The working fluids study has revealed that achieving 873 K is not reconcilable with health and safety requirements. Furthermore, the material of the heat pipe shell is 316 stainless steel.

The only sizing restriction stated so far has been that the setup should fit a tabletop. Practically, this translates into a heat pipe length of 0.5 to 1.0 m. In the dimensioning process, the length of the heat pipe will be fixed and the diameter is adjusted accordingly so that other criteria can be met. Table 3.1 contains an overview of the specifications relevant for this chapter so far.

Table 3.1: An overview of specifications relevant for design calculations. The minimum pressure is the approximate vapor pressure of biphenyl at 293 K.

Working fluid(s)	Shell material	Max. temperature	Max. pressure	Min. pressure	Heat pipe length
biphenyl, phenanthrene	316 SS	773 K	0.5 MPa	2.4 Pa	0.5 - 1.0 m

Table 3.2: The specifications of the Port Talbot CAPL installation [43].

	Strip			Temperature [K]			
	thickness [mm]	width [m]	length [m]	entry	exit	Speed [m s ⁻¹]	
Port Talbot CAPL	1.15	1.437	500	293	1016	3.65	

3.1.1. Specifications of an annealing line

An important reference in this chapter, especially for the calculation of the heat load, is an existing continuous annealing line. The heat pipe assisted continuous annealing line needs to be competitive with conventional, gas-fired, continuous annealing lines. Therefore the specifications need to be similar.

The heat and mass transfer phenomena that are to be studied with the high temperature setup should occur in the same physical regimes as present in a heat pipe of the annealing line. E.g., Reynolds numbers should be similar. How this works out will become more clear as the design calculations are carried out. For now it is important to look at the specifications of an existing continuous annealing line. As a reference Tata Steel's Port Talbot CAPL installation is taken. This installation has also been referred to for the design of the Tata Steel test rig and the known specifications are listed in Table 3.2 [43].

3.2. Dimensioning

3.2.1. Flow regime based

The initial approach for choosing an inner diameter for the heat pipe has been the application of a dimensional analysis to approach similarity between the conditions in a heat pipe of the annealing line and the heat pipe in the test setup. An important dimensionless number, which gives an indication of the flow regime in the evaporator and the condenser, is the radial Reynolds number of the vapor flow Re_{rad}. In these sections it is used because it describes the flow from the heat transfer surface to the center whereas the axial Reynolds number represents the flow in the adiabatic section [51]. The two dimensionless numbers can be related in case of a uniform evaporation rate. The radial Reynolds number is defined as

$$Re_{rad} = \frac{\rho_{v} v_{rad} r_{v}}{\mu_{v}}$$
 (3.1)

where $\rho_{\rm v}$ is the vapor density, $v_{\rm rad}$ the average radial velocity of the vapor at the liquid-vapor interface, $r_{\rm v}$ is the vapor space radius and $\mu_{\rm v}$ is the vapor viscosity. Re_{rad} can alternatively be expressed in terms of the radial heat flux $q_{\rm rad}$ with the following equations:

$$q_{\rm rad} = \frac{Q_{\rm in}}{A_{\rm evp}} \tag{3.2}$$

$$Q_{\rm in} = \dot{m}_{\rm v} L \tag{3.3}$$

$$\dot{m} = \rho_{\rm v} v_{\rm rad} A_{\rm evp} L \tag{3.4}$$

where Q_{in} is the heat flow entering the evaporator, A_{evp} is the area of the evaporator and \dot{m} is the mass flow. Rearranging eqs. (3.1) to (3.4) gives

$$Re_{rad} = \frac{q_{rad}r_{v}}{L\mu_{v}}$$
 (3.5)

This expression shows that $q_{\rm rad}$ and $r_{\rm v}$ are the only fluid independent variables for Re_{rad}. The heat flux cannot be increased however, for it is desired that it resembles the heat flux from strip to heat pipe in the continuous annealing line (Section 3.4). For obvious reasons, the working fluid cannot be changed either. Thus it is not possible to achieve similar values of Re_{rad} for the small-scale setup.

3.2.2. Annealing heat pipe geometry based

A typical rotating heat pipe in an experimental setup, or in most other applications, has a rather large length over diameter ratio (typically l/d > 10). For it increases the detectability of non-condensable gases by leading to a relatively larger heat transfer surface compared to the volume. The length and

3.2. Dimensioning 23

diameter of a heat pipe in the continuous annealing line are both dictated by other factors. The length depends on the width of the steel strips —it should accommodate two strips and leave room for an adiabatic section— as well as on the overall geometry of the continuous annealing line. The minimum diameter should correspond to the bending radius of the steel strip for which no plastic deformation (or coil-set) occurs. Altogether this results in an exceptionally small l/d ratio. The vapor flow behavior inside a rotating heat pipe of the continuous annealing line might deviate considerably due to the the relatively large vapor space. For example, back flow can occur close to the center (i.e. the rotational axis). To capture such phenomena, the heat pipe in the experimental setup should have a l/d ratio similar to that of an annealing heat pipe. As the length is restricted to 0.5 to 1.0 m, keeping the ratio constant can lead to a final value of the diameter and thus the dimensions can be fixed.

Unfortunately, no fixed value of the annealing heat pipes' l/d ratio is provided yet. A diameter can be calculated based on the yield stress and the strip thickness. E.g., coil-set calculations indicate the diameter is 2100 times the strip thickness [45]. A length can be estimated based on the strip width. However, no definitive values have been decided on by Tata Steel and will only be established after a dynamic model of the whole concept is finalized. Altogether this approach would be build upon uncertainties. Additionally, taking a relatively large diameter results in the necessity of large capacity heaters, as a consequence of fixed heat flux (Section 3.4.2).

3.2.3. Literature based

The third —and used— approach involves l/d ratios from experimental rotating heat pipe setups in literature. If the dimensions are chosen accordingly, this would enable comparison with data, models and observations from the corresponding literature. This way, a good understanding of the rotating heat pipe can be formulated that can be extended to unconventional geometries such as the ones encountered in the continuous annealing line.

A number of relevant studies that offer useful information have been identified. In Table 3.3 an overview is given. Unfortunately, no studies treating rotating biphenyl heat pipes have been found. The l/d ratios vary from 5.3 to 21.1. Based on these numbers, a value of l/d=10 is taken for the TU Delft test rig.

Table 3.3: An overview of studies consulted for the selection of a l/d ratio.	The ratio is calculated for the diameter of the
evaporator. Cond. stands for condenser section.	

	Daniels	Daniels	Ponnappan	Lee et	Song et al. [55],	Song et al. [55],
	et al. [16]	et al. [17]	et al. [50]	al. [37]	[56] non-tapered	[56] tapered
$\begin{array}{c} l \; [\text{mm}] \\ d_{\text{i}} \; [\text{mm}] \\ \text{taper} \\ l/d \\ T \; [\text{K}] \\ \omega \; [\text{rpm}] \\ Q_{\text{in}} \; [\text{kW}] \\ \text{Shell} \\ \text{Fluid} \end{array}$	325 55 - 30 whole (2°) 5.9 - <2000 2 copper water Arcton 113 Arcton 21	405 76 - 37 cond. (3°) 5.3 273 - 328 600 - 1000 0.8 - 1.4 copper Arcton 113	249 19.1 - 14.6 cond. (1°) 13.0 273 -523(-423) <30 000 0.25 - 1.3 316 SS water methanol	360 25.5 none 14.1 - 300 - 1650 0.4 copper water	400 19.0 none 21.1 293 - 363 2000 - 4000 0.2 - 0.7 copper water	400 19.8 cond. (2°) 20.2 293 - 363 2000 - 4000 0.2 - 0.7 copper water

For reasons concerning the heating power, it is preferred to keep the heat pipe small. Therefore the heat pipe length is fixed at 500 mm and consequently the inner diameter is 50 mm.

3.2.4. Outer diameter

The outer diameter, and with it the thickness of the shell, depends on a compromise between strength and space to accommodate sensors. The trade dimensions of standard 316 stainless steel pipes indicate that the general thickness for pipes of $d_{\rm i}=50\,{\rm mm}$ lies around 1 to 2 mm. Such a thickness is too little to accommodate the heat flux sensors in the shell. Fortunately there are thick-walled (5 mm) pipes available and for now, it is assumed that these will provide enough space. Therefore further design calculations are carried out for an outer diameter of 60 mm.

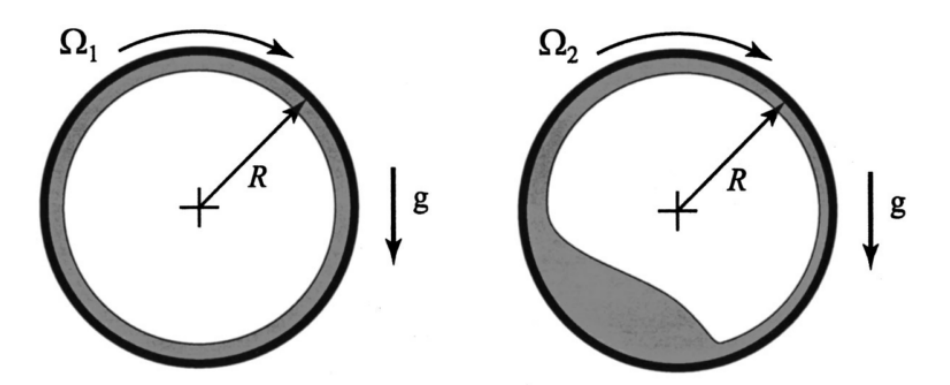


Figure 3.1: A schematic representation of annular flow on the left and rimming flow on the right. From: Baker et al. [9].

3.2.5. Division into sections

To define the sizes of an evaporative, adiabatic and condenser section, the heat pipe is simply split into three equal parts. By doing so, the radial heat fluxes in the evaporator and condenser are equal, as long as the heating and cooling loads are as well, as would be approximately the case when heat transfer is brought about by the steel strips. Yet it has to be noted that in a dynamic situation, the width of the steel strips at the evaporator and condenser section can differ. The consequential heat flows can be simulated by varying the heating and cooling loads during operation, although the heat fluxes would not be equal due to the fixed section geometry.

Depending on restrictions of the heating and cooling equipment dimensions, the actual size of the three sections can slightly deviate from the specified values (Chapter 4). To enable further design calculations, each section's length is assumed to be one third of the total heat pipe length (500 mm).

3.3. Rotation

The velocity of the rotating heat pipe, being the driver of liquid flow to the evaporator, has a significant effect on its performance. Nevertheless, in the continuous annealing line the rotational velocity is imposed by the line speed and cannot be varied for optimal heat transfer without affecting other process parameters. This is no critical issue since the heat pipe is able to transfer sufficient heat, even when operating below its optimum. Besides the performance, the rotational velocity, in combination with the amount of working fluid and the pipe diameter, affects the flow pattern of liquid inside the heat pipe [9]. A number of distinguished flow regimes exist and can therefore occur in the rotating heat pipes of the continuous annealing line, depending on the specific heat pipe characteristics. It is important that the heat pipe in the test setup can operate within these same regions. Since the exact specifications of the various heat pipes in the final system have not yet been established, neither are the present flow regimes. For this reason it is decided that the test heat pipe should be capable of covering all the possible flow regimes.

Given a certain working fluid, the liquid layer is nonuniform in the radial direction up to a certain critical velocity, which is characterized as rimming flow. Its thickness profile depends on interaction of wall shear stress, centrifugal force and gravity [9]. If there is an adequate amount of fluid present —a parameter that is described by the fill factor— even a pool can form at the bottom of the heat pipe. Above the critical velocity, the profile has transitioned to uniformity and the flow is annular. In Figure 3.1 a schematic cross-section is shown of both flow types. Baker et al. [9] conducted experiments with a transparent acrylic cylinder capable of rotating at sufficiently high velocities to determine the Froude number corresponding to the critical velocity. Water was used as fluid and the authors state, based on previous research, that properties such as viscosity and surface tension are not critical as the Froude number is the appropriate dimensionless parameter. This gives reason to use this study for biphenyl heat pipes as well. Although the research was carried out in the context of rotating heat pipes, no heat or cooling was applied to the cylinder. Based on the experimental observations within the region 5 < Fr < 180, a correlation for the critical Froude number for complete annular flow was derived

$$Fr_c = 20.03 (1 - \phi)^{-2.421}$$
 (3.6)

3.4. Heat fluxes 25

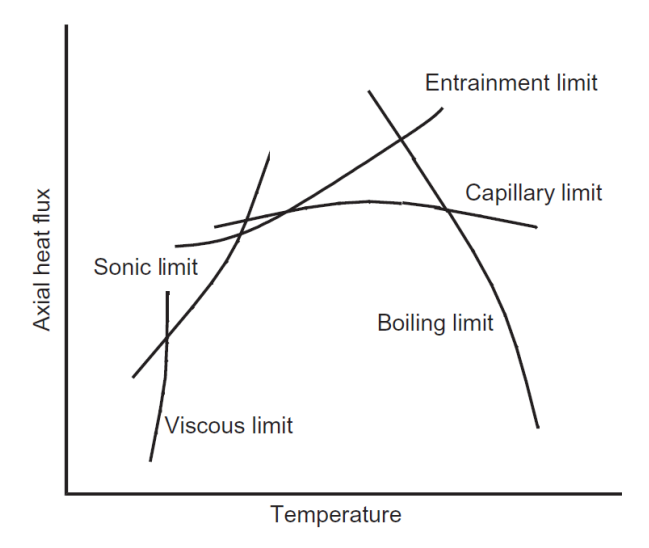


Figure 3.2: The heat transfer limits in a wicked heat pipe. Most of these also apply to rotating heat pipes, except for the capillay limit. From: Reay et al. [51].

where ϕ is the fill factor, i.e. ratio between the volume of the fluid at room temperature and the volumetric capacity of the heat pipe. Using the definition of the Froude number, the critical rotational velocity can be calculated for a specific geometry

$$\omega_{\rm c} = \sqrt{\frac{{\rm Fr}_{\rm c}g}{\frac{1}{2}d_{\rm i}}} \tag{3.7}$$

For the TU Delft test setup, it is decided to keep the fill factor relatively low, both to limit the quantities of chemicals that the heat pipe is charged with, as well as to restrict the rotational velocity, as these both have an impact on safety. The maximum fill factor the heat pipe is designed for is 0.1, resulting in a maximum charge of 1.15 kg biphenyl.

The critical Froude number for the established fill factor is 25.85 which corresponds to a rotational velocity of $100.72\,\mathrm{rad\,s^{-1}}$ (962 rpm). A small quantity is added on account of conservative design and the maximum rotational velocity of the heat pipe in the test rig is fixed at 1000 rpm.

3.4. Heat fluxes

3.4.1. Operating limits

Several physical phenomena limit the heat transfer in heat pipes, e.g. entrainment, boiling and sonic flow. Correlations to determine these limits are extensively described in literature, although they have been primarily derived for non-rotating, wicked heat pipes. Some are equally valid and relevant for rotating heat pipes as well, others need modification or are simply not applicable. The various limits are of effect in different operating regimes, dependent on the temperature where the phenomenon it relates to occurs and typically they are named after it. Figure 3.2 shows where the limits occur depending on temperature.

The first limit discussed was already mentioned in Section 2.1.1, and arises at lower temperatures when the flow is dominated by viscous forces. Hence it is called the viscous limit. The correlation is equally applicable to rotating heat pipes and has been theoretically derived by Busse [11], who showed it agrees reasonably well with experimental data. It is given by

$$Q_{\text{viscous}} = A_{\text{v}} \frac{d_{\text{v}}^2 L}{64\mu_{\text{v}} l_{\text{eff}}} \rho_{\text{v}} p_{\text{v}}$$
(3.8)

where $A_{\rm v}$ and $d_{\rm v}$ are the cross sectional area and the diameter of the vapor space respectively and $l_{\rm eff}$ is the effective length over which the vapor transport occurs. The fluid properties in eq. (3.8) refer to conditions in the evaporator. The effective length is calculated as follows

$$l_{\text{eff}} = \frac{l_{\text{evp}}}{2} + l_{\text{adi}} + \frac{l_{\text{con}}}{2} \tag{3.9}$$

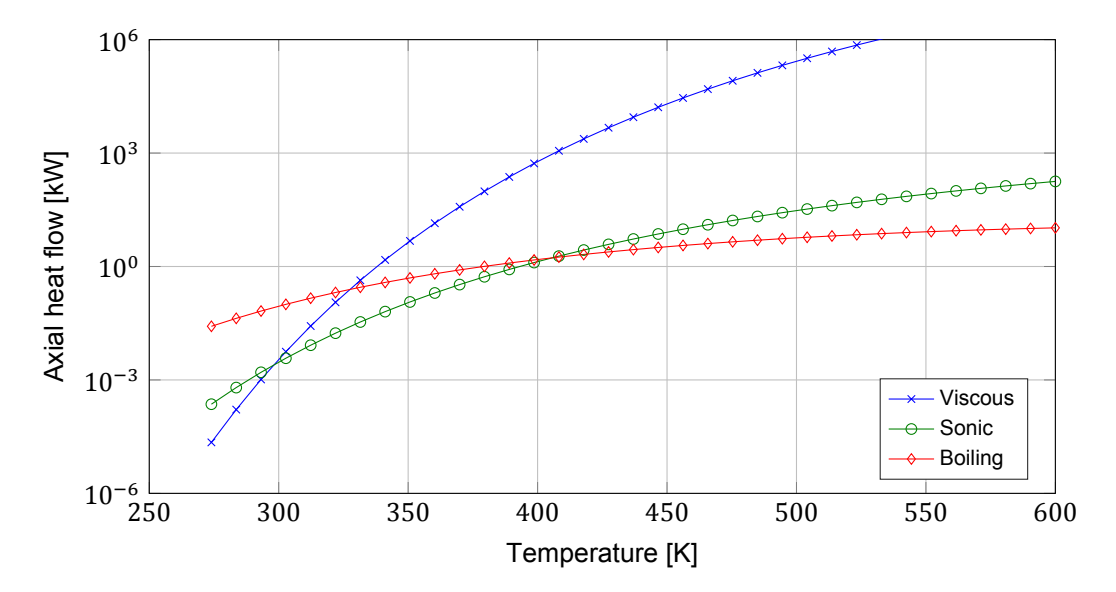


Figure 3.3: The heat transfer limits in a biphenyl filled rotating heat pipe with l = 500 mm and $d_i = 50$ mm.

where l_{evp} , l_{adi} and l_{con} are the lengths of the evaporator, adiabatic section and condenser respectively.

Like the viscous limit, the sonic limit arises at relatively low temperatures. It typically occurs during heat pipe startup. The vapor velocity increases along the evaporator and reaches a maximum at the exit, where the flow can become choked; leading to pressure shock waves and high mechanical loads. Busse [11] theoretically derived the following equation describing the heat transfer rate corresponding to the sonic flow

$$Q_{\text{sonic}} = 0.474 A_{\text{v}} L \sqrt{\rho_{\text{v}} p_{\text{v}}} \tag{3.10}$$

The entrainment limit involves limited flow-back of liquid to the evaporator due to shear forces at the interface caused by high velocity counter-directional vapor flow. As a consequence, the evaporator dries out and burn-out can occur. The relations describing this phenomenon are mostly derived for the condensate flowing in wicks or for thermosyphons and therefore not applicable to rotating heat pipes. Tien and Chung [60] developed correlations for various types of heat pipe, including a rotating one, but it is relying on the presence of a taper. Alternatively, a relation for thermosyphons could be modified, where gravitational acceleration driving the liquid is replaced by acceleration as a result of rotation. In order for this to work, a thickness profile of the liquid along the heat pipe is required, which is not readily available. Although there are no means to calculate the entrainment limit, it can be predicted that the possibility of it appearing significantly decreases with increasing rotational velocity. Centrifugal forces press the liquid against the inner shell and resist the rupture of droplets out of the layer.

The capillary limit does not apply to rotating heat pipes because they do not contain a wick.

The final limit, i.e. occurring at the highest temperatures is caused by the formation of a vapor film on the inner surface of the evaporator. Such a film significantly increases thermal resistance and inhibits heat transfer. Contrary to the other limits, the boiling limit concerns radial instead of axial heat flow. The axial transport limit can still be defined however, for they are related through evaporator surface area. The boiling limit is given by

$$Q_{\text{boiling}} = 0.14 A_{\text{evp}} \rho_{\text{V}}^{1/2} L \left(\sigma g \left(\rho_{\text{I}} - \rho_{\text{V}} \right) \right)^{1/4}$$
 (3.11)

where A_{evp} is the inner surface of the evaporator, σ is the surface tension of the working fluid and g is the gravitational acceleration.

In Figure 3.3 a plot is shown of the relevant limits that could be calculated, using the properties of biphenyl and the dimensions that were established in Section 3.2. Note that at lower temperatures there is a considerable limit to the heat input, something to keep in mind during startup when the heat pipe is at room temperature. At first sight, the limits provide a maximum value for the heat supplied to the heat pipe. It should be noted however that there is a factor of uncertainty to these values due to the

3.4. Heat fluxes 27

methods used to obtain the properties of biphenyl (see appendix A). Furthermore, there is a preferred method for determining the amount of heat that should be supplied to the heat pipe in the setup, as will become clear in Section 3.4.2.

3.4.2. Heat input

When determining the heat transfer through the heat pipe, once more a value is chosen so that the conditions in the test setup are similar to those in the the continuous annealing line. Table 3.2 provides the data to calculate the heat flux that a heat pipe should be able to supply to the steel strip at the condenser. Additionally, the density and specific heat of the strip are needed. Using the values from Table A.5, an average radial heat flux of 30 kW m⁻² is yielded. Since the evaporator and condenser surface each cover one third of the heat pipe, the total amount of heat supplied and removed is roughly 0.9 kW. In reality, less heat is expelled at the condenser due to heat losses over the length of the heat pipe. A supplementary amount of heat should be added to the evaporator to cover for these. It is assumed that only convection and radiation losses are relevant and that conduction from the outer surface to the surrounding air can be neglected.

When considering the convection losses, it should be kept in mind that under certain operating conditions, the heat pipe is rotating at high velocities. The resulting air flow over the outer surface could significantly improve heat transfer. Anderson and Saunders [1] derived the heat transfer coefficient for convection from a heated horizontal cylinder rotating about its longitudinal axis in air at varying rotational velocity. They found that up to a certain tangential velocity, the heat transfer is very similar to that of a free convection around a cylinder. This critical velocity is approximately equal to the upward free convection velocity of a stationary cylinder. Above it, the heat transfer increases exponentially with the rotational velocity. The Reynolds number that corresponds to this critical velocity (for air) is expressed in terms of the Grashof number and the Prandtl number

$$Re_{d,c} = 0.93 \sqrt{\frac{Gr_d}{Pr}}$$
 (3.12)

To determine whether the critical velocity is exceeded, the Reynolds number at the cylinder surface can be calculated with

$$Re_d = \frac{\rho v_s d_o}{\mu} \tag{3.13}$$

where $v_{\rm s}$ is the tangential velocity at the cylinder surface. The Grashof number is defined as

$$Gr_d = \frac{g\beta (T_S - T_{\infty}) d_0^3}{v^2}$$
 (3.14)

where β is the thermal expansion coefficient of air, $T_{\rm s}$ is the temperature of the cylinder's surface, T_{∞} is the temperature of the surrounding air (293 K) and ν is the kinematic viscosity of the air. β and ν are taken at the mean film temperature, i.e. $T = (T_{\rm s} + T_{\infty})/2$. The Prandtl number in Equation (3.12) is defined as

$$Pr = \frac{c_p \mu}{\lambda} \tag{3.15}$$

where c_p is the specific heat of air.

At Reynolds numbers exceeding the critical value (eq. (3.12)), the following equation for the Nusselt number is valid

$$Nu_d = 0.10 Re_d^{2/3} (3.16)$$

Subsequently the heat transfer coefficient for unforced convection from a rotating cylinder is given by

$$h_{d,\text{conv}} = \frac{\text{Nu}_d \lambda}{d_0} \tag{3.17}$$

The experiments conducted by Anderson and Saunders [1] have been reproduced in various other studies and in all of them, a very similar correlation was derived [22]. Finally, the heat loss as a result of convection can be calculated with

$$Q_{\text{conv}} = h_{d \text{ conv}} A \left(T_{\text{S}} - T_{\infty} \right) \tag{3.18}$$

where *A* is the surface area over which the loss takes place.

In the calculation of supplementary heating requirements, the heat losses are determined at the conditions where they are maximal; for the convective losses this means at the highest rotational velocity of 1000 rpm. In Figure 3.4 it can be seen that the Reynolds number is above the critical value over the entire temperature range and thus eq. (3.16) is valid.

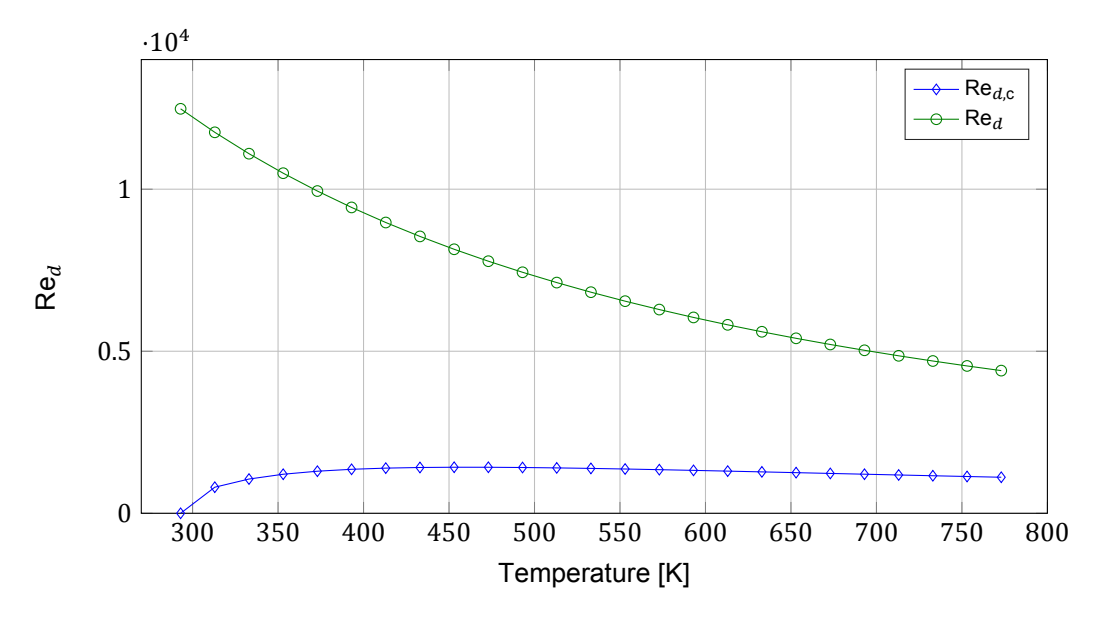


Figure 3.4: The critical Reynolds number for convective heat loss and the Reynolds number at $\omega = 1000$ rpm.

For the calculation of the radiative losses, only the following equation is needed

$$Q_{\mathsf{rad}} = \epsilon \sigma_{\mathsf{SB}} A \left(T_{\mathsf{S}}^4 - T_{\mathsf{\infty}}^4 \right) \tag{3.19}$$

where ϵ is the emissivity coefficient (Table A.5) and σ_{SB} is the Stefan-Boltzmann constant. Since the condenser is actively cooled, the losses only need to be accounted for over the surface of the evaporator and the adiabatic section. Thus the surface term in eqs. (3.18) to (3.19) is

$$A = \pi d_{\rm o} \left(l_{\rm evp} + l_{\rm adi} \right) \tag{3.20}$$

In Figure 3.5, all the relevant heat flows are plotted over the entire temperature range, including the startup from room temperature. The temperatures on the horizontal axis are in fact not the operating temperature but that of the outer surface. In reality there will be a gradient over the heat pipe shell; at the evaporator the surface temperature is higher, yet at the adiabatic section it is expected to be somewhat lower.

The sum of the heat flows indicates how much heat should be supplied to the evaporator by a heater. At a temperature of 773 K this is 2.27 kW. The radial heat flux at the evaporator is $86.6 \, \text{kW m}^{-2}$ and the axial heat flux is $1.15 \, \text{MW m}^{-2}$.

At temperatures below approximately 390 K, the heat flow supplied by the heater exceeds the acting limit (sonic), as can be seen in Figure 3.5. As a consequence, in this region the heat flow required for simulation of heat transfer from and to the steel strips cannot be achieved. However, one should note that this occurs outside of the working range of biphenyl, i.e. only during the startup from room temperature. A rotating heat pipe containing water should in fact be able to operate in these lower regions under the described heating conditions. Although it is poorly visible in Figure 3.5, at temperatures close to room temperature the convective heat loss by itself is already larger than the sonic limit. Since losses are for the highest rotational velocities, it is preferred to run the heat pipe at lower values during startup.

3.5. Mechanical and thermal loads

A basic static stress analysis is carried out, to ensure that the heat pipe, at the specified dimensions, can contain the working fluid at its maximum pressure of 0.5 MPa. Furthermore the thermal expansion

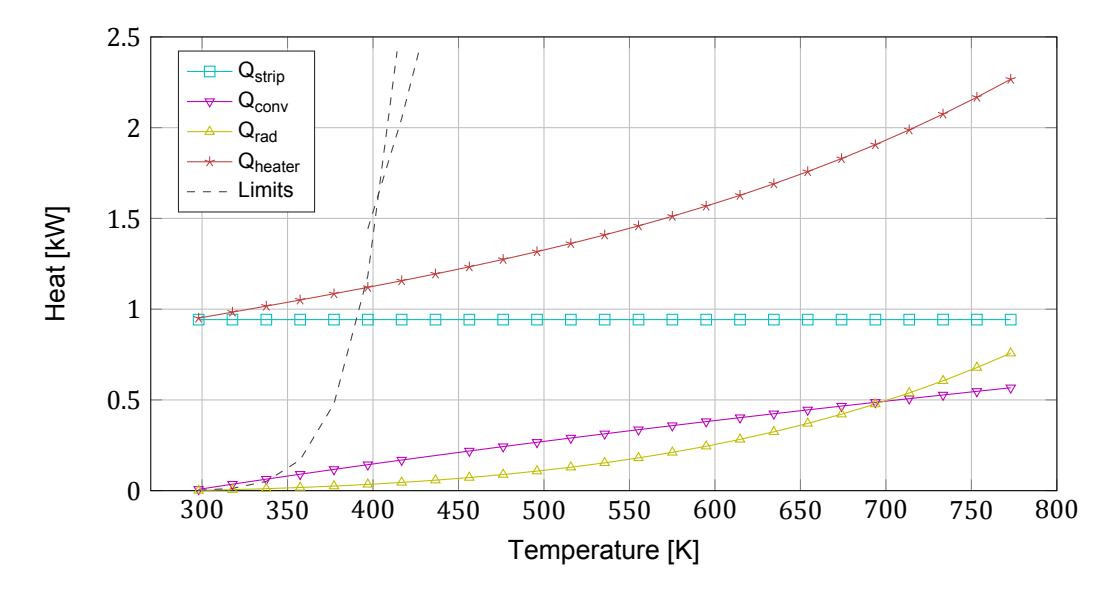


Figure 3.5: The radiative losses, convective losses (at 1000 rpm) losses, heat from the strip and the sum of all these, which should be the heat suplied by the heater. Acting heat transfer limits for biphenyl are also depicted.

needs to be considered, for the heat pipe will have its temperature substantially increased. More advanced calculations are required to cope with the large rotational velocities but these are carried out with regards to the frame that will carry the setup.

3.5.1. Stresses

Geometrically speaking, the heat pipe is a hollow cylinder with its sides covered by circular plates. As it is pressurized, both the tangential, axial and radial stresses need to be considered. The directions in which they act are illustrated in Figure 3.6.

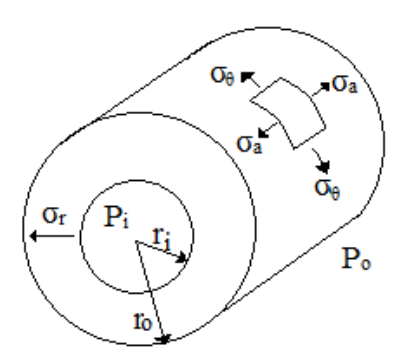


Figure 3.6: The stresses due to a pressure difference over a hollow cylinder shell.

The first also known as the hoop stress. For a thick-walled vessel, the radius being less than 10 times the thickness, the hoop stress is calculated with the following equation

$$\sigma_{\theta} = \frac{p_{i}r_{i}^{2} - p_{0}r_{0}^{2}}{r_{0}^{2} - r_{i}^{2}} - \frac{r_{i}^{2}r_{0}^{2}(p_{0} - p_{i})}{r^{2}(r_{0}^{2} - r_{i}^{2})}$$
(3.21)

where p_i and p_o are the pressure inside and outside the vessel respectively. The point where the stress acts is represented by r. The stress is maximal at a point closest to the center, i.e. at $r = r_i$.

The stress in the radial direction at a point in the (thick) cylinder wall can be expressed as

$$\sigma_{\text{rad}} = \frac{p_{\text{i}}r_{\text{i}}^2 - p_{\text{o}}r_{\text{o}}^2}{r_{\text{o}}^2 - r_{\text{i}}^2} + \frac{r_{\text{i}}^2 r_{\text{o}}^2 (p_{\text{o}} - p_{\text{i}})}{r^2 (r_{\text{o}}^2 - r_{\text{i}}^2)}$$
(3.22)

The radial stress reaches its maximum at a point furthest away from the center, i.e. $r=r_0$. Equations (3.21) and (3.22) are known as Lame's Equations. Finally, the stress in axial (or longitudinal) direction at any point in the (thick) cylinder wall is given by

$$\sigma_{\rm ax} = \frac{p_{\rm i}r_{\rm i}^2 - p_{\rm o}r_{\rm o}^2}{r_{\rm o}^2 - r_{\rm i}^2} \tag{3.23}$$

None of these stresses should come near the maximum tensile stress for 316 stainless steel. When considering this limit, special care should be taken of the high temperatures and the risk of creep that they bring forth. At 773 K the maximum stress for a creep rate of $1\,\%$ over a period of $10\,000\,\text{hours}$ is approximately 200 MPa [7]. Using eqs. (3.21) to (3.22) with a pressure difference of 0.4 MPa, the highest stress (tangential) calculated is $2.12\,\text{MPa}$. With such a low value, $1\,\%$ of creep will not take place over $100\,000\,\text{hours}$ at $773\,\text{K}$ [7].

3.5.2. Thermal expansion

As the shell temperate rises, the heat pipe expands in length as well as in diameter. This process is not exactly linear because the thermal expansion coefficient α , a property of the steel shell, is temperature dependent. The elongation of the shell is given by

$$\Delta l = \alpha l_0 \left(T_1 - T_0 \right) \tag{3.24}$$

The increase in diameter is calculated in a very similar fashion

$$\Delta d = \alpha d_0 \left(T_1 - T_0 \right) \tag{3.25}$$

Employing eqs. (3.24) to (3.25), for a temperature difference of 773-293=480 K, and the mean thermal expansion coefficient (Table A.5) over the temperature range gives an increase of 4.20 mm in length and 0.504 mm in diameter.

4

Equipment and Instrumentation

A selection of equipment is needed to accomplish the specifications that were defined in the previous chapter. Not only should this equipment provide the necessary loads, e.g. in terms of cooling; it should also comply with the specified design restrictions, such as safety. Moreover, to enable the desired observation of heat and mass transfer phenomena, a selection is to be made of measurement instrumentation. This chapter will cover the selection processes by discussing the tradeoffs of each technology and show the calculations that reveal whether a technology is suitable. First, the measurement instrumentation is treated. Later, the heating and cooling are discussed.

It has been decided to use alternative technologies to generate the heat flows. In the test setup located at Tata Steel, the heat is supplied and removed by the steel strips. This drastically complicates the required equipment however, as well as its operation. For instance, the strips needs to be tensioned and heated properly during operation or else its edges start to deform due to thermal expansion [46]. Furthermore, the thin, moving strip is extremely sharp and dangerous, which makes it unsafe to be operated by students. Since the emphasis lies on the internal phenomena, the strips are deemed unnecessary and omitted from the TU Delft setup.

4.1. Measurement techniques

Previously, in the Introduction a list was provided containing all the observations that the TU Delft test rig should enable. The reasons why these observations are relevant were not yet mentioned however. Clearly, it is important to be aware of the exact purposes and therefore the items on the list are now discussed in more depth.

Heat flux To monitor the uniformity and exact amount of heat that is supplied and extracted from the heat pipe, and to be aware of the heat that is lost over the adiabatic section, measurements of the heat flux need to take place at multiple locations in the shell, at least one in every section. This way, an energy balance over the entire system, with the shell as boundary, can be set up. Furthermore, this measurement will indirectly enable the derivation of heat transfer coefficients from the shell to the liquid at both the condenser and evaporator.

Liquid layer thickness Knowing the thickness of the condensate layer is relevant for the creation of a mass balance of the heat pipe's contents. The thickness also has an influence on the heat transfer from the shell, especially at the condenser, since the liquid acts as an insulating layer. Furthermore, the thickness profile can be related to the rotational velocity and heat flows for better comprehension of the driving forces behind the condensate return flow and the overall performance.

Liquid velocity Being aware of the liquid velocity leads to similar insights as for the thickness. It can assist in the formation of a mass balance. Moreover, relating (changes in) velocity to rotation and the heat balance is crucial for understanding how a rotating heat pipe works.

Vapor velocity Again, a velocity is needed for a mass balance of the heat pipe's contents. Thereby, the vapor velocity gives insight about the type of flow inside the heat pipe. This is critical in

understanding the rate of evaporation and condensation, as well as the vapor channel resistance.

Inside temperature profile Monitoring of the temperature at various heat pipe locations provides an overview of heat pipe functioning. The properties of the two phases of working fluid are dependent on the temperature. Moreover, transient temperature development with varying heat flux should be clearly understood. This is important because the final dynamic model of the heat pipe assisted annealing concept should incorporate the transient behavior of all the heat pipes with different working fluids and loads. Additionally, the temperature profile at the condenser would enable the detection and quantification of non-condensable gases inside the heat pipe. Finally, the temperatures are also required for the derivation of heat transfer coefficients.

Pressure profile Overseeing of the internal pressure is necessary to avoid the crossing of safety boundaries. Just like the case with temperature, the pressure profile provides an overview of the heat pipe's functioning. The pressure drop can directly be determined from the profile giving valuable information about the performance. The formation of non-condensable gases is also detected by monitoring the pressure profile.

Shell temperature profile For feedback to the heating and cooling equipment, it is important to monitor the temperature of the shell. In combination with the inside temperature profile, it is critical for the determination of the heat transfer coefficients. Finally, a shell temperature profile enables quantification of axial conduction through the heat pipe shell.

Rotational velocity This quantity influences the return of the condensate to the evaporator. It is therefore required to know it for the overall understanding of the rotating heat pipe's functioning.

The working fluid study in Chapter 2 has revealed that the heat pipe's performance can become unstable over time due to reactions of the working fluid. The possibility of this occurring is reduced as much as possible through design but the risk is never fully eliminated and therefore an extra observation inside the heat pipe is necessary. The stability of the working fluid and the formation of adverse reaction products should be monitored.

4.1.1. Reduction of measurements

Some of the listed items are related in a way that the measurements of one, will indirectly enable the measurement or derivation of the other, provided relevant theory is applied. Therefore not all these observations require a separate measurement and the list can be reduced to only a number of essential measurements.

A measurement of heat flux through the shell can be conducted by placing two temperature sensors at radially varying locations. If the thermal conductivity of the shell material and the exact locations are known, the heat flux is directly calculated from the temperature difference. The same temperature sensors can also serve to measure the temperature profile in the shell, thus eliminating the need for two measurements.

Since the heat pipe is a closed system, the mass is conserved and the size of the vapor stream is coupled to the size of the liquid stream. Besides that, the average velocity of the vapor stream can be derived from the evaporation rate (with eq. (3.3)) and the radius of the vapor space. The latter is dependent on the liquid layer thickness. Accordingly, measurement of the flow velocities of both streams would be redundant. Furthermore, models exist that relate the liquid velocity to the layer thickness [10]. Hence, a measurement of the thickness of the liquid layer at multiple axial locations can cover the liquid and vapor velocity as well.

If the heat pipe solely contains the working fluid —which should be the case— the vapor pressure is directly related to the temperature, as was used in Chapter 2 to determine a fluid's operating range. This means that separate measurements for both temperature and pressure is unnecessary. A measurement of the inside temperature at multiple axial locations will provide both the desired temperature and pressure profiles. The formation of non-condensable gases and thus the lifetime of the fluid can be monitored via the stability of pressure gradients between various locations in the condenser. Placing multiple temperature sensors in the vapor space of the condenser will enable such a measurement and is a proven method [3].

The rotational velocity of the heat pipe is likely to be controlled via the rotating drive and does not require an independent measurement if the right drive controller is selected.

Altogether, the list of independent measurements has been reduced to the following items:

- Temperature measurements in the shell, at two radial locations and at multiple axial locations, at least one in every section.
- · Liquid layer thickness measurement.
- Temperature of the vapor in the heat pipe, at various axial locations, at least one in the evaporator and adiabatic section and multiple in the condenser.

4.1.2. Instrumentation

Thermocouples provide a good means to conduct temperature measurements and are the most common type of sensors used in heat pipe testing [51]. The type K (chromel-alumel) is affordable and maintains its accuracy within the entire temperature range of the setup. The tip, which performs the measurement, can be shielded so that any contact with the working fluid that might result in adverse reactions is avoided. Besides, it can be kept small enough (<0.5 mm) to be accommodated inside the heat pipe shell and vapor space.

The heat flux sensor consists of two thermocouples closely placed in the shell. An estimation of the required precision of these thermocouples can be made by using Fourier's law

$$q = -\lambda \frac{\mathrm{d}T}{\mathrm{d}r} \tag{4.1}$$

The required precision is evaluated at only $5\,\mathrm{kW\,m^{-2}}$ because it is most critical at low heat fluxes. The spacing between the thermocouples is 3 mm, so that they will fit in the shell close to the inner and outer surface. The thermal conductivity of the 316 stainless steel shell is taken at room temperature, where it is the lowest (Table A.5). Altogether this conservative estimation yields a temperature difference of 1.13 K, which is very small and indicates that extra care and advice from suppliers is needed for the selection of these sensors.

The measurement of the liquid layer thickness is more problematic than the temperature. Commonly applied methods such as capacitive and conductive measurements rely on electromagnetic properties of the liquid. To facilitate these measurements an extra criterion to the liquid selection should be asserted. However, in this case the selection process has left little options and there are no alternative fluids available that comply with the fluid selection criteria and possess properties suitable in terms of electrical conductivity or differences between the dielectric constant of the liquid and gas phase. Alternatively, property enhancing additives could be added but these require an additional stability assessment.

Remaining methods are either of optical or acoustic nature. The former requires placement of instrumentation inside the heat pipe which is likely to affect the measurements by obstructing the flows. This could be avoided by allowing for visual access from the outside of the heat pipe; which in turn is problematic because it requires a (partially) different shell material —which was already carefully selected. The problem with visual access could be tackled later on, by making use of the planned modularity of the setup. Another heat pipe could be designed, that fits in the setup and has, e.g. transparent side covers.

Acoustic measurements of thickness are generally applied for solids. For liquids this method is less common and it could prove to be difficult to find the appropriate instrumentation commercially available. Yet the technology has been tried in a number of studies with positive results. Acoustic thickness measurements rely on ultrasonic waves that are attenuated and reflected at material or liquid-gas interfaces. An ultrasonic transducer generates sound waves directed through the respective materials. Based on the time it takes a wave to return to the ultrasonic transducer, the distance traveled and thus the thickness of the material layers is calculated. In Figure 4.1 a schematic showing the components of a typical measurement setup is depicted.

Lu et al. [42] measured the thickness of condensing R113 and FC-72 working fluid films down to 300 µm inside a horizontal rectangular duct. The thickness of the copper duct was 6.4 mm. The authors found that the technology works well as long as the film is smooth and lacking large-amplitude interfacial waves. It has to be noted that they used and analog oscilloscope and suspected that a digital one could serve to measure films that do not comply with these restrictions. More recently, Pedersen et al. [48] used the technology to perform measurements with condensing water and methanol and a

downward-facing surface. A 10 mm layer of copper separated the transducer from the film. Measured liquid film thicknesses ranged from 50 to 500 µm. The smallest thickness measured by Chen et al. [13] was 50 µm of ethylene glycol, through a copper block of 15 mm. They successfully measured on various film types; both static and growing non-condensing films, a non-condensing film with surface waves, and stable (upward-facing) and unstable (downward-facing) condensing films. In Figure 4.2 a photograph shows the ultrasonic transducer they used.

An experimental setup where the transducer was not mounted perpendicular to and directly on a flat surface was designed by Kamei and Serizawa [36]. Both the transducer and a rotating reflector were mounted inside a tube so that the thickness of the liquid film on the outside could be measured. The tube was filled with water to consolidate the ultrasound propogation. A 10 mm thick acrylic tube wall separated the instrumentation and the liquid film. By rotating the reflector a detailed map of the thickness around the full circumference of the tube could be created.

The studies described above show that the acoustic technique can successfully be employed for the purpose of measuring film thickness. There will be some specific conditions in the rotating heat pipe setup however, that have not been encountered in the literature. The inner and outer surface of the heat pipe cannot be flattened for proper mounting of the transducers. The forces due to the rotation could also be problematic, yet possibly a silicone sealant similar to the one used by Chen et al. [13] can withstand them. Indirect mounting can only be achieved through a propagation enhancing fluid, as Kamei and Serizawa [36] showed. Furthermore, the studies showed that a calibration of the sensors is absolutely necessary, which is difficult inside a closed heat pipe. Despite these problems, it is decided to employ the technique since it is still the most promising, yet it should be kept in mind that the realization will be challenging.

4.2. Heating

In Section 3.4 it was established that a radial heat flux of $86.6\,\mathrm{kW\,m^{-2}}$ should be provided over the 167 mm long surface of the evaporator, resulting in a total heat input of $2.27\,\mathrm{kW}$. The actual power required for a heater is even larger, due to its inevitable losses. A heating technology should comply with certain requirements. The temperature at which it supplies the heat should at least be higher than $500\,\mathrm{K}$ so that a gradient with the maximum operating temperature can be established. Additionally, a uniform heat supply most accurately resembles the heat input as brought about by a steel strip. Finally, the heater has to be safe enough to be operated by students.

A number of heating methods have been considered but most have been eliminated due to these requirements. A burner's heating profile is not uniform enough and is less safe due to open flames.

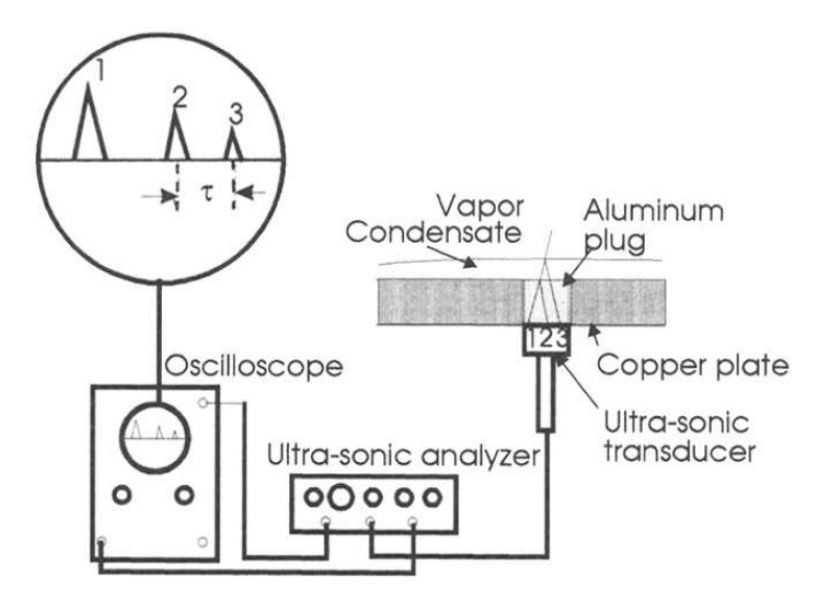


Figure 4.1: A schematic diagram of the test setup used by Lu et al. [42]. The travelling time of the waves is measured with an analog oscilloscope and analyzer. The aluminium plug is used because it was it found that the attenuation was too large through the copper.

4.2. Heating 35



Figure 4.2: The Parametrics Model 5077PR ultrasonic transducer that was used by Chen et al. [13]. The diameter of a unit is 12.7 mm. A silicone sealant fixes the transducers to the copper surface and ensures good acoustic coupling efficiency.

And a radiative heater of the desired scale is unlikely to achieve high enough temperatures. Two remaining concepts have been studied in more detail, to assess their suitability: induction heating and trace heating.

4.2.1. Induction heating

Induction heating is often applied in experimental rotating heat pipe setups [50, 55, 56]. It can rapidly heat a material to high temperatures, depending on the power of its supply unit. More importantly, it can provide contactless heating. An induction heating system consist of a frequency transformer that supplies an alternating current to a coil, which creates an electromagnetic field around it. If a conductive material (the workpiece) is placed correctly near the coil, the electromagnetic field will induce circulating eddy currents inside it, as illustrated in Figure 4.3. This current then dissipates in the workpiece, causing it to heat up. The process is enhanced when the material is ferromagnetic. The magnetic particles in the workpiece will constantly resist alignment with the alternating magnetic field, causing additional 'friction' in the material. The coil of an induction heating system is usually made of copper since its low resistivity leads to little dissipation in the device itself. To maintain it at suitable working temperatures, its tubes are hollow and a cooling water stream runs through it. The shape of the coil can vary depending on the shape of the workpiece. In the Tata Steel setup the steel strip is the workpiece and therefore the coil is flat and rectangular [46]. A round workpiece is usually placed inside a solenoid coil and this configuration can also be applied to a rotating heat pipe.

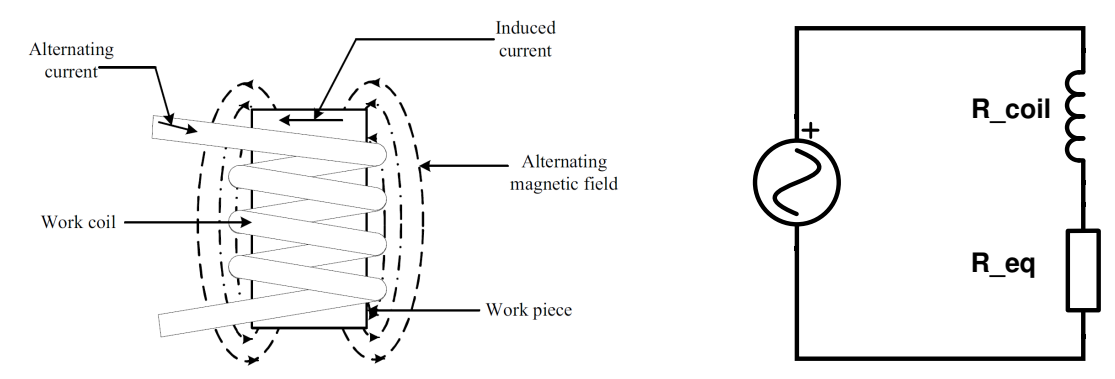


Figure 4.3: A schematic representation of an induction heating coil, workpiece and magnetic field [8].

Figure 4.4: The virtual electrical circuit used to calculate the electrical efficiency of an induction heating system.

An induction heating system has a certain electrical efficiency dependent on the geometry and electromagnetic properties of both the coil and workpiece, and the frequency of the alternating current. This efficiency is needed to calculate the required capacity of the heating system. To define it, an equivalent resistance of the workpiece is formulated, as if it would be part of the electrical circuit containing the power supply and the coil. The equivalent resistance of the workpiece is placed in series with the resistance of the coil as is shown in Figure 4.4. The heating system is efficient when power is dissipated in the workpiece and not in the coil. Therefore the efficiency can be described as

$$\eta = \frac{P_{\text{workpiece}}}{P_{\text{workpiece}} + P_{\text{coil}}} \tag{4.2}$$

where P is the power dissipated. Now using Ohm's law, eq. (4.2) can be written as

$$\eta = \frac{I^2 R_{\text{eq}}}{I^2 R_{\text{eq}} + I^2 R_{\text{cl}}} = \frac{R_{\text{eq}}}{R_{\text{eq}} + R_{\text{cl}}}$$
(4.3)

where I is the current, R_{eq} the equivalent resistance and R_{cl} the resistance of the coil. Note that indeed the efficiency is high when the equivalent resistance is high and the coil resistance low.

An important figure in induction heating calculations, also when determining the equivalent resistance, is the penetration depth δ . It stems from the non-uniform current distribution caused by an alternating current. When an alternating current flows through a conductor the current density is highest at its surface and decreases exponentially towards its center. This phenomenon is known as the skin effect and is also present in the workpiece and coil. The penetration depth is the distance from their surface to the point where the power is reduced to $1/e^2$ of the value at the surface. This means that approximately 86 % of the power is concentrated in the penetration depth. For a solid round bar the penetration depth can be calculated with Equation (4.4), provided SI units are used [53].

$$\delta = 503 \sqrt{\frac{\rho_{\rm e}}{\mu_{\rm m} f}} \tag{4.4}$$

where $\rho_{\rm e}$ is the electrical resistivity, f is the frequency and $\mu_{\rm m}$ is the relative magnetic permeability. The latter is the ratio of the permeability of a specific medium to the permeability of free space. For non-magnetic materials, such as 316 stainless steel, it is equal to unity. The electrical resistivity is a temperature dependent property and therefore the penetration depth varies slightly with temperature. Figure 4.5 shows how the penetration depth in 316 stainless steel varies with frequency for the highest and lowest temperature. Table A.5 contains information on how the electrical resistivity was obtained.

The equivalent resistance itself, for a round hollow workpiece, is calculated with the following relation

$$R_{\rm eq} = \frac{\pi \rho_{\rm e} d_{\rm o}}{\delta l_{\rm evp}} K_{\rm eq} N_{\rm cl} \tag{4.5}$$

where $N_{\rm cl}$ is the number of windings of the induction coil and K is a geometry dependent resistance factor. This factor depends on two ratios, $d_{\rm o}/\delta$ and $(d_{\rm o}-d_{\rm i})/(2d_{\rm o})$. Unfortunately no explicit correlation exists but Tudbury [61] has plotted values of $K_{\rm eq}$ versus both ratios.

Only the resistance of the coil itself is still needed to calculate the efficiency of the system. Basically, this is done by

$$R_{\rm cl} = \frac{\rho_{\rm e,cl} l_{\rm cl}}{A_{\delta,\rm cl}} \tag{4.6}$$

where l_{cl} is the total length of the current path in the coil and $A_{\delta,cl}$ is the effective area in which current flows and can be taken as the reference depth in the coil times the width of one turn. Tudbury [61] modified eq. (4.6) so that it is expressed in terms of the coil's geometrical parameters, yielding

$$R_{\rm cl} = \frac{\pi \rho_{\rm e,cl} \left(d_{\rm i,cl} + \delta_{\rm cl} \right) N_{\rm cl}^2}{\delta_{\rm cl} l_{\rm cl} \xi} \tag{4.7}$$

where ξ is the dimensionless space factor, which takes into account that there must be spacing between the coils turns. It is defined as

$$\xi = \frac{w_{\rm cl} N_{\rm cl}}{l_{\rm cl}} \tag{4.8}$$

4.2. Heating 37

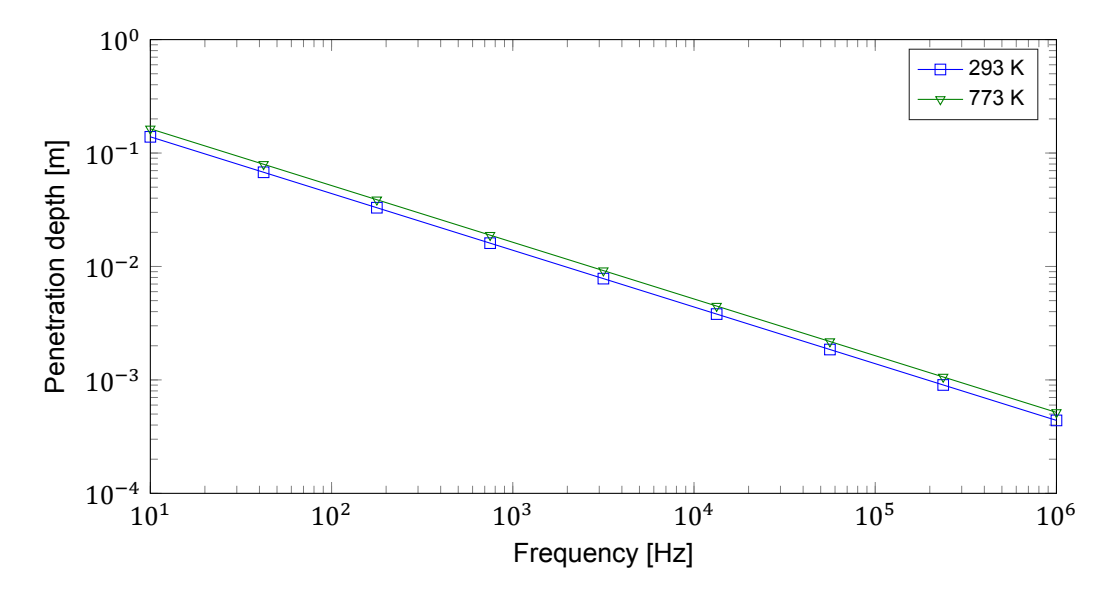


Figure 4.5: The penetration depth in 316 stainless steel for the lowest and highest value of the temperature range (Equation (4.4)).

where w is the width of a turn.

If the workpiece geometry is based on the heat pipe dimensions and the coil geometry based on a typical coil (10 mm spacing between the workpiece and the coil, $\xi=0.85$, 5 windings [61]), application of eqs. (4.2) to (4.8) yields a maximum efficiency of approximately 84 %. This maximum is achieved at the frequency that results in the highest value of $K_{\rm eq}$, i.e. $f=3.14\,\rm kHz$. Such an electrical efficiency means that about 2.7 kW of heating power is needed. In reality, this number is higher since the indispensable control unit (frequency transformer) contributes to losses as well. Additionally, the frequency is often not based on the highest value of $K_{\rm eq}$, but rather on reducing losses in the frequency transformer.

4.2.2. Trace heating

Trace heating relies on the dissipation of electrical current in a cable, therefore it is also known as resistance heating. As a result of the dissipation, the cable heats up and supplies heat to an object it is in contact with. For a cylindrical object such as a heat pipe, the heating cable can simply be wound around the surface of the evaporator. A problem with such a cable is the non-uniformity of the heating profile due to its circular shape. This can be overcome however, by reducing the cable diameter and placing it in a sheath that equally distributes the heat, so that a uniform heating element is created. Such an element can be cylindrically shaped and isolated on the outside so that it can efficiently supply heat to a pipe.

The losses in a trace heating system originate in the power control unit and the loss of heat to the environment. The latter is often reduced by applying an insulating layer around the heating element. Furthermore, such losses are already roughly covered by the contribution to heating power to account for thermal radiation and convection from the evaporator (Section 3.4). Therefore the required power is more or less equal to the previously defined amount (2.27 kW) and cannot be determined accurately before specifications from a power unit supplier are received.

Using a band heater for the heating of the evaporator is certainly possible but one major issue has to be overcome. Unlike an induction heating system, direct contact between the power supply and the dissipation element is required. As the heat pipe is rotating, a rotational electrical coupling capable of transferring large currents is necessary.

Alternatively, a heating cable could be integrated into the heat pipe shell, to some extent resembling the induction heating. This approach could improve control since the heat is supplied as direct as possible. However, regarding modularity; each heat pipe would need its own integrated heater, whereas a band heater can simply be clamped to another unit.

4.3. Cooling

At the condenser $30 \, \text{kW} \, \text{m}^{-2}$ has to be removed over a length of $167 \, \text{mm}$, resulting in a total heat flow of $0.9 \, \text{kW}$. In order to achieve this, active cooling is required, as the convective and radiative losses are not enough to achieve this rate over the entire temperature range (Figure 3.5). The selection of the technology able to do this, is discussed here.

4.3.1. Liquid cooling

Many heat pipe test setups employ cooling at the condenser by means of a fluid jacket [17, 37, 55, 56]. A cool liquid stream extracts heat as it flows over the surface. Initially, this was the considered cooling technology for the TU Delft setup but there are a couple of issues that complicate the application. First, the heat pipe is rotating, unlike many of other experimental setups. In order to contain the fluid to the condenser section and avoid spillage, two rotary fluid seals should be present. Although this is certainly possible, it is expected to restrict modularity by impeding the replacement of heat pipes. Second, a cooling fluid is needed that can handle surface temperatures up to approximately 773 K. A typically used fluid such as water would be subject to film boiling, resulting in reduced cooling rates due to the lower thermal conductivity of the vapor layer. High mass flows could be deployed to limit the temperature increase of the coolant but this requires a large, temperature resistant pump. Alternatively another cooling fluid could be selected, although not many materials are suitable for these high temperatures. Third, a secondary cooling circuit is needed to reduce the temperature of the coolant. Especially for other coolants, since cool water could be taken from the tap, although this would be wasteful. Anyhow, a secondary cooling circuit involves a substantial amount of extra equipment.

4.3.2. Air cooling

A simpler solution would be the application of air cooling. By itself, the convective heat transfer is insufficient (Figure 3.5) but the addition of a strong crossflow could significantly increase the rate. An air guiding duct would be required to contain the flow and create high velocities over the condenser surface. Again, such a structure would impede modularity, yet it does not require tight seals since it is not critical if air escapes into the environment; a simple brush is expected to suffice. Furthermore, the air duct could be opened so that a heat pipe can be replaced.

The question remains if air cooling is capable of removing all the heat. To investigate this, a literature study was executed for heat transfer over an axially rotating cylinder in a radially directed crossflow. Peller et al. [49] conducted relevant experiments on a cylinder rotating at velocities up to 5200 rpm and heated to temperatures up to 393 K. The rotating cylinder was subjected to a crossflow with free stream Reynolds numbers in the range of 8.35×10^3 to 7.13×10^4 . The velocities were expressed in terms of the velocity ratio, i.e. the tangential velocity at the cylinder surface over the free stream velocity, or

$$\gamma = \frac{v_{\rm s}}{v_{\infty}} = \frac{{\rm Re}_{\rm rot}}{{\rm Re}_{\infty}} \tag{4.9}$$

where Re_{rot} is the Reynolds number of the rotation cylinder and Re_{∞} the free stream Reynolds number. The former is defined as

$$Re_{rot} = \frac{d_0^2 \pi \omega}{60 \nu_f} \tag{4.10}$$

where $\nu_{\rm f}$ the kinematic viscosity at the film temperature. Note that ω is in rpm. The free stream Reynolds number was defined as

$$Re_{\infty} = \frac{v_{\infty}d_{0}}{v_{\epsilon}} \tag{4.11}$$

where v_{∞} is the air velocity of the free stream. The film temperature is an average between the cylinder surface temperature and the free stream air temperature

$$T_{\rm f} = (T_{\rm S} + T_{\infty})/2$$
 (4.12)

Peller et al. [49] found that for a sufficiently high rotational velocity, at $\gamma > 2$, the heat transfer becomes independent of the crossflow and may theoretically be described as heat transfer from a cylinder rotating in a quiescent medium. For $\gamma < 0.5$, the Nusselt number rapidly increases with γ . In

4.3. Cooling 39

the range $0.5 < \gamma < 2$, the heat transfer is independent of rotation rate and reaches a maximum value, solely dependent on the free stream velocity. The Nusselt number in this region is described by

$$Nu_{rot} = (1 + 0.019 Re_{\infty}^{0.221}) Nu_{(\gamma=0)}$$
(4.13)

where $Nu_{(\gamma=0)}$ is the Nusselt number for a non-rotating cylinder in a crossflow. Equation (4.13) is valid for $5\times 10^3 < Re_{\infty} < 1\times 10^5$. The authors found that their results agree well with other experimental data.

It is assumed that, in the heat pipe setup, the region $\gamma > 2$ is never achieved because it would void the necessity of active air cooling, yet it is known that active cooling is required. Thus the free stream velocity will be high enough to avert the region. Therefore Equation (4.13) provides a means to estimate the maximum achievable cooling rate and test whether air cooling is possible. To use it, an expression for $Nu_{(\gamma=0)}$ is needed. Compared with correlations for rotating cylinders, heat transfer from non-rotating cylinder in crossflow has been covered much more extensively. Peller et al. [49] ran their experiments for a non-rotating cylinder as well and compared it to other studies. They found that it agrees well, provided a number of corrections were applied. The first correction accounts for the aspect ratio of the cylinder, i.e. the length over diameter ratio. For the current geometry is it given by

$$\frac{\text{Nu}}{\text{Nu}_{l=\infty}} = \left[1 + 1.0338 \left(\frac{l_{\text{con}}}{d_{\text{o}}} \right)^{-0.85} \text{Re}_{\infty}^{0.221} \right]$$
 (4.14)

where $Nu_{l=\infty}$ is the Nusselt number for an infinitely long cylinder. The second correction accounts for the blockage caused by the cylinder in the free stream. This creates turbulence and increases the air velocity when it passes the cylinder. According to the method used by Peller et al. [49], it is defined by

$$\frac{\text{Nu}}{\text{Nu}_{y=\infty}} = \left[\left(1 + 1.18 \left(\frac{d_0}{y} \right)^2 \right)^3 \right]^{0.633}$$
 (4.15)

where *y* is the height of the channel. Both corrections results in a substantial increase in heat transfer. Finally, an expression for the non-rotating cylinder in a crossflow is provided by Churchill and Bernstein [14], who validated it for a broad range of experimental data. The correlation is as follows

$$Nu_{(\gamma=0)} = 0.3 + \frac{0.62Re_{\infty}^{1/2}Pr^{1/3}}{\left(1 + (0.4/Pr)^{2/3}\right)^{1/4}} \left[1 + \left(\frac{Re_{\infty}}{282000}\right)^{5/8}\right]^{4/5}$$
(4.16)

Equation (4.16) is valid for $Re_{\infty}Pr > 0.2$, which holds for all the temperatures and relevant velocities. After calculating the Nusselt number, the heat transfer coefficient is obtained from

$$h_{\rm rot} = \frac{\mathsf{Nu}_{\rm rot}\lambda_{\rm f}}{d_{\rm o}} \tag{4.17}$$

Subsequently, the heat flow is calculated by

$$Q = h_{\rm rot} A_{\rm con} \left(T_{\rm s} - T_{\infty} \right) \tag{4.18}$$

It is unclear whether Peller et al. [49] applied the corrections to Equation (4.13) as well. Figure 4.6 shows the maximum achievable heat transfer using the equation with and without the corrections from Equation (4.14) and (4.15) for the lowest and highest operating temperatures. At free stream air velocities above $6.28\,\mathrm{m\,s^{-1}}$, i.e. $\gamma < 0.5$, the capacities most certainly lie below the maximum, yet inside regions enclosed by the dashed curves. Peller et al. [49] did not provide a correlation for the Nusselt number for this range. Nevertheless, the cooling capacities can still be estimated to lie within the enclosed regions. For the upper dashed curve indicate the maximum, as if Equation (4.13) is still valid, and the lower dashed curve indicate the minimum, i.e. for a non-rotating cylinder as calculated with Equation (4.16). At lower rotational velocities, the range $0.5 < \gamma < 2$, shifts towards the left and the area where estimations are uncertain becomes even larger. It can be concluded that in terms of air

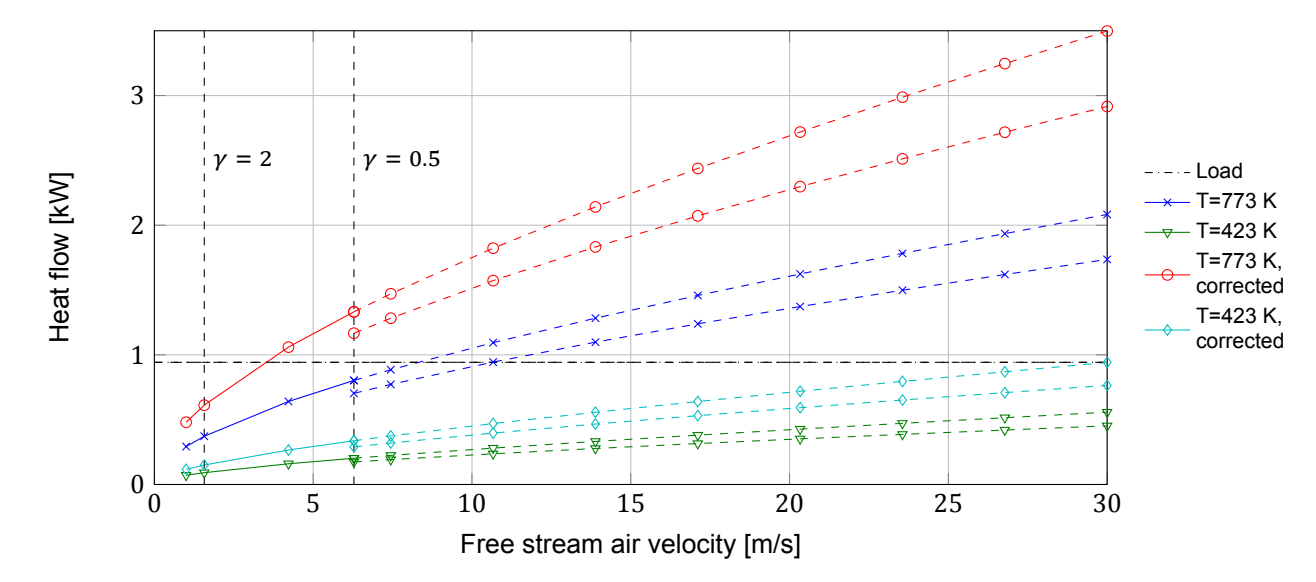


Figure 4.6: The maximum air cooling capacity as a function of free stream velocity. Lines are present for the highest and lowest operating temperature and with or without the corrections from Equations (4.14) and (4.15). The rotational velocity is fixed at $\omega = 1000 \, \text{rpm}$. The vertical dashed lines indicate the range wherein Equation (4.13) is valid.

cooling, the rotational speed is relatively low, since the region where it truly influences the cooling capacity (above $\gamma > 2$) is small even for the maximum rotational speed.

Figure 4.6 shows that air cooling alone, is not enough to remove 0.9 kW from the heat pipe. Even when assuming the corrections can be applied, which is unclear, the heat flow is too low at lower temperatures. At higher temperatures the technology provides enough cooling but still it requires a significant air velocity. To be certain that all the heat can be removed, it is decided to further enhance the air cooling by adding small droplets of water.

4.3.3. Mist cooling

The addition of liquid droplets can significantly increase the cooling capacity of an air stream. If this is done by atomizing water by the pressure in a nozzle it is know as spray cooling. Less common is mist cooling, where water is atomized in a nozzle by compressed air. The typical droplet size in spray cooling is in the order of $100\,\mu m$ or larger, whereas droplets in mist cooling are smaller than $100\,\mu m$ [57]. Mist cooling has a somewhat lower cooling capacity than spray cooling, due to the smaller mass flows involved. The uniformity of the heat transfer is better however and therefore it is the preferred method for the heat pipe setup. Figure 4.7 shows a comparison between spray and mist cooling.

As the small droplets in the air stream heat up and subsequently evaporate, they absorb extra heat from the hot surface. At sufficiently high surface temperatures, this can be primarily due to radiation, before there has been any contact with the surface. The onset of a vapor film on the surface should be avoided since this inhibits heat transfer [39]. No literature has been found concerning the mist cooling of a rotating surface but it could be that centrifugal forces reduce the risk of steady film formation. Lee et al. [38] performed mist cooling experiments on heated surfaces up to 573 K, with heat fluxes varying from 15 to $53 \, \text{kW m}^{-2}$, air velocities in the range of 4 to $32 \, \text{m s}^{-1}$ and water mass fractions of 1.5 to $10 \, \%$. They found that under the right conditions, the addition of mist can enhance the heat transfer coefficient at a heated surface by a factor 3 to 7. The heat flux is relatively uniform and temperature of the heated surface remains steady.

A correlation describing the heat transfer as a results of air/mist flow over a cylinder surface was derived by Finlay [23], who based it on experimental results with air velocities ranging from 23 to 76 m s $^{-1}$ and a maximum mass fraction of 9 % water. The maximum surface temperature remained below 323 K and heat fluxes were in the range of 5 to 30 kW m $^{-2}$. The local heat transfer coefficient depended strongly on both the water fraction and the Reynolds number. The Reynolds number of the combined air and water flow was used to correlate the data; it is given by

$$Re_{m} = \frac{(x\rho_{air,f} + \rho_{water,f})v_{\infty}d_{o}}{\mu_{m,f}}$$
(4.19)

4.3. Cooling 41

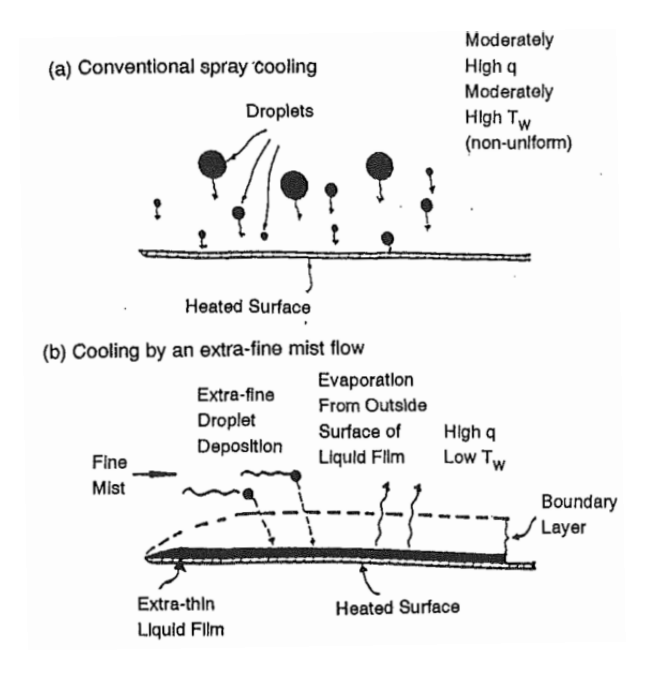


Figure 4.7: An overview of the characteristics of (a) spray cooling and (b) mist cooling. From: Lee et al. [38].

where x is the mass fraction of air in the water/air stream and v_{∞} is the velocity of the free stream. The dynamic viscosity of the assumed homogeneous mist mixture is denoted by $\mu_{\rm m}$ and can be calculated as follows

$$\mu_{\rm m} = \left(\frac{x}{\mu_{\rm air}} + \frac{1-x}{\mu_{\rm water}}\right)^{-1} \tag{4.20}$$

The average Nusselt number over the entire cylinder surface was related to the Nusselt number at the forward stagnation point Nu_{sp}, which is given by

$$Nu_{sp} = Re_{m}^{1-6(1-x)} \exp \left[56(1-x)^{0.8} - 4.1 \right]$$
 (4.21)

The average Nusselt number for the entire cylinder is defined as

$$Nu = Nu_{sp} \left(Re_{m}^{0.1+2(1-x)} \exp\left[-17.6(1-x) - 0.58 \right] \right)^{-1}$$
(4.22)

Equation (4.21) and (4.22) correlated the experimental data within $\pm 10\,\%$ and $\pm 12\,\%$ respectively. They have been derived for $29000 < Re_m < 95000$. There are a number of reasons that call for caution when applying the correlations to the heat pipe situation. The experimental conditions strongly deviate at some points, especially when it comes to surface temperature. As it does not exceed 323 K, no evaporation of the mist droplets takes place. Moreover, there has been no verification of the correlations with other data. And finally, the stagnation point of a non-rotating cylinder is likely to be different than those of a rotating one. Since these played a significant role in the analysis of the heat transfer, it is very reasonable to assume that the characteristics are different in the two situations. Nevertheless, the work by Finlay [23] shows the strong influence of water content and air velocity and it is used to obtain a rough prospect of the heat transfer enhancement provided by the addition of mist at low film temperatures, when no evaporation can take place.

It is decided to predict the mist cooling capacity by using an enhancement factor from the work of Lee et al. [38]. At a heat flux of 32.6 kW m $^{-2}$ and a water mass fraction of 5 %, the heat transfer coefficient is approximately 4 times the heat transfer coefficient of an air cooled surface. The droplet size in this scenario is the range of 30 to 60 µm, which relates to an evaporation regime where no film boiling takes place, as is expected to be the case in the rotating cylinder scenario. For the estimation, the heat transfer coefficient for the air cooled surface is the uncorrected value obtained from Equation (4.13).

In Figure 4.8 the mist cooling rates are depicted for various surface temperatures, if 5% of water is added. The method by Finlay [23] is only applied at a temperature where no evaporation can take

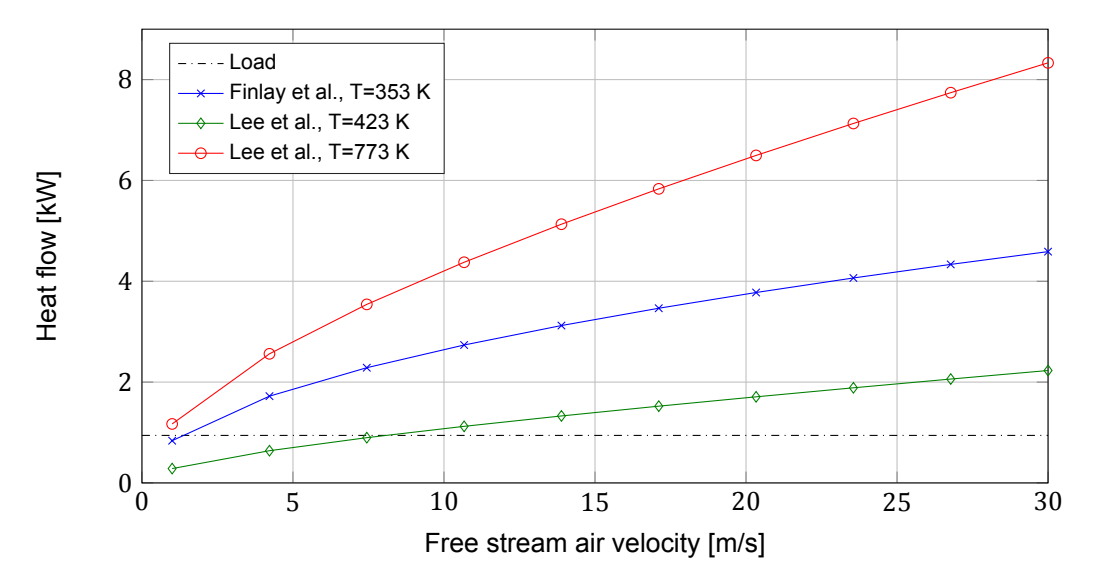


Figure 4.8: The maximum mist cooling capacity as a function of free stream velocity. The rotational velocity is fixed at $\omega = 1000$ rpm. The mass fraction of water droplets added to the air stream is 5%.

place but nevertheless it seems to give rather over predicted values. The method of Lee et al. [38] is expected to give more reasonable values and shows that mist cooling provides enough capacity, even at the lowest temperature of the working range, provided the free stream velocity is higher than $7.5\,\mathrm{m\,s^{-1}}$.

Altogether, the applied methods only give estimations of the cooling capacity. The necessary equipment should be capable of operating within an additional margin so that proper functioning at the specifications is ensured. The exact heat flow brought about by the mist cooling cannot be accurately predicted and therefore it is critical that the heat flux sensors provide a good feedback.

4.3.4. Pressure drop estimations

If air or mist cooling is to take place, a fan is required to provide the air flow. Such a device should be able to overcome the pressure drop in the duct and over the cylinder. High velocities are required and to create them, the duct will be narrow. Moreover, the flow is obstructed by the rotating cylinder positioned centrally in the flow. Therefore a substantial pressure drop can be expected. The pressure drop over an air duct can be calculated with the Darcy-Weisbach equation

$$\Delta p = \left(f_{\rm f} \frac{l}{d_{\rm h}} + \Sigma C \right) \frac{\rho v_{\infty}^2}{2} \tag{4.23}$$

where f_f is the friction factor, l is the length of the duct, d_h is the hydraulic diameter and C is a loss factor. An explicit correlation for the friction factor is provided by White [65]

$$f_{\rm f} = -1.8 \ln \left[\frac{6.9}{\text{Re}_d} + \left(\frac{\epsilon_{\rm r}/d}{3.7} \right)^{1.11} \right]$$
 (4.24)

where ϵ_r is the roughness of the wall. The hydraulic diameter is needed in case of a non-circular duct and for a rectangular cross-section it is defined as

$$d_{\mathsf{h}} = \frac{2wy}{(w+y)} \tag{4.25}$$

where w is the width and y is the height of the duct. The loss factors \mathcal{C} account for minor losses encountered in the duct, e.g. contractions, expansions and bends. Their values have been well established through derivation from many experimental data and can be obtained from literature [65]. Unfortunately, no loss factors have been encountered for cylindrical obstructions of the flow, let alone rotating ones. However, a conservative estimation of a loss factor could provide a safe pressure drop value for the selection of a fan.

4.4. Rotational drive

The characteristics of a fan can be compared with the pressure drop profile as obtained from Equation (4.23) to determine whether the device is capable of providing the air flow. Additionally, the air velocities through the duct can be derived from the delivered volume flow and duct geometry. In Figure 4.9 such a comparison is shown. The fan specification belongs to a typical radial fan, which is normally used for supplying air flow to ducts. It has been selected for its capability of realizing velocities high enough to achieve the needed cooling capacity, in combination with a practical duct size. The width of such a duct basically defines the size of the condenser and should therefore be equal, or at least similar, to the specified length. A duct height that is too small results in very high air velocities at the heat pipe crossing, accompanied by high pressure drop and noise; a duct height that is too large results in the necessity of a larger fan to obtain the required cooling velocities. For the cooling duct the height has been specified as roughly two times the heat pipe diameter, i.e. 120 mm.

The fan specification used to create the plot in Figure 4.9 is the same fan as discussed in Section 5.6.4. An advantage of this unit is that the geometry of its outlet closely resembles the required duct dimensions and that a coupling piece is therefore unnecessary. The combination of this fan and the duct results in air velocities in the range of 9.26 to 37 m s⁻¹ while providing sufficient static pressure at all times. A smaller fan could also be selected however, since at some point, the delivered velocities become far higher than needed. The parameters entered in Equation (4.23) have been based on expected duct characteristics. A roughness of 0.09 mm was taken for galvanized steel [65], which is a typical duct material. The required length is estimated at 800 mm, although this could become higher when a discharge line is added. A loss factor of 0.21 for a 90° bend has been included [65]. Additionally a conservative estimation of the loss over the cylinder has resulted in a factor of 2.

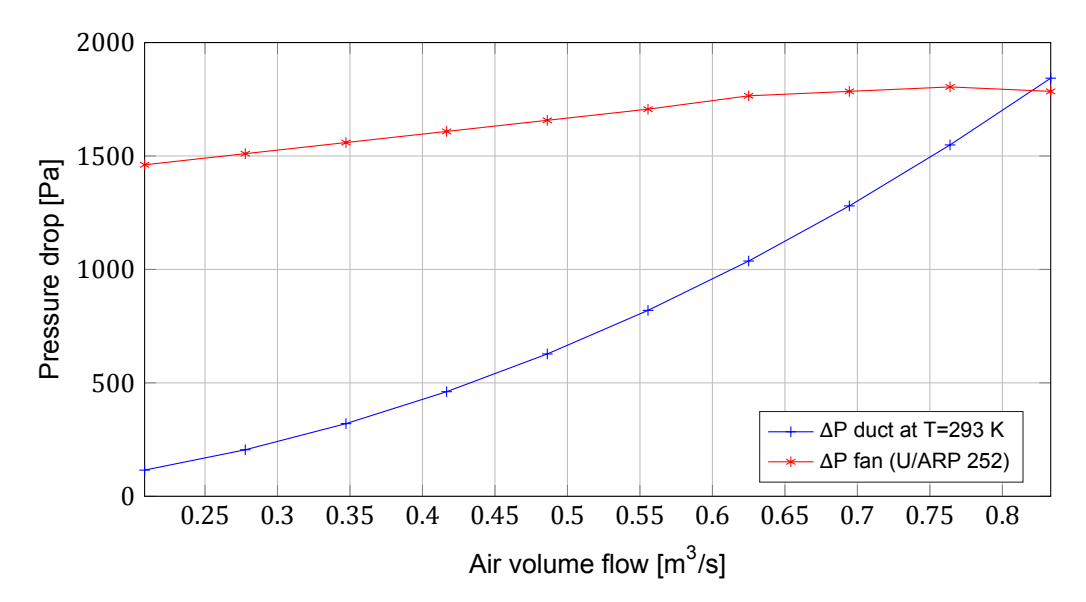


Figure 4.9: The pressure drop over the duct with geometry equal to a fan outlet ($w = 180 \, \text{mm}$, $y = 125 \, \text{mm}$) and the fan specification of an Induvac U/ARP 252 type fan. The air volume flow range corresponds to a free stream velocity range from 9.26 to 37 m s⁻¹.

4.4. Rotational drive

4.4.1. Characteristics

To accelerate to a rotational velocity and maintain it for steady operation, a rotational drive needs to be coupled to the heat pipe. If such a drive is to be selected, the required torque and motor power need to be known. The power is calculated by

$$P = \tau \frac{\omega \pi}{30} \tag{4.26}$$

where au is the torque and ω the rotational velocity in rpm. The torque is given by

$$\tau = \Sigma I_{\rm m} \frac{\pi}{30} \frac{\mathrm{d}\omega}{\mathrm{d}t} \tag{4.27}$$

where $I_{\rm m}$ denotes the moment of inertia about the axis of rotation. The rotating part of the heat pipe setup will consist of a number of elements with each their own moment of inertia. It will at least comprise: the shell (a hollow cylinder), the sides (thin disks) and shafts (solid rods). Respectively, their moments of inertia are

$$I_{\text{m,shell}} = \frac{\pi \rho l}{2} \left(\left(\frac{d_{\text{o}}}{2} \right)^4 - \left(\frac{d_{\text{i}}}{2} \right)^4 \right) \tag{4.28}$$

$$I_{\text{m,side}} = \frac{\pi \rho t_{\text{S}}}{2} \left(\frac{d_{\text{O}}}{2}\right)^4 \tag{4.29}$$

$$I_{\text{m,shaft}} = \frac{\pi \rho l}{2} \left(\frac{d_{\text{shaft}}}{2}\right)^4 \tag{4.30}$$

where ρ is the density of the steel (Table A.5), $t_{\rm S}$ the thickness of the sides and l the length of the shafts. Equation (4.27) suggests that only a small amount of torque is needed as long as the acceleration is low. This is only partly true, in reality the dynamic friction in the bearings and surface drag from air need to be overcome. At standstill, there is static friction as well. Additionally, there will be a mass of fluid inside that is, depending on the rotational velocity, not always evenly spread. Furthermore, equipment like the band heater and instrumentation will add extra, unevenly spread mass to the rotating body. Altogether, exact values of the required motor characteristics cannot be determined. Based on the relations in this section, it is estimated that a drive with 0.1 kW power and 1 N m torque will suffice.

4.4.2. Type

When it comes to selection a electronic motor, there is generally the division between the alternating current (AC) and direct current (DC) type. For low power applications, DC motors offer easier regulation because the velocity is directly proportional to the input voltage. AC motors need a frequency controller and have lower efficiencies at low velocities. Furthermore, DC motors can be controlled over a wide velocity range while maintaining sufficient torque. For these reasons, a DC motor will be selected to rotate the heat pipe.

Procedures and Manufacture

So far this thesis has mostly been focused on the selection of materials and components, supported by calculations and arguments to assess their capability of enabling the specified requirements. Some important procedures require attention as well. A closer look at safety is needed to ensure that the test setup can be placed and operated at the TU Delft Process and Energy laboratory. The operation itself requires a good control system and a commissioning procedure. While regarding this, the capability of the setup to serve as a student's practical will come forward. All the components and procedures are brought together in a design concept and in this process, specifics such as exact sensor locations, auxiliary equipment dimensions and more, are fixed. The essential parts that have not yet been discussed and selected, will be treated as well. Finally, a number of third parties are identified that can supply the equipment or manufacture parts of the setup. A report is given of their products and the quotes they have provided.

5.1. Composition of equipment

5.1.1. Additional equipment

The selection of equipment has mostly been a process of calculations and some auxiliary devices have therefore not yet been specified. In Section 4.2.2 it was concluded that a rotary electrical coupling is necessary to transmit power to a band heater. Such a device could also serve to transmit the signals of the various sensors mounted in and on the heat pipe. This could be done wirelessly as well but this would require even more equipment besides the rotary coupling, which is non-replaceable when it comes to high currents. A slip ring is a device capable of transferring both power and electrical signals. It consists of multiple circular brushes, or rings, that make contact between a rotor and a stator. Depending on the amount of signals and their current, the number and the size of the rings can be expanded. Besides being applied in widely encountered technologies such as electric motors, they are also present in many rotating heat pipe setups [16, 17, 37, 56].

5.1.2. Overview

In Figure 5.1 a schematic diagram of the rotating heat pipe setup is shown that provides an overview of the equipment specified and includes the feed and discharge lines. Note that there is a filling line present, which has not yet been discussed. It will be treated in Section 5.3. The schematic reveals that a band heater has been selected as the preferred heating system; this choice will be justified in Section 5.6.

The volume flow, and thus the velocity, of air supplied to the duct by the fan is regulated by a frequency controller on the power supply. The air is taken from the environment although this might result in strong drafts across the laboratory. Alternatively a feed hose can be added to direct the inflow. The mist nozzle gains its water from the cooling water supply present at the P&E laboratory. The mass fraction of water can be adjusted through a control valve on the feed line and feedback is provided by the flow meter. The stream exiting the duct contains air, steam and unevaporated water at possibly high temperatures and must therefore be treated with caution. At the laboratory there is a knock-out drum present in which the air can be separated from the water.

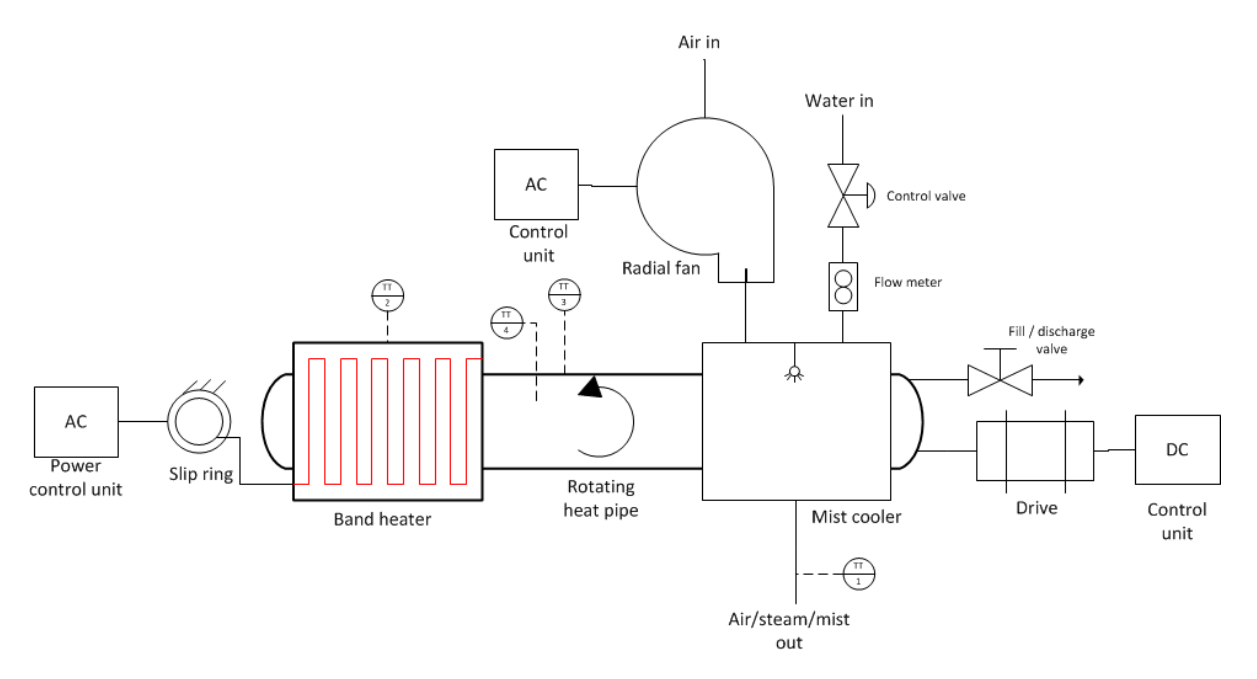


Figure 5.1: A schematic diagram of the rotating heat pipe setup.

Two additional temperature readings are added to the test rig. One is included in the band heater as part of its feedback system. The second reports the temperature of the mist cooler exit stream to provide insight about the cooling process.

5.2. Safety

Throughout this thesis a number of restrictions have been imposed and design choices made on account of safety. It was partially the reason to restrict the maximum internal pressure to 0.5 MPa. During the selection of the working fluid the safety criterion has eliminated a number of potential working fluids and contributed to the limitation of the maximum working temperature. Furthermore, the fill factor was kept low to minimize the amount of potentially hazardous material in the heat pipe. Note that although the selected working fluids passed the health and safety criteria, this does not necessarily mean that they are non-toxic.

In the further design process there are two main ways through which more safety can be achieved; the first is through a control system and the second is through mechanical safeguards. Additionally, an operation protocol and trained operators would be beneficial for safety. The control system is more elaborately discussed in Section 5.4, but here it is already noted that multiple emergency stops will be present and that the various devices in the setup will be coupled in a way that overheating is prevented.

The setup will contain a safety screen, shielding the operators and spectators from the rotating and heated parts. This shield will therefore encompass the entire heat pipe and its shafts, as well as the slip ring, the heater, the cooler and the drive. The shielding is made of a material allowing for visual access to the heat pipe so that the operator can perceive whether stable and safe operation is taking place. This means that either the shielding is made of a though transparent material, e.g. a thick sheet of acrylic glass, or of a metal grid. The holes in such a grid should be smaller than the smallest parts that can accidentally be hurdled from the heat pipe during rotation, e.g. a nut or bolt. The shield can be (partially) removed if the setup is idle so that the heat pipe and other equipment can be accessed or replacement of the heat pipe can take place. An electrical contact between the removable part of the shield and the frame it is mounted on, ensures that the operation cannot be started if the shield is not in place.

In case of failure of the control system, or any other unforeseeable reason, the temperature inside the heat pipe and with it the pressure, can rise above the safe limits. If for example, the heat pipe is loaded with biphenyl and the temperature rises 50 K above its maximum working temperature to 657 K, the pressure nearly doubles to 1 MPa (see Figure 2.1(c)). As it rises even further, for instance to the

5.3. Preparation 47

maximum operating temperature of the setup at 723 K, the pressure doubles again to 2 MPa. These high pressures involve risks of explosion or leakage of the working fluid into the environment. Although the stress calculations in Section 3.5 indicate that with a 5 mm shell, the heat pipe can withstand very high pressures, weak points such as welds and sensor fixations could still facilitate a rupture. In order to avoid the risks of explosions and uncontrolled fluid discharge, the heat pipe is equipped with a pressure relief system. Above a certain threshold pressure this device allows for a controlled discharge of the working fluid. By suction at the location where the discharge is taking place, any hazardous materials can be contained.

Two different pressure relief systems have been under consideration, a valve and a rupture disk. The valve requires more space —which will turn out to be scarce— whereas the rupture disk can be fixed in one of the sides. Yet the valve allows for reuse of the heat pipe after setting it off, because fluid is only ejected and no air is let in; whereas the rupture disk completely opens the heat pipe. This means that when the disk bursts, it needs to be replaced and the heat pipe needs to be cleaned again, or the entire heat pipe needs to be replaced. The valve can be connected to a discharge line so that suction of the ejected fluid can take place at a distance from the heat pipe. In case of the rupture disk, permanent suction needs to take place at one of the heat pipes' sides. In any case, the pressure relief system should not be triggered too lightly, for the heat pipe itself is capable of handling pressures above the 0.5 MPa limit and the triggering could result in disabling of the heat pipe.

5.3. Preparation

Proper preparation of the heat pipe during and after manufacture is critical for steady operation later on. Reay et al. [51] give a detailed description of the necessary process. Before the heat pipe is started or even sealed, a thorough cleaning of the inside should take place. This process involves degassing and rinsing with a solvent. Degassing of stainless steel is necessary for heat pipes operating above 673 K. Stainless steel contains dissolved hydrogen that is released at accelerated rates at high temperatures and is then likely to react with the working fluid [51]. The degassing can be carried out by placing the heat pipe in an oven, under vacuum at at temperature of at least 673 K. It is advised to clean with a solvent prior to this process to remove any non-atmospheric contaminants. Jouhara and Robinson [34], who performed experiments on a thermosyphon filled with biphenyl based working fluids (Dowtherm A and Therminol VP1), used xylene and methanol for cleaning. Preferably, the heat pipe is kept in a clean environment after the cleaning and during the sealing, e.g. a glove box. The advised sealing technique is by argon arc welding because it reduces risks of contamination.

For the TU Delft setup it is decided to fully seal the heat pipe prior to filling it. A small tube, mounted through the side of the condenser, will allow for addition of fluid after the sealing has taken place. The tube is fitted with an open-close valve through which it can be connected to a vacuum pump and filling station. It is critical that the valve is 316 stainless steel like the rest of the heat pipe. The location at the condenser is chosen to facilitate non-condensable gas bleeding during operation, as it is the place where it will accumulate. The filling tube adds extra vapor space to the heat pipe and through it heat transfer can take place that is unmonitored by the flux sensor. Therefore it is essential to keep it as small as possible and mount the valve that seals up the space, as closely to the heat pipe as possible. To avoid the gathering of condensate in the tube, the part inside the heat pipe is slightly bent away from the center so that droplets will be thrown out due to centrifugal forces.

After the sealing, atmospheric contaminants are removed by creating a vacuum inside the heat pipe through the filling tube and a vacuum pump. An inert gas like argon can be used to purge out all the air prior to the vacuuming itself. By doing so, any remainders left —although still undesired— are at least not compromising the stability. Before the vacuuming, a pressure test can be conducted to test all the welds or other seals for leaks. The purity of the working fluid can be guaranteed by obtaining it at high grade from a supplier or by performing additional purification steps. If multiple heat pipes need to be filled it can be beneficial to design a separate filling station, where the processes of cleaning, vacuuming and filling are combined. Layouts of such stations and the corresponding procedures are described in literature [51].

5.4. Control

A control system is implemented in the heat pipe test rig for various reasons. These are:

- · Operation within specified limits
- · Safety
- Overview for the operator
- Suitability for student's practicals

Note that steady operation is absent on this list. The regulation of the equipment will be done manually by the operator. The heater power will be set manually and feedback is obtained from the integrated temperature sensor on the heater and the heat flux sensors at the evaporator. The cooling is regulated similarly, via manual control of the fan speed and the water mass flow. Either data is provided by the fan supplier concerning the relation of the motor power to the air volume flow, or an additional air flow meter needs to be installed before the duct. This information is required to determine the mass fractions in the mist stream. Feedback of the cooling process is provided by the flux sensors at the condenser.

The regulation of the rotational velocity is performed manually by adjusting the motor power. The velocity of a DC motor is directly proportional to the applied voltage. Therefore a voltage controller will suffice and this is usually included by the supplier.

At a later stage a Programmable Logic Controller (PLC) could be added to the test rig that integrates (most of) these actions into an automated system. A more advanced control system could be designed that automatically adjusts the heating, cooling and rotation based on e.g. a preset operating temperature. Before this is possible, a better understanding of the relation of certain parameters is required, for instance between the cooling capacity, the fan power and the water mass fraction.

5.4.1. Operation within limits

Although the operation itself is controlled by the operator, the control system will ensure that certain boundaries are not crossed. These are mainly the maximum temperature and rotational velocity. Limitation by the system of the maximum temperature will avoid overheating of the heat pipe and high internal pressures. The band heater will be supplied with an advanced controller. The motor power supply (controller) is connected to it to prevent operation of the heater when the heat pipe is not rotating. The temperature sensor integrated in the band heater is connected to the controller to regulate the device. Additionally the thermocouples in the shell and vapor space of the evaporator section can be connected as well for better control. In any case, the temperature at the evaporator is continuously monitored by the controller and if a threshold is exceeded, the band heater is immediately disabled. It is extremely important to adjust the maximum values to the charged working fluid. As previously described in Section 5.2, the vapor pressure of biphenyl at the maximum operating temperature of phenanthrene is approximately 2 MPa, which is far above the limit. Therefore specific operating limits have to be set for each heat pipe containing a different fluid.

The rotational velocity is limited via the controller of the DC motor to avoid too large forces and vibrations. The power to the electric motor driving the fan is regulated via a frequency controller, through which the maximum power and thus fan speed, is limited.

5.4.2. Safety

Most of the control setup already contributes to safety by avoiding (too) high temperatures, pressures and rotational velocities. Extra measures are taken to enable a quick shutdown in case an accident occurs (or is about to occur). Three emergency stops will be mounted on strategic locations at the test rig, one in the front and one at each side. These stops are hardwired to the motor power supply; if at least one of them is triggered, the motor is disabled and with it the band heater. Even when the stop is released, the motor interlock is still active. The test rig can only be operated again after restarting of the motor. The safety shield is connected to the motor power supply as well. When it is opened, neither the motor or the band heater can be started.

5.4.3. Overview

In Figure 5.2 a schematic of the control scheme is depicted. All the connections between the controllers and devices are shown. A data logger unit is used to acquire all the data from the sensors and controllers. It is connected to a PC that displays the properties they measure. Software such as Labview or any other program compatible with the data logger can be used to process the signals.

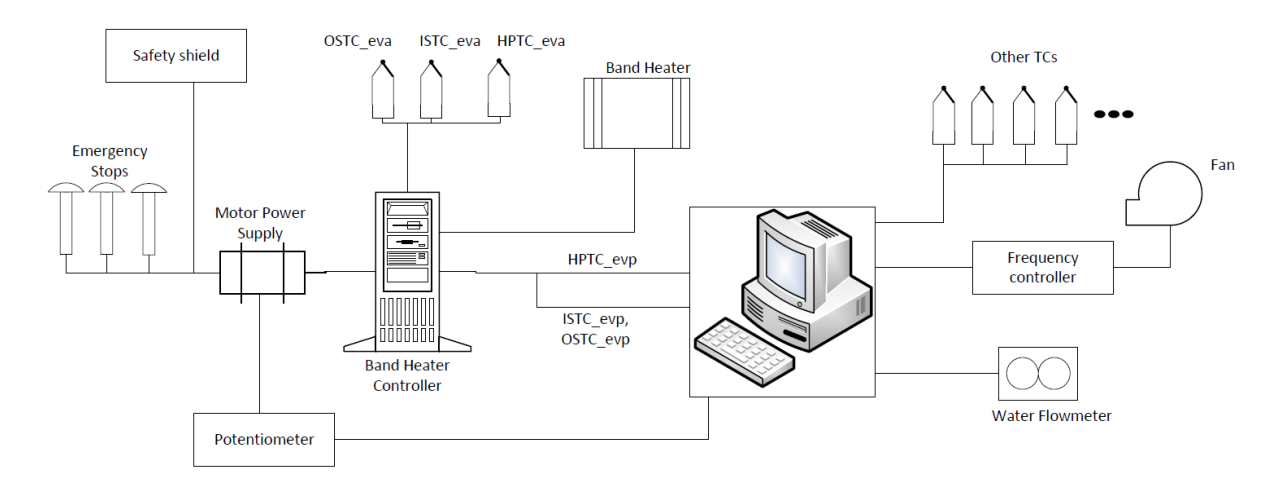


Figure 5.2: A diagram showing the connections in the control scheme. OSTC and ISTC denote the thermocouples in the shell at the outer surface and inner surface respectively, together they form a heat flux sensor. HPTC denotes the thermocouples inside the heat pipe. The icon of the PC resembles both the PC and the data logger connected to it.

Thus the temperatures, volume flows and rotational velocities can be read from the PC. Their display is essential for manual control by the operator since he/she needs to adjust the controllers based on the measurements.

5.4.4. Practicals

The manual control situation provides a good basis for the setup of practicals. Students have a direct influence on the operation, contrary to operating a control system instead that then in turn operates the test rig. The consequences of every action quickly become clear which provokes a better understanding of the system. It also requires overthinking of the counter action, which then further improves the understanding. For example, if the heater power is increased, the heat pipe is likely to transport more heat which will lead to an increase of the condenser temperature; the students need to anticipate this by raising the cooling capacity, either by increasing the fan speed or by increasing the mass fraction of water.

The test rig offers many opportunities for both elementary and complicated calculations in the fields of thermodynamics and fluid mechanics that can be performed by the students. Efficiencies of equipment and the influence of parameters can be checked. A heat balance could be created, where correlations for convective and radiative losses are checked. Or a more complicated estimation of heat transfer coefficients at the inner surface can be made. Overall, many tasks can be thought of.

Since after all, the test rig is a complicated system with many different controllable parameters, it is perhaps better to restrict some of these at first. The rotational velocity could be fixed for instance, while students experiment in finding the balance between the heater and the cooler.

The variety of sensor readings and control options make the setup well suited for operation by groups. Different tasks can be divided and discussion can take place on the consequences of each action. A special safety protocol should be created for the practicals and the limits allowed by the control system could be lowered.

5.5. Drawings and manufacture

Conceptual drawings of the setup have been made in a CAD program (SolidWorks), to assign exact positions and orientations for each piece of equipment and specify the assembling procedures. The drawings assist in the assessment of manufacturability and communications with suppliers and manufacturers. Some essential parts of the test rig have not yet been discussed but will be highlighted in this section. The same applies to certain topics, such as sensor locations and handling of the leads. Since the drawings concern detailed images, they are scaled as little as possible and placed in Appendix C. To provide some overview during the following descriptions a rendering of the entire setup is already displayed in Figure 5.3.

When it comes to design, and drawing in particular, it is essential that the manufacturing process is

kept in mind. A design can fulfill all the functions it was required to do, but if it cannot be manufactured it is still useless. Therefore, in this section's discussion of the designs, the intended manufacturing process is treated as well.

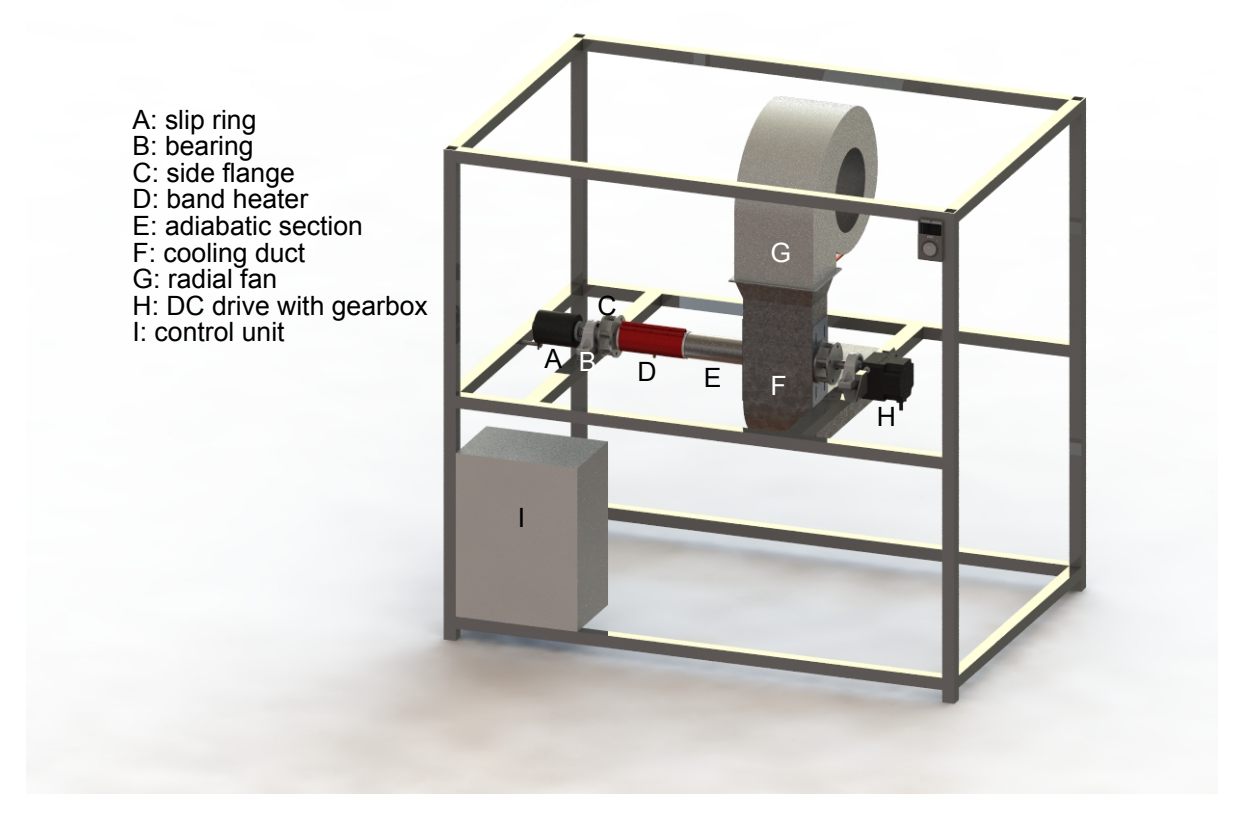


Figure 5.3: A rendering of the drawn setup with components indicated. The height of the setup is 1.2 m.

5.5.1. The heat pipe and its sensors

The dimensions of the heat pipe were already announced, but the locations of the sensors it contains were not. Drawing C.1 shows all the relevant dimensions of the heat pipe. The sides are depicted as 5 mm thick —like the shell— but this dimension is likely to be increased for manufacturing purposes. A trade dimension sized flange could be used, which is generally thicker. In any case, thicker side disks will ease the welding, as thin ones are likely to deform.

Each section has two heat flux sensors in the shell, positioned at one third and two thirds of the section. It is assumed that the heating profile and temperature distribution over the shell is axisymmetrical and therefore the tangential position of the sensors does not matter. Accordingly, the sensors are all placed in a straight line at the same tangential location. Each section contains two units to detect a profile or non-uniformities in the axial direction and to have a backup in case of a failure. The two thermocouples that comprise the heat flux sensor need to be placed in such a way that the tips or leads do not obstruct the heat flow, since this would affect the measurement. This entails that the lead should not be situated above or below the tip but rather come horizontally from the side. The thermocouples are placed at radially varying locations, one close to the outer surface and one close to the inner surface. The leads of these sensors need to be directed to the slip ring, via one of the shafts at the sides of the heat pipe. This is problematic as the leads generally cannot be lead to the shaft over the outer surface. At the evaporator, the band heater is tightly clamped around the heat pipe and the presence of the leads would significantly impede the heat transfer. Therefore these leads need to be led inside the heat pipe and exit it at one point in order to continue to the slip ring. The flux sensor leads at the remaining sections could in fact be lead over the surface, since they are not likely to significantly influence the heat transfer there. However, in order to minimize the risk of a leak, it is preferred that the heat pipe is pinged for lead outlets as little as possible and it is therefore decided that all the leads exit the heat pipe at one single location. Thus, the leads at the adiabatic section and condenser will be led into the heat pipe as well.

A hollow axis is placed at the center of the heat pipe that can accommodate all the sensor leads. The ones coming from the surface are directed into it through the vapor space. By doing so, they cross the liquid layer at the surface and the vapor flow. Indeed this will affect the flows but the effect is expected to be minor since the diameter is only very small (it can be as small as 0.25 mm) and the disruption only takes place at one tangential location —hence the placement in one straight line. The axis will exit the heat pipe at one point through the side disk, as can be seen in Drawing C.1. In the drawing the axis only protrudes a small distance from the heat pipe, but in the actual device it will protrude more in order to create space for an advanced seal that lets the leads out and prevents anything else from coming in.

The lead guiding axis can fulfill another function by serving as a mount for the vapor space thermocouples. The evaporator and adiabatic section each contain one of these at their center. The condenser contains two extra units, of which one is positioned very close to its end, to enable the detection of noncondensable gases. The exact locations are indicated on Drawing C.1. The leads of the vapor space thermocouples are directed out of the heat pipe through the axis as well. Thereafter, all the leads are led to the slip ring via one of the shafts. Note that the leads are not depicted in any of the drawings.

Drawing C.2 presents more views of the heat pipe and gives detail of the filling tube. The lead axis is kept as thin as possible, being only 5 mm across, since it resides in the vapor space and could affect the vapor flow. Other experimental rotating heat pipe setups containing sensors in the vapor space have been encountered and no reports have been made on significant disruption of the flow [56].

The manufacturing of the heat pipe and specifically the sensors and their leads can prove to be very problematic. To place the thermocouples for the flux measurements, tiny holes would have to be drilled from the inside of the heat pipe. Not only would this be extremely difficult, especially deep down the pipe at the adiabatic section, but also nearly impossible to do so with the required high precision. A better approach would be to drill a plug out of the shell for each sensor, place the thermocouples in it with high precision and braze the plug back in so that the heat pipe is again sealed. Afterwards the inner and outer surface can be machined so that they are smooth again. This concept is illustrated in Figure 5.4.

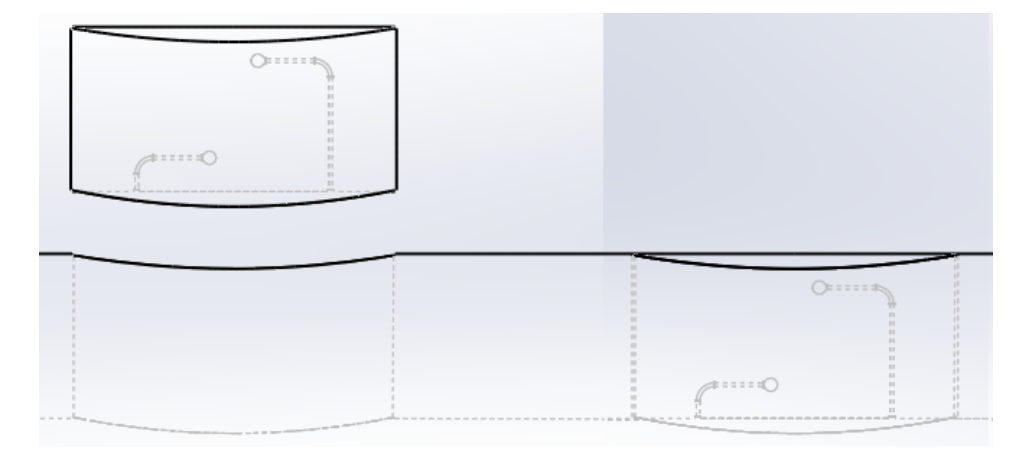


Figure 5.4: The intended way of mounting the thermocouples comprising the heat flux sensor. On the left a 'plug' has been drilled out of the shell. The thermocouples can be placed inside it with high precision. Thereafter the plug can be placed back in, as is shown on the right. The leads are led into the heat pipe. The diameter of the plug in this graphic is 10 mm, a thermocouple tip is 0.5 mm and its leads 0.2 mm.

A company specialized in thermocouples, Thermo-Electra (Pijnacker)[†], has been contacted for advice and assistance. They have had similar challenges before and expect to be able to supply the required sensors. Furthermore, they have applied the approach, where a plug is drilled to create a flux sensor in a shell, with success. Axes containing multiple leads can also be manufactured; so far up to 17 leads have been placed in a 3 mm inner diameter axis. The leads in such an axis are separated by magnesium oxide. The axis itself can be made out of 316 stainless steel. Since Thermo-Electra

[†]http://www.thermo-electra.com/

can produce the shell containing the sensors as well as the lead axis, it has been decided that they will produce the entire heat pipe, including the sides. At the moment of writing this thesis, analysis of the manufacturing process is still ongoing and the company will provide feedback regarding the minimum dimensions of the shell and central axis they can achieve. Therefore, it can turn out that the shell or central axis will need to be somewhat thicker than 5 mm.

One more possible issue needs to be considered. Because of the presence of the central axis and the leads inside the heat pipe, condensation can take place on their surface, leading to disturbed functioning of the heat pipe. It is assumed that this will only occur during startup and that at steady operation, the temperature of the metal bodies is equal to the operating temperature and condensation will only take place where heat is removed, i.e. at the condenser. However, if droplets would still originate at the surfaces, they could gather and flow via the leads directly towards the heat flux sensors. This would seriously affect the heat flux measurement and therefore it is possibly better if the leads are bent at the surface and are only directed towards the axis, after traveling a small distance along the inner surface of the shell. An additional beneficial effect of this approach would be the relocation of the flow disturbance to a spot further away from the flux sensor.

5.5.2. Connection to the shafts

The setup has to contain a replacement system for the various heat pipes, so that modularity is supported. The shafts are therefore not directly mounted to the sides of the heat pipe, but instead onto a secondary flange. This construction is shown in Drawing C.2. Although the shaft is not depicted in the drawing, a hole in the flange is visible, in which the shaft can be mounted for better welding. In Drawing C.3 multiple views of the setup are presented and the connection of the shafts to the flanges is visible. If a heat pipe is to be replaced, the sides can be disconnected from the flanges so that the heat pipe is no longer connected to the setup —provided all electrical connections are undone as well. This way, the drive and slip ring can stay in place.

In the current design, spacers separate the sides and the flanges for multiple reasons. It provides a location for the small filling tube valve, which needs to be as close to the heat pipe side as possible, to minimize the added vapor space by the tube. After this valve, the space is sealed off and the tube can continue through a hole in the flange to a point where a more convenient connection to a filling system can be established. Since the second part of the tube is no part of the heat pipe, it can even be made from a different material, e.g. copper.

Another reason for which space is required is the protruding of the lead axis from the side. The seal attached to this lead axis is not depicted in the drawing, since its exact shape is yet unknown. The lead axis exits the heat pipe at the evaporator side. The band heater is located there as well and the cables of both devices need to be led to the same slip ring, as is visible in Drawing C.3.

A third reason is the pressure relief system that needs to be integrated in one of the sides. A final decision on its form has not yet been made. If it becomes a disk, permanent suction has to take place in between the respective side and flange. In case of a valve, it has to be placed as close to the side as possible for the same reasons that apply to the filling valve. Thereafter, a relief tube could make a bend in between the side and flange and continue into the shaft to a further location where suction can take place.

The final reason is that air the between the sides and the flanges provides thermal insulation. Since the shafts are not directly connected to the heat pipe, its high temperatures will not be reached. This prevents significant thermal expansion and overheating of additional equipment fixed to the shaft, e.g. the slip ring.

The sensor leads exit the lead axis' seal at the midpoint of the side, i.e. at the axis of rotation. From this point they will be directed away from the center through a hole in the flange. For the slip ring they are connected to is of the through-bore type, which implies that the cables enter the rotor part at the outer surface of the shaft and not inside the axis. For more information on the slip ring, see Section 5.6.3. The cables from the band heater can join the bundle of sensor cables through the same hole in the flange and follow the same path to the slip ring.

A potential problem with the spacer approach could be the realigning of rotational bodies after a replacement has been conducted. Because of the high rotational velocities that the setup can be subjected to, proper alignment is critical. An initial alignment procedure can take place during the assembly of the setup, but this is an extensive procedure. It is highly undesirable as it has to take place every time a heat pipe is replaced. Marking of the spacers and the corresponding holes they

were connected to during alignment, and reassembling them accordingly, can substantially improve the rotational stability. Alternatively a different mounting system can be considered, for instance a commercially available self aligning clamping system, although compatibility with the space requiring equipment is still required.

5.5.3. Cooling duct

The fan providing the air flow is placed above the heat pipe so that gravity assists in keeping water droplets from flowing in. In Figure 5.5 a part of the assembly is shown where important parts of the cooling system are clearly visible. The water tube enters the duct on the side and is bent towards the heat pipe before finishing with the mist nozzle. The duct itself consists of two parts that can be decoupled to allow for replacement of the heat pipe. The separation lies in the horizontal plane through the center of the heat pipe. The upper part is connected to the fan so that they can be carried off as a whole in case of replacement. To ensure proper sealing when the duct is assembled, each side houses two sealing plates with slots cut out through which sliding bolt can be fitted; so that they can be securely fixed after closing. Since these sliding plates are the parts that will be in contact with the rotating heat pipe, they need to contain the seal that prevents large quantities of the air mixture coming out. This seal can be a heat resistant brush or a wearing resistant, low friction ring.

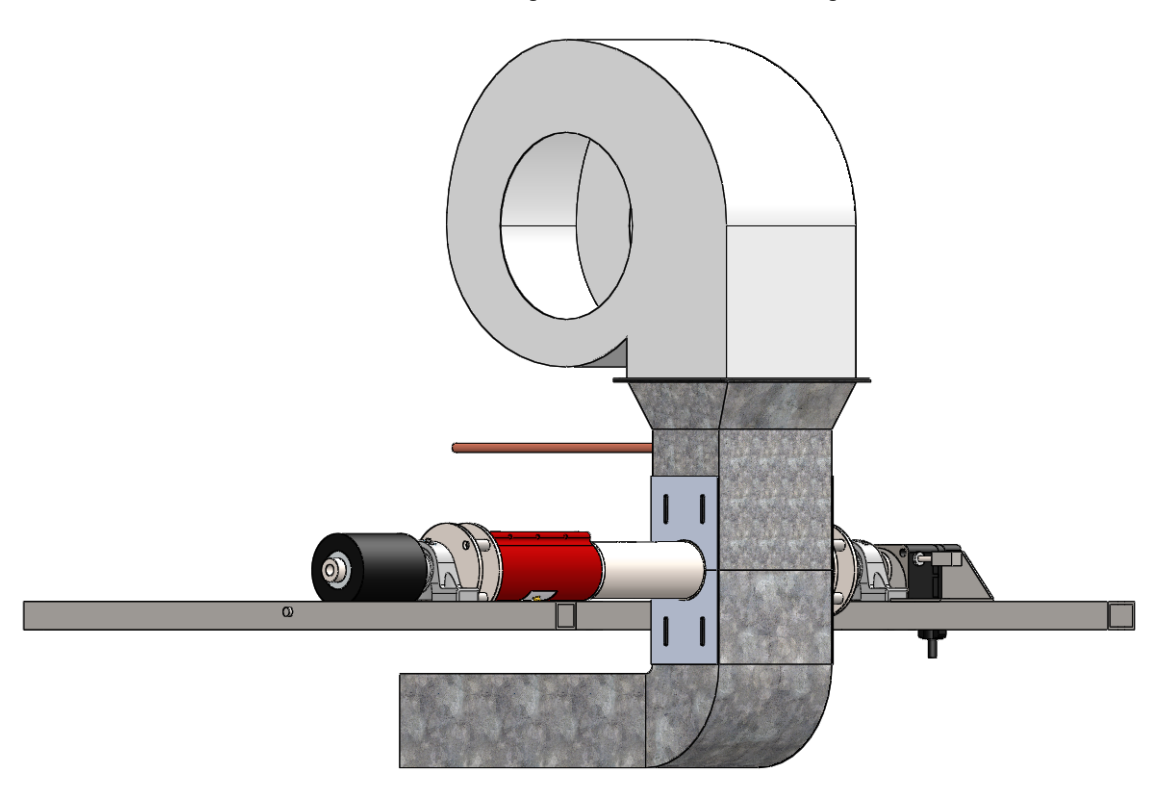


Figure 5.5: A view of the assembly where the cooling system is clearly visible.

The duct can either be purchased as a whole, e.g. from a HVAC equipment supplier, and then manipulated to meet the modularity requirements. Alternatively, it can be manufactured by plate working. In any case, galvanized steel seems like a good material for the duct, as it is generally applied for these purposes.

Some additional parts are required for the air duct. A coupling piece for the fan and duct could be needed, depending on their geometry. Furthermore, with the current fan orientation, a bend has to redirect the exit towards the knock-out drum.

5.5.4. Rotation

In the top view shown in Figure 5.6 the DC motor and its gearbox are visible on the right. The gearbox is mounted directly on the shaft. Transmission of power by e.g. a belt, entails risks of skipping and therefore the rotational velocity indicated by the controller could deviate from the actual rotation of the

axis. Moreover, use of a chain transmission would imply considerable noise, as well as safety hazards. Transmission via a coupling would require extensive aligning or a the use of a flexible version. By direct mounting on the shaft, no alignment is necessary and only a basic fix preventing rotation of the motor is required. This approach has also been applied in the Tata Steel test rig.

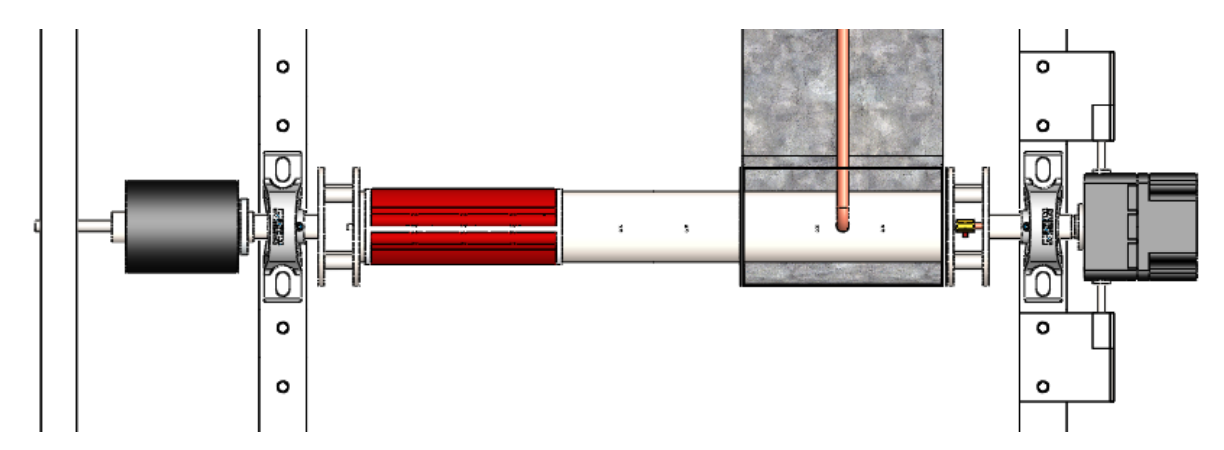


Figure 5.6: A top view of the heat pipe with the fan and coupling piece made invisible. At the right end, the DC motor and its gearbox are directly mounted on the shaft.

Normally, the shaft of a DC motor is protruding out of the device. To mount it directly on the heat pipe shaft, a gearbox is needed with a hollow shaft. Furthermore, the motor end of the heat pipe shaft requires machining in order to fit the gearbox shaft dimensions. The outer diameter of the heat pipe shafts is dimensioned at 20 mm, which is more than sufficient when it comes to bearing the mechanical loads. The large size is chosen to enable the accommodation of cables and tubes through the center, as well as to be compatible with larger slip rings, since many circuits need to be fitted. The inner diameter can be as high as 15 mm depending on the size of the bundles and tubes.

Roller bearings are selected for the fixation of the shafts to the frame, because they allow for easy alignment which is convenient when it comes to replacement of the heat pipe. The thermal expansion calculated in Section 3.5.2, although seemingly small, can lead to high stresses when the shafts are fixed in place. Accordingly, the shaft on the evaporator side is allowed to move axially in the bearing to eliminates this issue. The shaft on the condenser side, thus closest to the drive, is fully fixed in the bearing.

5.5.5. Frame

The frame, as depicted in the drawings, is rather spacious. This way there is enough place for the various control units, of which one is already depicted in the bottom left of the setup (or at least its volume is). The size of most of the units is not yet known and therefore they have not been added in the drawings, yet the depicted one is roughly the size of the band heater's control unit.

Besides extra space for the controllers, the frame needs to accommodate the safety shield and emergency buttons. Other equipment, like the fan, the duct, the slip ring and the motor fixes, need to be connected to it as well. Overall, these connections have not yet been depicted due to unfamiliarity with the exact equipment sizes.

The frame is constructed out of steel, rectangularly shaped beams, welded at the intersections for structural strength. Alternatively an aluminium construction system can be used, e.g. extruded profiles with T-nuts. The exact appearance of the frame is likely to change. Because of the high rotational velocities, it needs to handle mechanical vibrations, which require some designing experience that can be provided by a frame manufacturer.

5.5.6. Manufacture

The drawings and models presented so far have been mainly conceptual, except for the locations of the sensors and heat pipe dimensions. As stated before, Thermo-Electra will be responsible for the manufacture of the heat pipe and the implementation of the thermocouples. Further construction will take place at the TU Delft central workshop (DEMO). The TU Delft test rig has proven to be a complex project for several reasons, among which, the required cleanliness of the heat pipe combined with the

5.6. Suppliers 55

placement of the sensors and the high rotational velocities in combination with the need for modularity. Via the P&E laboratory, an engineering bureau has been contracted to finalize the design and prepare it for manufacture. Cadans Engineering (Noordwijkerhout), has worked with DEMO before and has designed various other setups for the TU Delft. Final decisions such as the pressure relief system, as well as the frame structure and the heat pipe to shaft coupling mechanism will be made by Cadans Engineering, based on more (practical) experience. Both companies involved in the manufacture of the test rig have been acquainted so that good communication is ensured.

5.6. Suppliers

The last part of this chapter concerns the communication with equipment suppliers. Inquiries have been submitted to obtain price indications and detailed specifications. Only the auxiliary equipment has been treated, i.e. the heater, the cooler, the drive and the slip ring. More mechanical parts such as bearings and frame parts have not been regarded yet, because their selection more or less depends on the design finalization, rather than influencing it, like the auxiliary equipment. Nevertheless some information on such parts is available and shared here as well. Relevant information concerning the inquiries, such as datasheets, are placed in Appendix D.

5.6.1. Induction heaters

Two companies have provided quotations for the supply of an induction heating system. More companies have been contacted and provided information about their products; all of them proposed to supply a frequency generator (controller), coil and cooling system for the coil. Generally, the lower limit of the power supply they suggested lay around 5 kW. Below this limit, the induction equipment they could supply, was often less suited.

- IEW GmbH (Vienna, AUS) delivers a 5 kW system (€ 15 000), including control (€ 8000 to 10 000), cooling system and installation (€ 3500) and shipping (€ 2500) for a total price of € 26 000 to 31 000.
- Ambrell (Hengelo) suggested a 10 kW system (€ 18 520), with controller (€ 4480) and design and manufacture of the coil (€ 2000). Including an educational discount the total was € 22 500.

Due to these high costs is has been decided to not implement induction heating technology in the TU Delft setup. Especially since there is a more affordable alternative available.

5.6.2. Band heaters

Again, multiple potential suppliers have been contacted. Two of them have provided concrete quotations. The proposed band heaters had the right clamping diameter and are generally able of achieving the desired temperatures and heat flows. It has to be noted that when the inquiry was made, a somewhat lower power demand (1.8 kW) was submitted. However, it is expected that, based on the supplier catalogs, the higher demands can also be met.

None of the devices could cover the length of the evaporator by itself. The suggested solution was to use of two units beside each other. In all cases this created a total length close to the desired 167 mm. The suppliers assured the band heaters provide a uniform heating profile. However the effects of combining two units were not mentioned. If this is expected to be problematic, a custom made solution could be requested. Although this is likely to be a more costly solution.

- Kurval (Nieuw-Vennep) delivers two 1 kW Watlow band heaters with a combined length of 177.8 mm for € 128 a piece. A control unit is included for € 860 and some additional equipment for € 20. The total price is € 1136.
- Vulcanic S.A. (Berchem, BE) suggested two 900 kW ceramic band heaters of a combined 160 mm length for € 234. A PID controller is included for € 617. The total price, including shipping, is € 1126

Clearly, trace heating is a much less costly solution than induction heating.

5.6.3. Slip ring

During the selection of a slip ring, special attention was given to the sensitivity (mV) of the thermocouple signals. The difference between the sensor and power circuits was emphasized, as well as the total number of circuits required. The suppliers ensured that there are clear barriers between the rings (circuits) and that the impedance and dynamic contact resistance are minimal. It was also stressed that slip rings are applied by other customers for similar applications. For the power circuit, high current rings are added. All parties suggested a through-bore type unit for the application. Two quotations were received.

- Penlink AB (Hägersten, SWE) can provide a slip ring with 4× 10 A, 600 V and 40× 2 A, 250 V rings for € 1050.
- Cosmau (Shenzhen, CN) supplies a very similar unit for \$1120.

Alternatively, Thermo-Electra has suggested the use of a brushless, mercury containing slipring, specially suited for transmission of thermocouple signals. A price of such a unit has not yet been received and it is unclear whether an additional unit is needed for the power transmission.

5.6.4. Fan

A suitable radial fan has been found at Induvac (Zoetermeer). The price of the unit (€661) does not include a controller. According to Induvac, a frequency controller can be connected to the power supply to regulate the air flow. The price of such a device is estimated at €500. The supplier has confirmed that the fan can be used in any orientation and that even the output direction can be reversed. Another advantage of the specified unit is its geometry; the dimensions of the outlet are 125×180 mm, which make it directly applicable without the need for a coupling. The specifications of the concerned fan have been used to generate the plot in Figure 4.9.

5.6.5. DC Motor

An inquiry for a DC Motor has been send to Orientalmotor (Basingstoke, UK). Multiple solutions have been provided, all in the range of 0.1 to 0.2 kW. The motors all come with a speed controller, working on AC input. The holding torques range from 0.6 to 1.7 Nm. However, these torques are adjusted with a gearbox to achieve the right velocity range. The price for a unit with gearbox lies around €400. With a hollow shaft gearbox included, this price becomes €700.

5.6.6. Ultrasonic transducers

No suitable suppliers have yet been found for the ultrasound thickness sensors. Therefore the exact price and specifications of these devices are unknown. More time is needed to examine this technology and thus the implementation in the TU Delft test rig is postponed.

5.6.7. Frame

Cadans Engineering has provided estimations that the manufacture of a steel frame, including purchase of the requisites will cost € 4000 to 5000.



Conclusion

In order to conclude this thesis, a summary of the design choices is presented together with their consequences and conclusive remarks. The problem statement from the introduction is then recalled to assess whether the imposed requirements have been met. Finally a number of recommendations is made.

6.1. Conclusive summary

A design has been made of an experimental rotating heat pipe setup. Its goal is to assist in the development of the heat pipe assisted annealing project, by facilitating observations that provide insight in the performance and internal phenomena of the rotating heat pipe.

For the operation, a temperature range (423 to 873 K) and upper pressure limit (0.5 MPa) were imposed. Two working fluids —biphenyl and phenanthrene— have been identified that are expected to cover the specified range up to 717 K while complying with the pressure limit and criteria concerning health, environment and stability. It was found that performance is subordinate to these criteria due to lack of alternatives and the capability of the selected materials to deliver sufficient heat transfer for implementation in a heat pipe assisted continuous annealing line. A third material, cesium, was found to cover the upper part of the specified temperature region (723 to 873 K) while satisfying the stability criterion. Yet for safe deployment, an inert environment is required, which cannot be provided at the P&E laboratory. Therefore this material can serve in a heat pipe assisted continuous annealing line but cannot be included in the TU Delft test rig. Thus the temperature range of the test rig is limited to 423 to 723 K. A fourth type of working fluid, containing siloxanes, seems suitable as well in the lower part of the temperature range. Although biphenyl is deemed a better option, siloxanes can be included in the tests as well for research purposes. It was found that 316 stainless steel is a suitable material in combination with all the suggested working fluids.

The working fluid study has disclosed how critical the cleanliness of the heat pipe and purity of the working fluid are. Even when taking all the necessary precautions, non-condensable gases can still form due to unforeseen reasons. Therefore the designed test setup gains the additional requirement of serving as a lifetest facility for the working fluids. Additionally, to avoid complications with the heat pipe cleanliness, each working fluid needs its own heat pipe. Consequentially, the setup needs to support the replacement of heat pipes.

Further design requirements, concerning the dimensions of the heat pipe, heat source and sink and rotational velocity have, as far as possible, been based on resemblance of the operating conditions in a heat pipe assisted continuous annealing line. The design calculations have been made conservatively, to ensure stable operation within the specified ranges. Accordingly, the maximum design temperature was $773\,\mathrm{K}$. Heat pipe dimensions were established at a $500\,\mathrm{mm}$ length, $60\,\mathrm{mm}$ outer diameter and $50\,\mathrm{mm}$ inner diameter in order to allow for a moderately sized setup and to enable comparison with data and models of other rotating heat pipe studies. With a shell thickness of $5\,\mathrm{mm}$ the heat pipe can withstand all the existing stresses and is not subjected to creep over the entire temperature range. The heat pipe can operate up to a maximal rotational velocity of $1000\,\mathrm{rpm}$ and covers all known flow regimes. At the condenser, $30\,\mathrm{kW}\,\mathrm{m}^{-2}$ can be extracted, which resembles the heat flux that is typ-

58 6. Conclusion

ically applied to a steel strip in the heat pipe assisted continuous annealing line. At the evaporator, an additional $56.6\,\mathrm{kW\,m^{-2}}$ is added to account for convective and radiative losses over the heat pipe shell. The resulting axial heat flow stays below the operating limits for a rotating heat pipe over the relevant temperature range. However, the entrainment limit was not tested and during startup from room temperature, a more restricted heat input is advised.

The heating and cooling technologies have primarily been selected based on their capacity to supply the desired heat flows and the uniformity of their heating profile. Induction heating is contactless, which is useful because of the rotation, and meets all the requirements. Yet the technology turns out to be too expensive to be included in the test rig. Liquid cooling is dismissed because the required equipment impedes modularity. For the addition of heat, trace heating is selected in the form of a band heater, of which two units are likely needed to cover the evaporator length. A rotary electrical coupling is needed to supply power to the device. A slip ring with high current channels is capable of doing so. The exact heat input can be controlled via a controller that receives temperature feedback from the heater.

The cooling can be performed performed by a fan providing an air flow to a duct with small water droplets ($<100\,\mu m$) added to it to create a mixture of air and mist. By itself, the air flow is not expected to provide enough capacity under all circumstances. The cooling capacity can be controlled by varying both the air flow and water mass fraction. The exact rates can only be roughly estimated and thus feedback concerning the heat flows is needed.

The rotation of the heat pipe is brought about by a DC motor. The device is placed directly on the shaft for easy alignment and is controlled by regulating its voltage.

The placement of multiple pairs of thermocouples in the heat pipe shell facilitates both the measurement of radial heat flux as well as the shell temperature. If two pairs are placed at each section, the temperature profile over the length can be observed. The heat flow at each section is obtained and a balance can be created. Furthermore, having an extra sensor at each section ensures that the heat pipe is not void in case of a failure, for replacement is not possible due to the complexity of the manufacturing. The shell thermocouples can participate in the feedback systems of the heating and cooling equipment. The temperature and (indirectly) the pressure inside the heat pipe can be monitored via thermocouples placed in the vapor space. Information concerning the stability of the working fluid and the formation of non-condensable gases can be derived from the development of temperature gradients in the vapor space. Therefore, extra thermocouples are placed in the condenser section. The measurement of the liquid layer thickness is required for derivation of the vapor and liquid velocities. Ultrasonic measurements from outside the shell are most suitable to obtain the thickness without compromising the measurement itself. The implementation is complicated however, due to unfamiliarity with the required equipment and the rotation of the heat pipe. Thus for now, the focus lies on temperature, pressure and heat flux observations. At a later stage, mass balance enabling observations can be implemented as well.

A control system ensures operation within specified limits and provides additional safety for the operator and spectators. Furthermore it registers measured data and provides a visual representation of it. Settling and maintaining of stable operating conditions is done by the operator, who relies on the control system for feedback on the operating parameters, such as temperature and rotational velocity.

Safe operation is established through a wide range of measures. Some of these concerned the selection of working fluids and equipment. The control system and presence of safeguards such as emergency buttons and shielding further assist in securing safety.

The cleaning and filling of the heat pipe prior to commissioning are critical and complicated procedures that require much caution and preparation. Even more troublesome could be the manufacture of the heat pipe due to the required sealing, delicate placement of sensors and handling of the leads; with the modularity and high rotational velocity, further complicating the process. To additional parties can provide the experience necessary for handling of these issues. Thermo-Electra will manufacture the heat pipe and Cadans Engineering will further develop the design so that modularity and the rotation can both be achieved. The entire setup will be manufactured by DEMO.

For the supply of auxiliary equipment, a number of parties have been contacted. Received equipment specifications confirm that the desired technologies are feasible. The total price of the equipment so far is approximately € 8500.

6.2. Discussion of requirements

The goal of the this thesis was to design a setup that could comply with a number of imposed requirements. These were presented in the introduction and are now recalled in order to assess whether the design goals have been met.

- A number of observations were to be facilitated by the test rig. All observations concerning temperatures, pressures, heat flows and rotational velocity have been met, either directly or indirectly. The observations concerning thickness and velocity of the liquid and vapor have not (practically) been met. The required technology has been identified, yet the implementation in the test setup is not yet completed due to its complexity.
- The setup can cover the largest part of the temperature range without passing the pressure limit, except for the last 150 K. This is due to conflict with the another requirement, i.e. safety.
- Working fluids have been identified that can cover the entire temperature range (and beyond)
 while meeting criteria of vapor pressure, heat transfer characteristics, long term stability and
 safety.
- The designed heat pipe is compatible with all the working fluids and facilitates a part of the measurements. The operating conditions closely resemble those of a continuous annealing line.
- The designed setup can serve as a test facility for the project but can also be used by students for educational practicals. This is enabled through manual control and visual feedback. Furthermore, necessary safety measures have been implemented.
- Arrangements have been made for the supply of auxiliary equipment and the manufacture of the setup.

As all of the requirements have (partially) been met, it can be concluded that the desired setup can and will be created.

6.3. Recommendations

Based on the experiences obtained during the design of the setup and the aforementioned conclusions a number of recommendations can be made.

6.3.1. Materials

In Chapter 2, it was seen that only a small number of working fluids are applicable if all requirements need to be met. If it turns out that the advised working fluids are unsuited after all, very few alternatives are available. Unfortunately, raising the pressure limit would not solve this problem. For most fluids have a too high decomposition rate at the temperatures corresponding to the their vapor pressures above 0.5 MPa. What could however be a solution is the use of highly inert alloys as shell material in combination with halide working fluids or the coating of the inner shell with an inert material.

Eutectic siloxane mixtures are currently under development and could also prove to be a viable heat pipe fluid.

6.3.2. High temperature alkali setup

If the heat pipe assisted annealing project is to succeed, the upper temperature range needs to be covered as well. By now it has become clear that cesium or other alkali metals such as potassium are needed. To gain experience with the operation and manufacturing of alkali heat pipes a third test setup could be constructed.

6.3.3. Visual access

Since the observation of internal flow still remains a difficult issue, a special heat pipe could be manufactured that enables visual observation of the liquid layer. The heat pipe sides could for example be made out of a transparent material. A fully transparent heat pipe could also be made although it would likely be operating at lower temperatures due to the higher thermal resistance or lower temperature resistance of the used materials.

60 6. Conclusion

6.3.4. Ultrasonic technology

It is expected that the use of an ultrasonic transducer is a suited technology to measure the liquid thickness without affecting the internal flows. Unfortunately the technology could not be implemented in the design. Because of the adequacy of the technology, it is advised to investigate how it can be implemented at a later stage.

6.3.5. Additional experiments

The heat pipe setup has been designed so that a number of important measurements are enabled. Yet it also facilitates a number of other unintended experiments. The convective heat loss from a high temperature surface could be investigated. Furthermore, literature concerning convection from a rotating cylinder in a crossflow is relatively scare. No literature regarding the specific situation of mist cooling of a rotating surface has been encountered at all.

- [1] J. T. Anderson and O. A. Saunders. Convection from an Isolated Heated Horizontal Cylinder Rotating about Its Axis. *Proceedings of the Royal Society A: Mathematical, Physical and Engineering Sciences*, 217(1131):555–562, May 1953. ISSN 1364-5021. doi: 10.1098/rspa.1953.0080. URL http://rspa.royalsocietypublishing.org/cgi/doi/10.1098/rspa.1983.0054http://rspa.royalsocietypublishing.org/cgi/doi/10.1098/rspa.1953.0080.
- [2] William G. Anderson, John H. Rosenfeld, Angirasa Devarakonda, and Ye Mi. Evaluation of Heat Pipe Working Fluids In The Temperature Range 450 to 700 K. In *AIP Conference Proceedings*, volume 699, pages 20–27. AIP, 2004. ISBN 0735401713. doi: 10.1063/1.1649553. URL http://scitation.aip.org/content/aip/proceeding/aipcp/10.1063/1.1649553.
- [3] William G. Anderson, Richard Bonner, Peter Dussinger, John Hartenstine, David Sarraf, and Ivan E. Locci. Intermediate Temperature Fluids Life Tests Experiments. *5th International Energy Conversion Engineering Conference and Exhibit (IECEC)*, (June):25–27, 2007. doi: doi:10.2514/6.2007-4808. URL http://dx.doi.org/10.2514/6.2007-4808.
- [4] William G. Anderson, Sanjida Tamanna, Calin Tarau, John Hartenstine, and David Ellis. Intermediate Temperature Heat Pipe Life Tests and Analyses. In 43rd International Conference on Environmental Systems, pages 1–23, Reston, Virginia, July 2013. American Institute of Aeronautics and Astronautics. ISBN 978-1-62410-215-8. doi: 10.2514/6.2013-3304. URL http://arc.aiaa.org/doi/abs/10.2514/6.2013-3304.
- [5] G. Angelino and C. Invernizzi. Cyclic Methylsiloxanes as Working Fluids for Space Power Cycles. *Journal of Solar Energy Engineering*, 115(August):130, 1993. ISSN 01996231. doi: 10.1115/1. 2930039.
- [6] D S Aribike and A A Susu. Kinetics and mechanism of the thermal cracking of n-heptane. Thermochimica Acta, 127:247-258, 1988. doi: 10.1016/0040-6031(88)87501-4. URL http://linkinghub.elsevier.com/retrieve/pii/0040603188875014\$\backslash\$nfile:///D:/EBooksandProfesionalDocuments/ProfesionalEngineeringDocuments/Papers/ScienceDirectPapers/ReactionNetworkGeneration/1-s2.0-0040603188875014-main.pdf.
- [7] ASM International. ASM Handbook, Volume 1, Properties and Selection: Irons, Steels, and High Performance Alloys, volume 1. 10th edition, 1990. ISBN 0-87170-380-7.
- [8] Soe Sandar Aung, Han Phyo Wai, and Nyein Nyein Soe. Design Calculation and Performance Testing of Heating Coil in Induction Surface Hardening Machine. *World Academu of Science, Engineering and Technology*, 2(6):416–420, 2008. doi: 10.1.1.192.9022.
- [9] J. Baker, T. Oliver, L. Lin, R. Ponnapan, and J. Leland. Correlations of Critical Froude Number for Annular-Rimming Flow in Rotating Heat Pipes. *Journal of Fluids Engineering*, 123(4): 909, 2001. ISSN 00982202. doi: 10.1115/1.1411967. URL http://fluidsengineering.asmedigitalcollection.asme.org/article.aspx?articleid=1484338.
- [10] Rémi Bertossi, Noëlie Guilhem, Vincent Ayel, Cyril Romestant, and Yves Bertin. Modeling of heat and mass transfer in the liquid film of rotating heat pipes. *International Journal of Thermal Sciences*, 52:40–49, February 2012. ISSN 12900729. doi: 10.1016/j.ijthermalsci.2011.09. 017. URL http://linkinghub.elsevier.com/retrieve/pii/S1290072911002869.

[11] C.A. Busse. Theory of the ultimate heat transfer limit of cylindrical heat pipes. *International Journal of Heat and Mass Transfer*, 16(1):169–186, January 1973. ISSN 00179310. doi: 10.1016/0017-9310(73)90260-3. URL http://www.sciencedirect.com/science/article/pii/0017931073902603http://linkinghub.elsevier.com/retrieve/pii/0017931073902603.

- [12] C. Camino, S. M. Lomakin, and M. Lazzari. Polydimethylsiloxane thermal degradation part 1. Kinetic aspects. *Polymer*, 42(6):2395–2402, 2001. ISSN 00323861. doi: 10.1016/S0032-3861(00)00652-2.
- [13] Z.Q. Chen, J.C. Hermanson, M.A. Shear, and P.C. Pedersen. Ultrasonic monitoring of interfacial motion of condensing and non-condensing liquid films. *Flow Measurement and Instrumentation*, 16(6):353–364, December 2005. ISSN 09555986. doi: 10.1016/j.flowmeasinst.2005.06.002. URL http://linkinghub.elsevier.com/retrieve/pii/S0955598605000683.
- [14] S. W. Churchill and M. Bernstein. A Correlating Equation for Forced Convection From Gases and Liquids to a Circular Cylinder in Crossflow. *Journal of Heat Transfer*, 99(2): 300, 1977. ISSN 00221481. doi: 10.1115/1.3450685. URL http://heattransfer. asmedigitalcollection.asme.org/article.aspx?articleid=1436684.
- [15] Andre Colas. Silicones: Preparation, Properties and Performances. Technical report, Dow Corning, 2005.
- [16] T.C. Daniels and F.K. Al-Jumaily. Investigations of the factors affecting the performance of a rotating heat pipe. *International Journal of Heat and Mass Transfer*, 18(7-8):961–973, 1975. ISSN 00179310. doi: 10.1016/0017-9310(75)90190-8.
- [17] T.C. Daniels and R.J. Williams. Experimental temperature distribution and heat load characteristics of rotating heat pipes. *International Journal of Heat and Mass Transfer*, 21(2):193–201, February 1978. ISSN 00179310. doi: 10.1016/0017-9310(78)90223-5. URL http://dx.doi.org/10.2514/6.1978-416http://arc.aiaa.org/doi/abs/10.2514/6.1978-416http://linkinghub.elsevier.com/retrieve/pii/0017931078902235.
- [18] D.R. De Halas. *Kinetics of the decomposition of organic reactor coolants*. Hanford Atomic Products Operation, 1958.
- [19] Angirasa Devarakonda. Thermo-Physical Properties of Intermediate Temperature Heat Pipe Fluids. In *AIP Conference Proceedings*, volume 746, pages 179–186, Washington, 2005. National Aeronautics and Space Administration, AIP. doi: 10.1063/1. 1867133. URL http://gltrs.grc.nasa.govhttp://scitation.aip.org/content/aip/proceeding/aipcp/10.1063/1.1867133.
- [20] Peter Dussinger, William G. Anderson, and Eric Sunada. Design and Testing of Titanium-Cs and Titanium-K Heat Pipes. In *3rd International Energy Conversion Engineering Conference*, pages 1–9, Reston, Virigina, August 2005. American Institute of Aeronautics and Astronautics. ISBN 978-1-62410-062-8. doi: 10.2514/6.2005-5631. URL http://arc.aiaa.org/doi/abs/10.2514/6.2005-5631.
- [21] S H Ehrman, S K Friedlander, and M R Zachariah. Characteristics of SiO2/TiO2 nanocomposite particles formed in a premixed flat flame. *Journal of Aerosol Science*, 29(5-6):687–706, 1998. ISSN 00218502. doi: 10.1016/S0021-8502(97)00454-0. URL <GotoISI>://WOS: 000074107300017.
- [22] Reda I. Elghnam. Experimental and numerical investigation of heat transfer from a heated horizontal cylinder rotating in still air around its axis. Ain Shams Engineering Journal, 5 (1):177–185, March 2014. ISSN 20904479. doi: 10.1016/j.asej.2013.09.008. URL http://www.sciencedirect.com/science/article/pii/s2090447913000944http://linkinghub.elsevier.com/retrieve/pii/s2090447913000944.

[23] I C Finlay. An analysis of heat transfer during flow of an air/water mist across a heated cylinder. *The Canadian Journal of Chemical Engineering*, 49(3):333–339, June 1971. ISSN 00084034. doi: 10. 1002/cjce.5450490307. URL http://pcp.sagepub.com/lookup/doi/10.1243/PIME_CONF_1967_182_239_02http://doi.wiley.com/10.1002/cjce.5450490307.

- [24] P. Gierszewski and R.E. Hollies. Organic coolants and their applications to fusion reactors. Nuclear Engineering and Design. Fusion, 4(2):223–236, January 1987. ISSN 0167899X. doi: 10. 1016/0167-899X(87)90006-1. URL http://linkinghub.elsevier.com/retrieve/pii/0167899X87900061.
- [25] Vernon H Gray. The rotating heat pipe-a wickless, hollow shaft for transferring high heat fluxes. 1969.
- [26] M. Groll, D. Heine, and T. Spendel. Heat recovery units employing reflux heat pipes as components. Technical report, Commission of the European Communities, Stutgart, 1984.
- [27] Lawrence R. Grzyll, D. D. Back, C. Ramos, and N. A. Samad. Characterization and Testing of Novel Two-Phase Working Fluids for Spacecraft Thermal Management Operating Between 300 Deg. C and 400 Deg. C. Technical report, MAINSTREAM ENGINEERING CORP ROCKLEDGE FL CHEMICAL SYSTEMS DIV., 1994.
- [28] L. E. Gusel'nikov, N. S. Nametkin, T. Kh. Islamov, A. A. Sobtsov, and V. M. Vdovin. The mechanism of the thermal conversions of methylcyclosiloxanes. *Bulletin of the Academy of Sciences of the USSR Division of Chemical Science*, 20(1):71–75, January 1971. ISSN 0568-5230. doi: 10.1007/BF00849322. URL http://link.springer.com/10.1007/BF00849322.
- [29] Walter J. Hamer, Marjorie S. Malmberg, and Bernard Rubin. Theoretical Electromotive Forces for Cells Containing a Single Solid or Molten Chloride Electrolyte. *Journal of The Electrochemical Society*, 103(1):8, 1956. ISSN 00134651. doi: 10.1149/1.2430236.
- [30] Walter J. Hamer, Marjorie S. Malmberg, and Bernard Rubin. Theoretical Electromotive Forces for Cells Containing a Single Solid or Molten Fluoride, Bromide, or Iodide. *Journal of The Electrochemical Society*, 112(7):750, 1965. ISSN 00134651. doi: 10.1149/1.2423683. URL http://jes.ecsdl.org/cgi/doi/10.1149/1.2423683.
- [31] Aydin Jalali, M M Yousef Motamedhashemi, Fokion Egolfopoulos, and Theodore Tsotsis. Fate of Siloxane Impurities During the Combustion of Renewable Natural Gas. Combustion Science and Technology, 185(6):953–974, June 2013. ISSN 0010-2202. doi: 10.1080/00102202.2013. 766606. URL http://www.tandfonline.com/doi/abs/10.1080/00102202.2013. 766606.
- [32] George J. Janz. Molten Salts Handbook. 2013. ISBN 9780323144834. doi: 10. 1016/B978-0-12-395642-2.50040-X. URL http://books.google.com/books?id= K9jXCwMCZeQC.
- [33] I.B. Johns, E.A. McElhill, and J.O. Smith. Thermal Stability of Some Organic Compounds. *Journal of Chemical & Engineering Data*, 7(2):277–281, April 1962. ISSN 0021-9568. doi: 10. 1021/je60013a036. URL http://dx.doi.org/10.1021/je60013a036http://pubs.acs.org/doi/abs/10.1021/je60013a036.
- [34] H Jouhara and a J Robinson. An experimental study of small-diameter wickless heat pipes operating in the temperature range 200c to 450c. Heat Transfer Engineering, 30(13): 1041-1048, 2009. ISSN 0145-7632. doi: 10.1080/01457630902921113. URL http://www.scopus.com/inward/record.url?eid=2-s2.0-67651229121&partnerID= 40&md5=fd6cff7b42a75dd239fab9d343bf43d4.
- [35] G. Juppe, M. Alvarenga, and H. Hannaert. The Pyrolytic Decomposition of Terphenyls. Technical report, European Atomic Energy Community, 1964.

[36] T. Kamei and A. Serizawa. Measurement of 2-dimensional local instantaneous liquid film thickness around simulated nuclear fuel rod by ultrasonic transmission technique. *Nuclear Engineering and Design*, 184(2-3):349–362, August 1998. ISSN 00295493. doi: 10.1016/S0029-5493(98)00208-8. URL http://linkinghub.elsevier.com/retrieve/pii/S0029549398002088.

- [37] Jin S Lee and Chul J Kim. Heat transfer and internal flow characteristics of a coil-inserted rotating heat pipe. *International Journal of Heat and Mass Transfer*, 44(18):3543–3551, 2001. ISSN 0017-9310. doi: DOI:10.1016/S0017-9310(00)00317-3. URL http://www.sciencedirect.com/science/article/pii/S0017931000003173.
- [38] S L Lee, Z H Yang, and Y Hsyua. Cooling of a Heated Surface by Mist Flow. Journal of Heat Transfer, 116(1):167, 1994. ISSN 00221481. doi: 10.1115/1.2910851. URL http://www.scopus.com/inward/record.url?eid=2-s2.0-0028042470&partnerID=40&md5=6662237f4b029ed6f5d8189f0e03fc1dhttp://heattransfer.asmedigitalcollection.asme.org/article.aspx?articleid=1441605.
- [39] Sookwan Lee, Jeeman Park, Piljong Lee, and Moohwan Kim. Heat Transfer Characteristics during Mist Cooling on a Heated Cylinder. *Heat Transfer Engineering*, 26(8):24–31, October 2005. ISSN 0145-7632. doi: 10.1080/01457630591003718. URL http://www.tandfonline.com/doi/abs/10.1080/01457630591003718.
- [40] E.W. Lemmon, M.L. Huber, and M.O. McLinden. *NIST Standard Reference Database 23: Reference Fluid Thermodynamic and Transport Properties REFPROP*. National Institute of Standards and Technology, Standard Reference Data Program, version 9.0 edition, 2010.
- [41] P. Leveque. Organic Liquids as Reactor Codants and Moderators. Technical report, IAEA, Vienna, 1967.
- [42] Qing Lu, N.V. Suryanarayana, and Christodoulous Christodoulu. Film thickness measurement with an ultrasonic transducer. *Experimental Thermal and Fluid Science*, 7(4):354–361, November 1993. ISSN 08941777. doi: 10.1016/0894-1777(93)90058-Q. URL http://linkinghub.elsevier.com/retrieve/pii/089417779390058Q.
- [43] G. Paulussen. Continuous heat treatment using heat pipes. Technical report, Corus, 2009.
- [44] G. Paulussen. Heat pipe assisted annealing treatment, 2011. Pat. nr. WO2011012257 A1.
- [45] G. Paulussen. Test plan for heat pipe assisted annealing proof of principle. Technical report, Tata Steel, 2012.
- [46] G. Paulussen. Heat pipe assisted annealing phase 2b final report. Technical report, Tata Steel, 2014.
- [47] Robert N. Pease and John M. Morton. Kinetics of Dissociation of Typical Hydrocarbon Vapors 1. *Journal of the American Chemical Society*, 55(8):3190–3200, August 1933. ISSN 0002-7863. doi: 10.1021/ja01335a021. URL http://pubs.acs.org/doi/abs/10.1021/ja01335a021.
- [48] Peder C. Pedersen, Zeljko Cakareski, and James C. Hermanson. Ultrasonic monitoring of film condensation for applications in reduced gravity. *Ultrasonics*, 38(1-8):486–490, March 2000. ISSN 0041624X. doi: 10.1016/S0041-624X(99)00214-0. URL http://linkinghub.elsevier.com/retrieve/pii/S0041624X99002140.
- [49] H. Peller, V Lippig, D Straub, and R Waibel. Thermofluiddynamic experiments with a heated and rotating circular cylinder in crossflow. Experiments in Fluids, 2(3):113–120, 1984. ISSN 0723-4864. doi: 10.1007/BF00296425. URL http://link.springer.com/10.1007/BF00296425.
- [50] R. Ponnappan, Q. He, and J. E. Leland. Test Results of Water and Methanol High-Speed Rotating Heat Pipes. *Journal of Thermophysics and Heat Transfer*, 12(3):391–397, July 1998. ISSN 0887-8722. doi: 10.2514/2.6350. URL http://arc.aiaa.org/doi/abs/10.2514/2.6350.

[51] D.A. Reay, P.A. Kew, and R.J. McGlen. Heat Pipes - Theory, Design and Applications. Butterworth-Heinemann, an imprint of Elsevier, Kidlington, Oxford, UK, 6th edition, 2014. ISBN 9780080982663. doi: 10.1016/B978-0-08-098266-3.00009-1. URL http://linkinghub.elsevier.com/retrieve/pii/B9780080982663000091.

- [52] Robert S Reid. Alkali Metal Heat Pipe Life Issues. pages 1–14, 2004.
- [53] Valery Rudnev, Don Loveless, Raymond L. Cook, and Micah Black. *Handbook of Induction Heating*. 2003. ISBN 0824708482. URL http://www.asminternational.org/web/hts/home/-/journal content/56/10192/75024G/PUBLICATION.
- [54] Elric W. Saaski and Peter C. Owzarski. Two-Phase Working Fluids for the Temperature Range 50° to 350°C. Technical report, NASA Lewis Research Center, Cleveland, Ohio, 1977.
- [55] F. Song, D. Ewing, and C. Y. Ching. Experimental investigation on the heat transfer characteristics of axial rotating heat pipes. *International Journal of Heat and Mass Transfer*, 47(22):4721–4731, 2004. ISSN 00179310. doi: 10.1016/j.ijheatmasstransfer.2004.06.001.
- [56] F. Song, D. Ewing, and C.Y. Ching. Heat transfer in the evaporator section of moderate-speed rotating heat pipes. *International Journal of Heat and Mass Transfer*, 51(7-8):1542–1550, April 2008. ISSN 00179310. doi: 10.1016/j.ijheatmasstransfer.2007.07.020. URL http://linkinghub.elsevier.com/retrieve/pii/S0017931007004838.
- [57] N. Sozbir, Y. W. Chang, and S. C. Yao. Heat Transfer of Impacting Water Mist on High Temperature Metal Surfaces. *Journal of Heat Transfer*, 125(1):70, 2003. ISSN 00221481. doi: 10.1115/1. 1527913. URL http://heattransfer.asmedigitalcollection.asme.org/article.aspx?articleid=1446224.
- [58] Calin Tarau, David B. Sarraf, Ivan E. Locci, and William G. Anderson. Intermediate Temperature Fluids Life Tests Theory. In AIP Conference Proceedings, volume 880, pages 137–146. AIP, 2007. doi: 10.1063/1.2437450. URL http://scitation.aip.org/content/aip/proceeding/aipcp/10.1063/1.2437450.
- [59] T. Howard Thomas and T. C. Kendrick. Thermal analysis of polydimethylsiloxanes. I. Thermal degradation in controlled atmospheres. *Journal of Polymer Science Part A-2: Polymer Physics*, 7 (3):537–549, 1969. ISSN 04492978. doi: 10.1002/pol.1969.160070308. URL http://doi.wiley.com/10.1002/pol.1969.160070308.
- [60] C. Tien and K. Chung. Entrainment limits in heat pipes. In 3rd International Heat Pipe Conference, Reston, Virigina, May 1978. American Institute of Aeronautics and Astronautics. doi: 10.2514/6.1978-382. URL http://arc.aiaa.org/doi/abs/10.2514/6.1978-382.
- [61] C.A. Tudbury. Basics of Induction Heating, volume 1. John F. Rider Publisher, Inc., 1960.
- [62] T.P. van der Stelt and P. Colonna. Experimental vapor pressures and thermodynamic models of perfluorocarbons PP80 and PP90. Fluid Phase Equilibria, 370:50-57, 2014. ISSN 03783812. doi: 10.1016/j.fluid.2014.02.027. URL http://www.sciencedirect.com/science/article/pii/S0378381214001228.
- [63] L. L. Vasil'ev, G M Volokhov, A S Gigevich, and M I Rabetskii. Heat pipes based on naphthalene. Journal of Engineering Physics, 54(6):623–626, June 1988. ISSN 0022-0841. doi: 10.1007/BF01102648. URL http://link.springer.com/10.1007/BF01102648.
- [64] Theresa Weith, Florian Heberle, Markus Preiß inger, and Dieter Brüggemann. Performance of Siloxane Mixtures in a High-Temperature Organic Rankine Cycle Considering the Heat Transfer Characteristics during Evaporation. *Energies*, 7(9):5548–5565, August 2014. ISSN 1996-1073. doi: 10.3390/en7095548. URL http://www.mdpi.com/1996-1073/7/9/5548/.
- [65] Frank M. White. Fluid Mechanics. McGraw-Hill, 4 edition, 1998.



Material data

This appendix contains all the methodology and sources that have been used to obtain the material properties encountered throughout this thesis. All the thermophysical properties were required as a function of temperature. For the more regularly applied materials, such relations could simply be obtained from databases like RefProp. For the other, less frequently applied materials, parametric equations derived from empirical data were used. In the case of insufficient data (only for enthalpies of vaporization) an estimative correlation was used. In some cases, mostly for the halides, properties have been calculated outside of the temperature range that they were derived for, possibly resulting in an unknown error. Since there was no alternative, and the data is only used for preliminary indications and performance estimations, this is deemed acceptable.

Properties used in the design calculations, i.e. biphenyl, steel and air are treated separately because different properties were needed.

A.1. Thermophysical properties

Table A.1 and A.2 provide references to the literature containing the property data. In some cases, the applied equation is listed as well. Often the calculation methods applied in the literature are commonly encountered property correlations. Since they are recurring and have proved to be useful tools, some attention has been given to describing them.

A.1.1. Empirical property correlations

Vapor pressures The Antoine equation is the most widely used for relating vapor pressure to temperature and is accurate within the range it was derived for. It is given by

$$\log_{10}\left(p^{\text{sat}}\right) = A - \frac{B}{C + T} \tag{A.1}$$

with A, B and C material dependent parameters.

The Wagner-Ambrose equation is very accurate for temperatures ranging from triple point to critical point [42]. It is given by

$$\ln(p_{\rm r}^{\rm sat}) = \frac{A\tau + B\tau^{1.5} + C\tau^{2.5} + D\tau^5}{T_{\rm r}}$$
 (A.2)

with $\tau = 1 - T_{\rm r}$ and $T_{\rm r} = T/T_{\rm c}$. A, B, C and D are material dependent parameters.

The Riedel equation, like the Wagner-Ambrose equation, performs well over a wide temperature range. It is given by

$$ln psat = A + B/T + C ln T + DT6$$
(A.3)

with A, B, C and D material dependent parameters.

68 A. Material data

Enthalpy of vaporization The Pitzer equation provides a close approximation of the enthalpy of vaporization within the region $0.6 < T_r < 1.0$. It is given by

$$\frac{L}{RT_{\rm c}} = 7.08(1 - T_{\rm f})^{0.354} + 10.95\omega(1 - T_{\rm f})^{0.456}$$
(A.4)

with ω the acentric factor:

$$\omega = -\log_{10}(p_{\rm r}^{\rm sat}) - 1 \tag{A.5}$$

where $p_{\rm r}^{\rm sat}=\frac{p^{\rm sat}}{p_{\rm c}}$ is the reduced saturation pressure at $T_{\rm r}=0.7$. The Watson equation fits a data point to the typical shape of a temperature versus enthalpy of vaporization curve. Doing so, other data points can be found as follows

$$L(T_2) = L(T_1) \left(\frac{1 - T_{r_2}}{1 - T_{r_1}}\right)^{0.38} \tag{A.6}$$

here $L(T_1)$ and T_{r_1} comprise the initial data point so that $L(T_2)$ can be calculated.

A.1.2. Reference tables

Table A.1: Correlations and sources for temperature dependent properties of organic materials.

Material	$p_{sat}(T)$	$ ho_{I}(T)$	$\mu_{I}(T)$	$\lambda_{I}(T)$	L(T)
D ₃	Riedel eq. [19]	-	-	-	-
D_4	RefProp [34]	RefProp	RefProp	RefProp	RefProp
D_5	RefProp [34]	-	-	-	-
D_6	RefProp [34]	-	-	-	-
D_7	Riedel eq. [19]	-	-	-	-
D_8	Riedel eq. [19]	-	-	-	-
D_9	Riedel eq. [19]	-	-	-	-
decane	RefProp [34]	RefProp	RefProp	RefProp	RefProp
dodecane	RefProp [34]	RefProp	RefProp	RefProp	RefProp
Dowtherm A	Dow Co. [12]	Dow Co.	Dow Co.	Dow Co.	Reay et al. [43]
heptane	RefProp [34]	RefProp	RefProp	RefProp	RefProp
MM	RefProp [34]	-	-	-	-
MDM	RefProp [34]	-	-	-	-
MD_2M	RefProp [34]	-	-	-	-
MD_3M	RefProp [34]	-	-	_	-
MD_4M	RefProp [34]	-	-	-	-
MD_5M	Riedel eq. [19]	-	-	-	-
MD_6M	Riedel eq. [19]	-	-	-	-
naphthalene	Wagner-Ambrose eq. [1]	Riedel eq. [24]	Yaws [61]	Yaws [61]	Pitzer eq. [42]
nonane	RefProp [34]	RefProp	RefProp	RefProp	RefProp
octane	RefProp [34]	RefProp	RefProp	RefProp	RefProp
PP80	Wagner-Ambrose eq. [56]	-	-	-	-
PP90	Wagner-Ambrose eq. [56]	-	-	-	-
phenanthrene	Riedel eq.(adapted) [38]	-	Yaws [61]	Yaws [61]	-
propylcyclohexane	RefProp [34]	RefProp	RefProp	RefProp	RefProp
m-terphenyl	Riedel eq.(adapted) [38]	-	-	-	-
o-terphenyl	Riedel eq.(adapted) [38]	Grzyll et al. [22]	Yaws [61]	Yaws [61]	Watson eq. [47]
p-terphenyl	Riedel eq.(adapted) [38]	-	-	-	-
toluene	RefProp [34]	RefProp	RefProp	RefProp	RefProp
undecane	CoolProp [7]	-	-	-	-
m-xylene	CoolProp [7]	-	-	-	-
o-xylene	CoolProp [7]	-	-	-	-
p-xylene	CoolProp [7]	-	-	-	-

Table A.2: Correlations and sources for temperature dependent properties of inorganic materials.

Material	$p_{sat}(T)$	$\rho_{I}(T)$	$\mu_{I}(T)$	$\lambda_{I}(T)$	L(T)
AlBr ₃	Antoine eq. [62]	Smithells [8]	Yaws [61]	Yaws [61]	Watson eq. [35]
Al_2l_6	Smithells [8]	-	-	-	-
BBr ₃	Smithells [8]	-	Yaws [61]	Yaws [61]	Watson eq. [35]
BI_3	Smithells [8]	-	-	-	Watson eq. [35]
BeBr ₂	Smithells [8]	-	-	-	-
BeCl ₂	Smithells [8]	-	-	-	-
Bel ₂	Smithells [8]	-	-	-	-
BiBr ₃	Smithells [8]	-	-	-	-
BiCl ₃	Smithells [8]	Janz [28]	Yaws [61]	-	Watson eq. [35]
cesium	Vargaftik et al. [58]	Lide [35]	Yaws [61]	Yaws [61]	Watson eq. [35]
GaBr₃	Smithells [8]	Smithells [8]	Yaws [61]	-	Watson eq. [35]
GaCl ₂	Smithells [8]	Smithells [8]	-	-	-
GaCl₃	Antoine eq. [62]	Smithells [8]	Yaws [61]	Yaws [61]	Watson eq. [35]
InCl	Smithells [8]	-	-	-	-
mercury	Wagner-Ambrose eq. [26]	Reay et al. [43]	Yaws [61]	Yaws [61]	Reay et al. [43]
potassium	Smithells [8]	Lide [35]	Yaws [61]	Yaws [61]	Watson eq. [35]
SbBr ₃	Smithells [8]	-	Yaws [61]	Yaws [61]	Watson eq. [35]
SbCl ₃	Smithells [8]	Smithells [8]	Yaws [61]	Yaws [61]	Watson eq. [35]
Sbl ₃	Smithells [8]	Janz [28]	-	Yaws [61]	Watson eq. [35]
sodium	Fink and Leibowitz [18]	-	-	-	-
SnBr ₄	Smithells [8]	-	-	Yaws [61]	Watson eq. [35]
SnCl ₄	Smithells [8]	Janz [28]	Yaws [61]	Yaws [61]	Watson eq. [35]
Snl₄	Smithells [8]	Smithells [8]	-	Yaws [61]	Watson eq. [35]
sulfur	Smithells [8]	Lide [35]	-	Yaws [61]	Watson eq. [35]
TiBr₄	Smithells [8]	Smithells [8]	-	-	Watson eq. [35]
TiCl ₄	Smithells [8]	Smithells [8]	Yaws [61]	-	Watson eq. [35]
Til ₄	Smithells [8]	Smithells [8]	-	-	Watson eq. [35]
water	RefProp [34]	RefProp	RefProp	RefProp	RefProp
TICI	Smithells [8]	-	-	-	-
ZnCl ₂	Smithells [8]	-	-	-	-

A.2. Decomposition rates

A large number of sources was studied in order to find decomposition rates as a function of temperature for as much relevant materials as possible. Since the conditions under which the decomposition takes place can significantly affect the rates, they are reported as well, in order to enable a comparison with the conditions inside the operating heat pipe. Table A.3 presents all the relevant information, if available.

70 A. Material data

Table A.3: The conditions and sources of the decomposition parameters used to generate Figures 2.4(a) to 2.5(c). A number of abbreviations is used in this table; their definition is as follows: CP - chromatographically pure, SR - static reactor, FR - flow reactor, SPST - single pulse shock tube, CFC - counterflow flame configuration, GC - gas chromotography, MS - mass spectrometry, S - separation, V - vacuum, ICoNG - in combustion of natural gas, PG - pyrex glass, SS - stainless steel, Q - quartz.

Material	Source	Purity [%]	Method	Analysis	Temperature [K]	Environment	Container
biphenyl	[63]	CP	SR	GC	695 - 719	V	PG & SS
biphenyl(2)	[14]	-	SR	MS	673 - 873	V	PG & SS
p-terphenyl	[29]	>99	SR	GC	693 - 760	V	PG
o-terphenyl	[52]	>99	SR	GC	692 - 755	V	SS
o-terphenyl(2)	[29]	>99	SR	GC	693 - 760	V	SS
m-terphenyl	[14]	-	SR	MS	673 - 873	V	PG & SS
toluene	[49]	-	-	-	=	-	-
toluene(2)	[55]	-	FR	S	953 - 1123	V	Si
m-xylene	[55]	-	FR	S	953 - 1123	V	Si
p-xylene	[55]	-	FR	S	953 - 1123	V	Si
o-xylene	[55]	-	FR	S	953 - 1123	V	Si
naphthalene(1)	[33]	-	SPST	GC	1350 - 1650	Ar	SS
naphthalene(2)	[9]	-	FR	MS & GC	<1273	Ar	Q
phenanthrene	[9]	-	FR	MS & GC	<1273	Ar	Q
MM	[50],[16]	-	FR	MS	300 - 673	V	Al_2O_3 , Q
MM(2)	[27]	99.5	CFC	MS & GC	<1800	ICoNG	-
MDM	[27]	98	CFC	MS & GC	<1800	ICoNG	-
MD_2M	[27]	97	CFC	MS & GC	<1800	ICoNG	-
D_4	[27]	98	CFC	MS & GC	<1800	ICoNG	-
$D_4(2)$	[13]	CP	SR	GC	767 - 842	V	Q
$D_4(3)$	[51]	98	FR	MS	1058 - 1197	Ar	Q
D_5	[23]	CP	SR & FR	GC	743 - 823	Ar	Q & SS
propylcyclohexane	[60]	>99	SR	MS & GC	648 - 723	V	SS
heptane(1)	[5]	99.7	SR	GC	933 - 1053	N_2	SS
heptane(2)	[41]	-	SR	S	823 - 903	V	PG
heptane(3)	[10]	-	SR	GC	793 - 953	Ar	SS
octane	[54]	95	FR	GC	1023 - 1073	N_2	SS
nonane	[32]	98.5	FR	GC	923 - 1023	N_2	SS
decane	[65]	>99	SR	-	673 - 723	V	Р
dodecane	[65]	>99	SR	-	673 - 723	V	Р
dodecane(2)	[64]	-	SR	MS & GC	673 - 723	N_2	SS

A.3. Properties of design materials A.3.1. Biphenyl

Table A.4: Correlations and sources for (temperature dependent) properties of biphenyl in liquid and vapor phase. The temperature range for which the properties were derived is listed as well.

Property	Range [K]	Source	Remarks
T_{c}		NIST Webbook [36]	
p_{c}		NIST Webbook [36]	
$p_{sat}(T)$	342 - 780	Mackay et al. [38]	
$\rho_{l}(T)$	574 - 673	Grzyll et al. [22]	
$\rho_{V}(T)$	342 - 780		Via Peng-Robinson EoS
$\mu_{l}(T)$	373 - 780	Yaws [61]	
$\mu_{V}(T)$	250 - 780	Yaws [61]	
$\lambda_{l}(T)$	342 - 650	Yaws [61]	
$\lambda_{V}(T)$	250 - 780	Yaws [61]	
L(T)	468 - 780	Pitzer eq. [42]	Checked by van der Stelt et al. [57]
$\sigma(T)$	574 - 673	Grzyll et al. [22]	

A.3.2. Air

All the properties of air have been obtained from the RefProp database [34].

A.3.3. Steel

Table A.5: The properties of stainless steel as used in the design calculations. In case the property has been applied as temperature dependent, the range for which the data was derived is given.

Property	Range	Source
ρ		ASM [6]
$ ho_{e}(T)$	273 - 900	Ho and Chu [25]
$\lambda(T)$	273 - 900	Ho and Chu [25]
$\epsilon(T)$	503 - 1143	Modest [39]
C_{p}		Cobb [11]
$\alpha(T)$	273 - 811	Cobb [11]



Life test data

B.1. Life test results and sources

Table B.1: Results of life test from various studies for working fluid - shell material combinations. A more detailed description of the shell materials can be found in Table B.2. Definitions: (S) success, (F) failure, (A) agrees, (D) disagrees, (NA) not available. For organics the results were compared with the decomposition model and for halides with the compatibility model. Notes: (1) 24 h cycles: 1.2 h at 653 K, 22 h at 598 K.

Working fluid	Shell	Temperature [K]	Duration [hours]	Outcome	Theory	Study
octane	mild steel (1)	503	39 420	S	Α	[20]
	stainless steel (3)	523	39 420	S	Α	[20]
toluene	mild steel (3)	392	700	S	Α	[49]
	aluminium (1)	403	3570	S	Α	[49]
	aluminium (1)	410	23 130	S	Α	[48]
	titanium (1)	523	8760	S	Α	[20]
	mild steel (1)	523	26 280	S	Α	[20]
	mild steel (2)	523	26 280	S	Α	[20]
	copper nickel(1)	553	8760	S	Α	[20]
	stainless steel (1)	553	26 280	S	Α	[20]
Dowtherm A	mild steel (4)	483	17 520	S	NA	[40]
	mild steel (3)	523	8382	S	NA	[31]
	stainless steel (11)	541	2453	S	NA	[31]
	titanium (1)	543	8760	S	NA	[20]
	mild steel (1)	543	39 420	S	NA	[20]
	mild steel (1)	573	39 420	F	NA	[20]
	mild steel (5)	623	39 420	F	NA	[20]
	stainless steel (3)	623	39 420	F	NA	[20]
	stainless steel (5)	541	2453	S	NA	[31]
	stainless steel (5)	664	1200	S	NA	[31]
	stainless steel (5)	673	1770	F	NA	[2]
	stainless steel (5)	723	180	F	NA	[2]
biphenyl	mild steel (3)	498	6174	S	Α	[31]
	aluminium (1)	514	8000	F	D	[48]
	mild steel (2)	523	8760	S	Α	[20]
	mild steel (3)	540	1675	S	Α	[49]
	stainless steel (1)	543	8760	S	Α	[20]
	aluminium (1)	548	2014	S	Α	[49]
	stainless steel (3)	548	6174	S	Α	[31]
	mild steel (3)	598	4040	F	D	[31]
	stainless steel (2)	623	5520	S	Α	[21]
	mild steel(2)	673	8760	F	Α	[20]
	stainless steel (1)	673	8760	F	Α	[20]

74 B. Life test data

Table B.1 continued

Working fluid	Shell	Temperature [K]	Duration [hours]	Outcome	Theory	Stud
	stainless steel (3)	673	1200	S	Α	[31]
	stainless steel (3)	695	366	F	D	[31]
	stainless steel (3)	748	72	F	Α	[31]
o-terphenyl	mild steel (3)	546	27 796	S	Α	[49]
	mild steel (3)	556	3570	S	Α	[49]
	aluminium (1)	563	672	F	D	[49]
	stainless steel (2)	598(1)	5520	S	Α	[21]
	stainless steel (2)	623	5520	S	D	[21]
o-terphenyl/	mild steel (2)	593	8760	F	D	[20]
m-terphenyl	stainless steel (1)	623	8760	F	Α	[20]
mixture	mild steel (2)	673	8760	F	Α	[20]
	stainless steel (1)	673	8760	F	Α	[20]
biphenyl/	mild steel (2)	623	8760	F	Α	[20]
o-terphenyl/	stainless steel (1)	623	8760	F	Α	[20]
m-terphenyl	mild steel (2)	673	8760	F	Α	[20]
mixture	stainless steel (1)	673	8760	F	Α	[20]
naphthalene	aluminium (1)	488	27 769	S	Α	[48]
	mild steel(3)	490	3570	S	Α	[49]
	mild steel(3)	490	6430	S	A	[49]
	aluminium (1)	491	3570	S	Α	[49]
	mild steel (1)	543	26 280	S	Α	[20]
	mild steel (2)	543	26 280	S	A	[20]
	titanium (1)	573	8760	S	A	[20]
	nickel chromium (3)	593	300	S	A	[59]
	titanium (4)	593	3000	S	A	[59]
	stainless steel (1)	593	8760	S	A	
	copper nickel (1)	593	8760	F	D	[20] [20]
		598(1)	5520	S		[21]
	stainless steel (2) stainless steel (2)	623	5520 5520	S	A A	[21]
cyclic	mild steel (1)	553	8760	F	D	[20]
siloxanes	mild steel (2)	553	8760	F	D	[20]
(XF218 oil)	copper nickel (1)	553	8760	F	D	[20]
linear	mild steel (1)	573	8760	F	A	[20]
siloxanes	mild steel (1)	623	8760	, F	A	[20]
(200 50 CS)	` '	623	8760	F	A	
	copper nickel (1)					[20]
GaCl₃	titanium (2)	613 623	19 632	F F	A	[4]
0.5	nickel chromium (1)		5000		A	[4]
SbBr ₃	aluminium (1)	500	5000	F	Α	[37]
SbCl ₃	mild steel (3)	476	5000	F	Α	[48]
	aluminium (1)	500		F	A	[48]
SnCl ₄	aluminium (1)	432		F	Α	[49]
	mild steel (3)	432	3570	S	D	[49]
	mild steel (3)	432	27 769	S	D	[48]
	nickel chromium (2)	553	20 160	F	Α	[2]
TiBr ₄	titanium (2)	653	3024	S	Α	[2]
TiCl ₄	mild steel (3)	425	3570	S	Α	[49]
	mild steel (3)	425	28 557	S	Α	[48]
	aluminium (1)	438	2210	F	Α	[49]
	titanium (3)	500	4019	S	D	[37]
	nickel chromium (1)	573	49 932	S	Α	[3]
	titanium (3)	653	20 060	F	Α	[2]

Table B.1 continued

Working fluid	Shell	Temperature [K]	Duration [hours]	Outcome	Theory	Stud
mercury	stainless steel (6)	603	10 000	S	NA	[15]
cesium	titanium (4)	673	2000	S	NA	[43]
	niobium zirconium (1)	1273	8700	S	NA	[43]
sulfur/	stainless steel (4)	623	1008	S	NA	[45]
10 %iodine	aluminium (2)	623	1028	F	NA	[45]
	titanium (3)	523	24	F	NA	[45]
	titanium (5)	623	1000	F	NA	[45]
	niobium zirconium (1)	623	950	F	NA	[45]
potassium	stainless steel (5)	783	6100	S	NA	[43]
	stainless steel (6)	783	6500	S	NA	[17]
	niobium zirconium (1)	838	14 071	S	NA	[53]
	nickel (1)	873	24 500	S	NA	[43]
	stainless steel (6)	923	6100	S	NA	[43]
sodium	stainless steel (1)	873	83 000	S	NA	[46]
	stainless steel (5)	923	7100	S	NA	[43]
	stainless steel (6)	923	7100	S	NA	[43]
	stainless steel (1)	923	115 000	S	NA	[46]
	nickel chromium (4)	973	20 000	S	NA	[46]
	nickel chromium (5)	973	41 000	S	NA	[46]
	nickel chromium (6)	988	8000	S	NA	[43]
	nickel chromium (6)	988	33 000	S	NA	[43]
	stainless steel (2)	1044	4000	S	NA	[43]
	niobium zirconium (1)	1123	10 000	S	NA	[43]
	stainless steel (7)	1153	16 874	S	NA	[30]
	stainless steel (7)	1158	25 4 1 7	S	NA	[30]
	stainless steel (4)	1163	29 187	S	NA	[30]
	stainless steel (4)	1183	23 505	S	NA	[30]
	niobium zirconium (1)	1273	105 120	S	NA	[44]
	niobium zirconium (1)	1373	1000	S	NA	[43]

76 B. Life test data

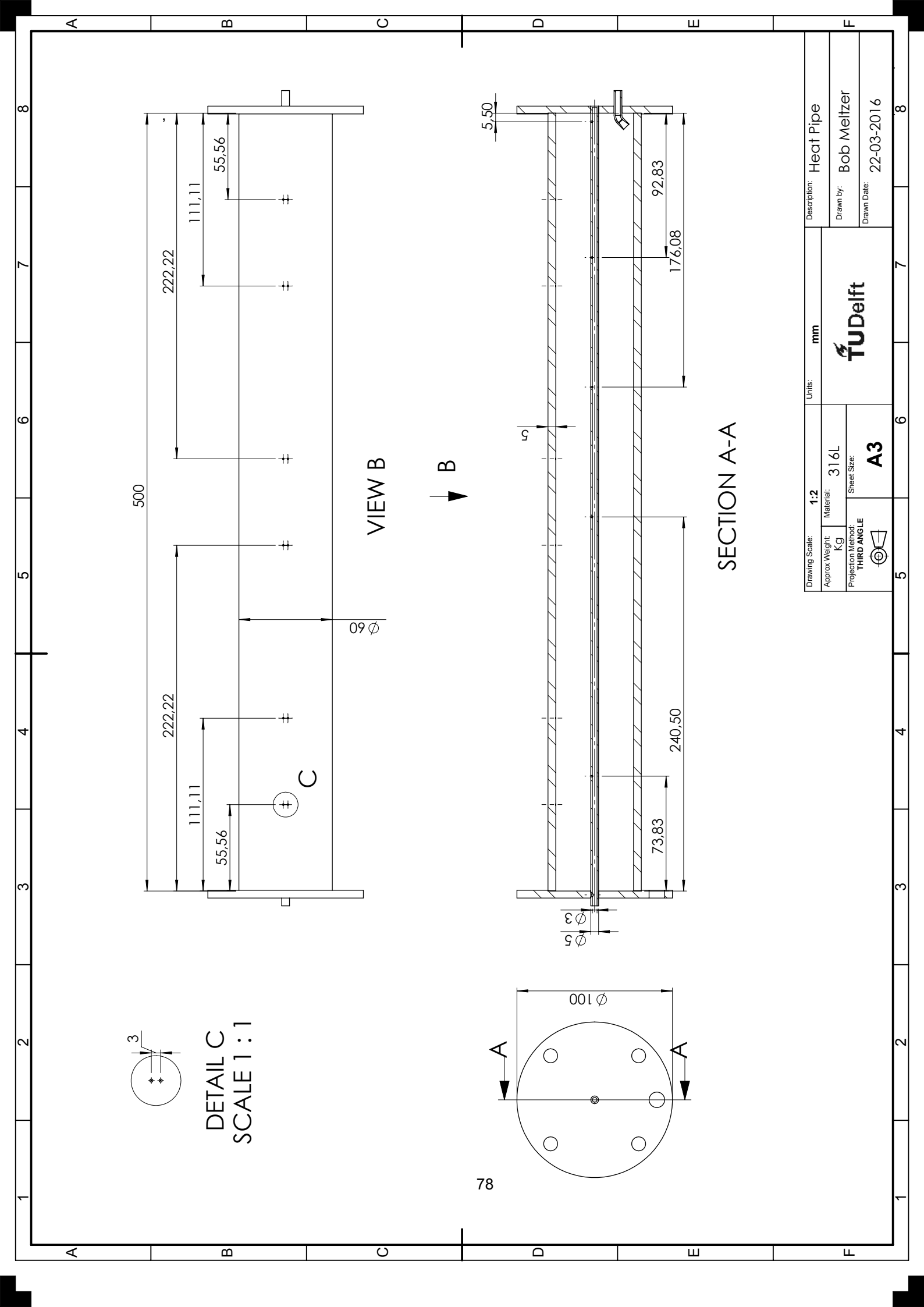
B.2. Composition of heat pipe shell materials

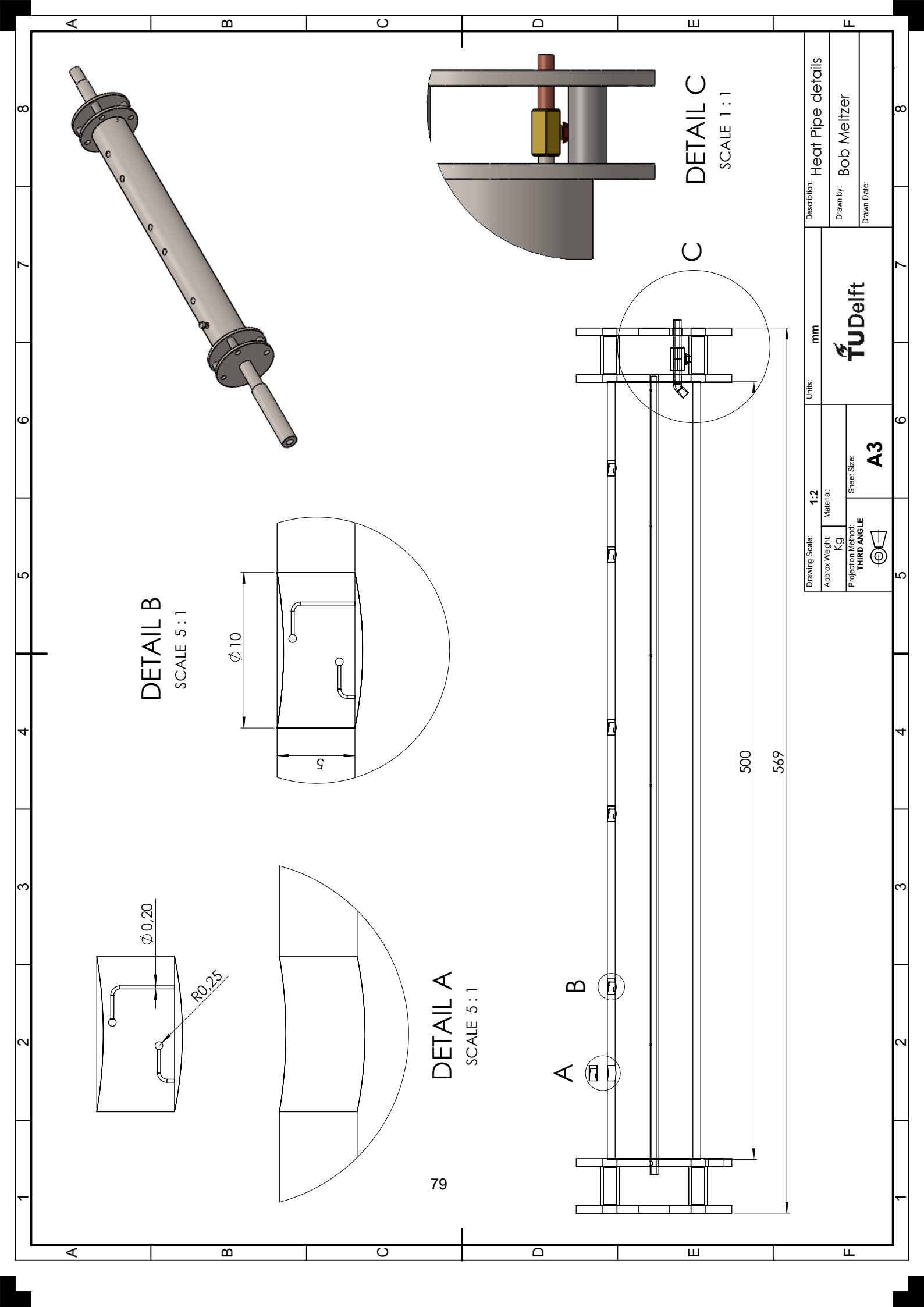
Table B.2: The composition of the shell materials listed in Table B.1.

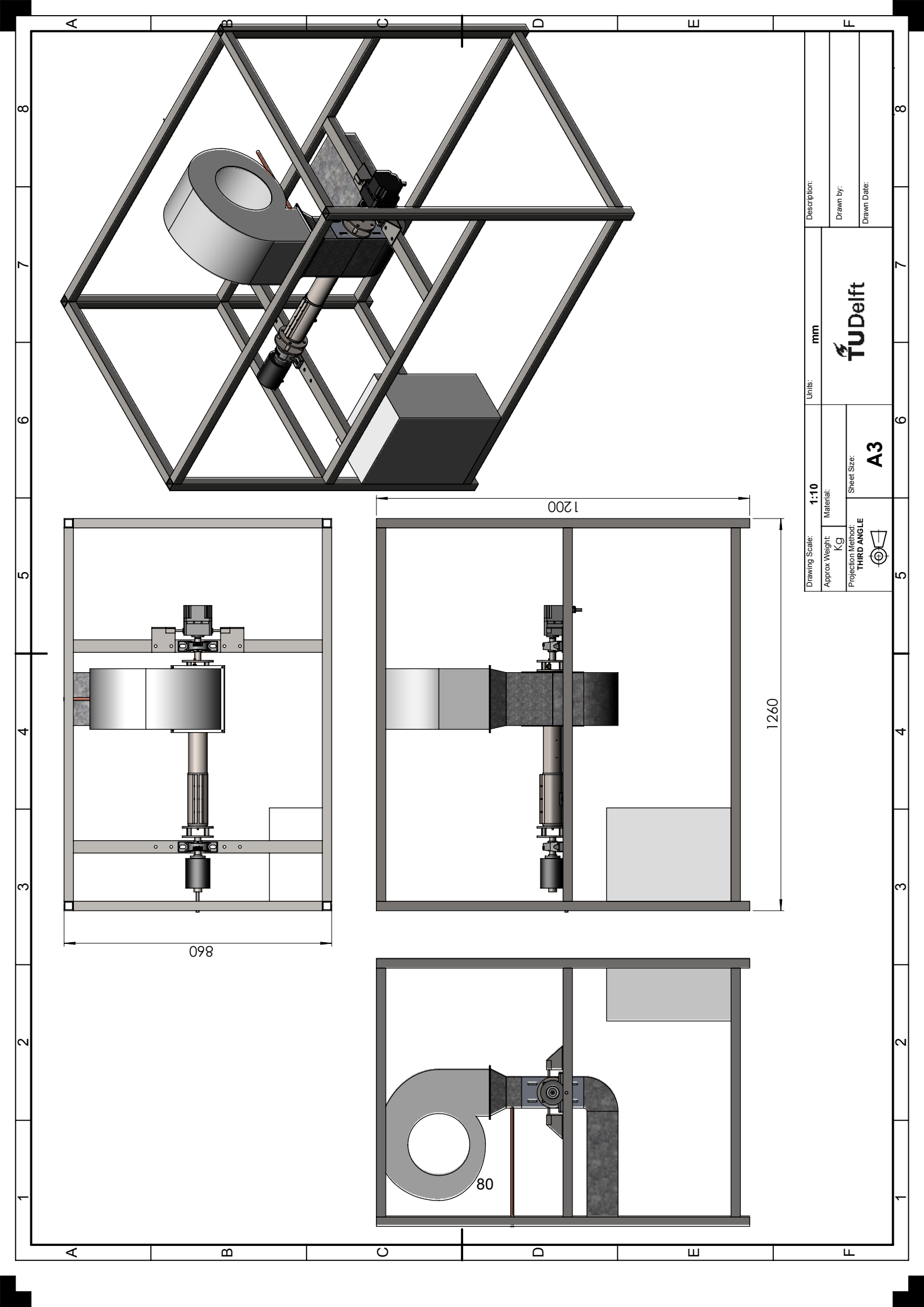
Shell	#	Name	Main constituents [max. weight]
mild steel	(1) (2) (3) (4)	ST35 13CrMo44 A-178 ST37	Fe, C 0.16, Mn 1.2, Si 0.35, Cr 0.3, Cu 0.03, Mo 0.08, Ni 0.3 Fe, C 0.14, Cr 0.98, Mo 0.6, Mn 0.55, Si 0.4 Fe, C 0.18, Mn 0.63, P 0.035, S 0.035 Fe, C 0.17, Mn 1.4, P 0.045, S 0.045
stainless steel	(1) (2) (3) (4) (5) (6) (7)	316L 316 321 304L 304 347 310S	Fe, Cr 18, C 0.03, Ni 14, Mo 3, Mn 2, Si 0.75 Fe, Cr 18, C 0.08, Ni 14, Mo 3, Mn 2, Si 0.75, Fe, Cr 19, C 0.08, Ni 12, Mn 2, Si 0.75, Ti 0.7 Fe, Cr 20, C 0.03, Ni 12, Mn 2, Si 0.75, N 0.1, P 0.045, S 0.03 Fe, Cr 20, C 0.08, Ni 12, Mn 2, Si 0.75, N 0.1, P 0.045, S 0.03 Fe, Cr 19, C 0.08, Ni 13, Mn 2, Si 0.75, Nb & Ta 1 Fe, Cr 26, C 0.08, Ni 22, Mn 2, Si 1.5, P 0.045, S 0.03
titanium	(1) (2) (3) (4) (5)	Ti99.4 CP-Ti CP-Ti 2 Ti-6Al-4V	Ti >99.4 Ti, Fe 0.2, O 0.18, C 0.08, N 0.03, H 0.015 Ti, Fe 0.3, O 0.25, C 0.08, N 0.03, H 0.015 exact composition unknown Ti, Al 6, V 4, Fe 0.25, O 0.2
aluminium	(1) (2)	Al6061 Al5052	Al, Mg 1.2, Si 0.8, Fe 0.7, Cu 0.4, Cr 0.35, Zn 0.25, Ti 0.15, Mn 0.15 Al, Mg 2.8, Fe 0.4, Cr 0.35, Si 0.25, Cu 0.1, Mn 0.1, Zn 0.1
nickel	(1)		exact composition unknown
copper nickel	(1)	CuNi10Fe	Cu, Ni 10, Fe 2, Mn 1
nickel chromium	(1) (2) (3) (4) (5) (6)	C22 C2000 Alloy20 Haynes 230 Inconel 718 Hastelloy X	Ni, Cr 22, Mo 13, Fe 3, W 3, Co 2.5, Mn 0.5, V 0.35, Si 0.08, C 0.01 Ni, Cr 23, Mo 16, Fe 3, Cu 1.6, Al 0.5, Mn 0.5, Si 0.08, C 0.01 Fe, Ni 35, Cr 21, Co 4, Mo 3, Mn 2, Si 1, Nb 1, C 0.06 Ni, Cr 22, W 14, Co 5, Fe 3, Mo 2, Mn 0.5, Si 0.4, Al 0.3, C 0.1, La 0.02, B 0.015 Fe, Ni 55, Cr 21, Nb 5.5, Mo 3.3, Co 1, Al 1.15, Cu 0.8, Mn 0.35, Si 0.35, Ti 0.3, C 0.08 Ni, Cr 22, Fe 18, Mo 9, Co 1.5, Mn 1, Si 1, W 0.6, C 0.1, B 0.008
niobium zirconium	(1)	Niobium-1 % Zr	Nb, Zr 1.2, Ta 0.5, Mo 0.05, W 0.05, O 0.025, Hf 0.02, C 0.01, Fe 0.01

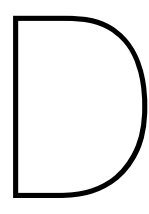


This appendix contains the following drawings: Drawing C.1: page 78 Drawing C.2: page 79 Drawing C.3: page 80









Supplier Inquiries

D.1. Datasheets

The links below will lead to datasheets of the equipment discussed in Chapter 5. If no direct link is available, a link to the website of the supplier is provided instead.

Induction heating

Band heater

Vulcanic S.A. http://www.vulcanic.com/en/

Slip ring

```
Penlink AB http://www.penlink.se/files/SRH2578en.pdf
Cosmau http://www.arslipring.com/products.html
```

Fan

Induvac http://www.induvac.com/downloads/productbladen/ventilatoren/uarp-pdf

DC Motor

- [1] D. Ambrose, M.B. Ewing, N.B. Ghiassee, and J.C. Sanchez Ochoa. The ebulliometric method of vapour-pressure measurement: vapour pressures of benzene, hexafluorobenzene, and naphthalene. *The Journal of Chemical Thermodynamics*, 22(6):589–605, 1990. ISSN 00219614. doi: 10.1016/0021-9614(90)90151-F.
- [2] William G. Anderson, Richard Bonner, Peter Dussinger, John Hartenstine, David Sarraf, and Ivan E. Locci. Intermediate Temperature Fluids Life Tests Experiments. *5th International Energy Conversion Engineering Conference and Exhibit (IECEC)*, (June):25–27, 2007. doi: doi:10.2514/6.2007-4808. URL http://dx.doi.org/10.2514/6.2007-4808.
- [3] William G. Anderson, Sanjida Tamanna, Calin Tarau, and John Hartenstine. Intermediate Temperature Heat Pipe Life Tests. pages 1–23, 2012.
- [4] William G. Anderson, Sanjida Tamanna, Calin Tarau, John Hartenstine, and David Ellis. Intermediate Temperature Heat Pipe Life Tests and Analyses. In 43rd International Conference on Environmental Systems, pages 1–23, Reston, Virginia, July 2013. American Institute of Aeronautics and Astronautics. ISBN 978-1-62410-215-8. doi: 10.2514/6.2013-3304. URL http://arc.aiaa.org/doi/abs/10.2514/6.2013-3304.
- [5] D S Aribike and A A Susu. Kinetics and mechanism of the thermal cracking of n-heptane. Thermochimica Acta, 127:247-258, 1988. doi: 10.1016/0040-6031(88)87501-4. URL http://linkinghub.elsevier.com/retrieve/pii/0040603188875014\$\backslash\$nfile://D:/EBooksandProfesionalDocuments/ProfesionalEngineeringDocuments/Papers/ScienceDirectPapers/ReactionNetworkGeneration/1-s2.0-0040603188875014-main.pdf.
- [6] ASM International. ASM Handbook, Volume 1, Properties and Selection: Irons, Steels, and High Performance Alloys, volume 1. 10th edition, 1990. ISBN 0-87170-380-7.
- [7] Ian H. Bell, Jorrit Wronski, Sylvain Quoilin, and Vincent Lemort. Pure and pseudo-pure fluid thermophysical property evaluation and the open-source thermophysical property library coolprop. *Industrial & Engineering Chemistry Research*, 53(6):2498–2508, 2014. doi: 10.1021/ie4033999. URL http://pubs.acs.org/doi/abs/10.1021/ie4033999.
- [8] E.A. Brandes and G.B. Brook. *Smithells Metals Reference Book*. Butterworth-Heinemann, 7 edition, 1992. ISBN 9780080517308.
- [9] Odolphus S.L. Bruinsma, Peter J.J. Tromp, Henry J.J. de Sauvage Nolting, and Jacob a. Moulijn. Gas phase pyrolysis of coal-related aromatic compounds in a coiled tube flow reactor. *Fuel*, 67 (3):334–340, 1988. ISSN 00162361. doi: 10.1016/0016-2361(88)90315-8.
- [10] Jp Chakraborty and D Kunzru. High pressure pyrolysis of n-heptane. *J. Anal. Appl. Pyrolysis*, 86(1):44–52, 2009. ISSN 01652370. doi: 10.1016/j.jaap.2009.04.001. URL http://linkinghub.elsevier.com/retrieve/pii/S0165237009000382.
- [11] Harold M. Cobb, editor. *Steel Products Manual: Stainless Steels*. The Iron & Steel Society, Warrendale, 1999. ISBN 1-886362-34-3.
- [12] Dow Chemical Company. Dowtherm A, Heat Transfer Fluid, Product Technical Data. Technical report, 1997.
- [13] Iain M. T. Davidson and John F. Thompson. Kinetics of the thermolysis of octamethylcyclotetrasiloxane in the gas phase. *Journal of the Chemical Society, Faraday Transac*tions 1: Physical Chemistry in Condensed Phases, 71:2260, 1975. ISSN 0300-9599. doi:

- 10.1039/f19757102260. URL http://xlink.rsc.org/?DOI=f19767201088http://xlink.rsc.org/?DOI=f19757102260.
- [14] D.R. De Halas. *Kinetics of the decomposition of organic reactor coolants*. Hanford Atomic Products Operation, 1958.
- [15] J. E. Deverall. Mercury as a Heat Pipe Fluid. Technical report, Los Alamos Scientific Laboratory, 1969. URL http://permalink.lanl.gov/object/tr?what=info:lanl-repo/lareport/LA-04300-MS.
- [16] S H Ehrman, S K Friedlander, and M R Zachariah. Characteristics of SiO2/TiO2 nanocomposite particles formed in a premixed flat flame. *Journal of Aerosol Science*, 29(5-6):687–706, 1998. ISSN 00218502. doi: 10.1016/S0021-8502(97)00454-0. URL <GotoISI>://WOS: 000074107300017.
- [17] G. Ewell, A. Basiulis, and T. Lamp. Reliability of low-cost liquid metal heat pipes. In *3rd International Heat Pipe Conference*, Reston, Virigina, May 1978. American Institute of Aeronautics and Astronautics. doi: 10.2514/6.1978-437. URL http://dx.doi.org/10.2514/6.1978-437http://arc.aiaa.org/doi/abs/10.2514/6.1978-437.
- [18] J.K. Fink and L. Leibowitz. Thermodynamic and Transport Properties of Sodium Liquid and Vapor. Technical report, Argonne National Laboratory, Chicago, 1995.
- [19] Ora L. Flaningam. Vapor pressures of poly(dimethylsiloxane) oligomers. *Journal of Chemical & Engineering Data*, 31(3):266–272, 1986. ISSN 0021-9568. doi: 10.1021/je00045a002. URL http://pubs.acs.org/doi/abs/10.1021/je00045a002.
- [20] M. Groll, D. Heine, and T. Spendel. Heat recovery units employing reflux heat pipes as components. Technical report, Commission of the European Communities, Stutgart, 1984.
- [21] Lawrence R. Grzyll, D. D. Back, C. Ramos, and N. A. Samad. Characterization and Testing of Novel Two-Phase Working Fluids for Spacecraft Thermal Management Operating Between 300 Deg. C and 400 Deg. C. Technical report, MAINSTREAM ENGINEERING CORP ROCKLEDGE FL CHEMICAL SYSTEMS DIV., 1994.
- [22] Lawrence R. Grzyll, Charlie Ramos, and Dwight D. Back. Density, Viscosity, and Surface Tension of Liquid Quinoline, Naphthalene, Biphenyl, Decafluorobiphenyl, and 1,2-Diphenylbenzene from 300 to 400 °C. *Journal of Chemical & Engineering Data*, 41(3):446–450, January 1996. ISSN 0021-9568. doi: 10.1021/je950266z. URL http://pubs.acs.org/doi/abs/10.1021/je950266z.
- [23] L. E. Gusel'nikov, N. S. Nametkin, T. Kh. Islamov, A. A. Sobtsov, and V. M. Vdovin. The mechanism of the thermal conversions of methylcyclosiloxanes. *Bulletin of the Academy of Sciences of the USSR Division of Chemical Science*, 20(1):71–75, January 1971. ISSN 0568-5230. doi: 10.1007/BF00849322. URL http://link.springer.com/10.1007/BF00849322.
- [24] J.L. Hales and R. Townsend. Liquid densities from 293 to 490 K of nine aliphatic alcohols. *The Journal of Chemical Thermodynamics*, 4:763 772, 1972. ISSN 00219614. doi: 10.1016/0021-9614(76)90126-9.
- [25] C. Y. Ho and T. K. Chu. Electrical resistivity and thermal conductivity of nine selected AISI stainless steels - Center for Information and Numerical Data Analysis and Synthesis. *Distribution*, page 15, 1977.
- [26] Marcia L. Huber, Arno Laesecke, and Daniel G. Friend. Correlation for the vapor pressure of mercury. *Industrial and Engineering Chemistry Research*, 45(21):7351–7361, 2006. ISSN 08885885. doi: 10.1021/ie060560s.
- [27] Aydin Jalali, M M Yousef Motamedhashemi, Fokion Egolfopoulos, and Theodore Tsotsis. Fate of Siloxane Impurities During the Combustion of Renewable Natural Gas. Combustion Science and Technology, 185(6):953–974, June 2013. ISSN 0010-2202. doi: 10.1080/00102202.2013. 766606. URL http://www.tandfonline.com/doi/abs/10.1080/00102202.2013. 766606.

[28] George J. Janz. Thermodynamic and Transport Properties for Molten Salts: Correlation Equations for Critically Evaluated Density, Surface Tension, Electrical Conductance, and Viscosity Data -Supplement No. 2. Journal of Physical and Chemical Reference Data, 17, 1988.

- [29] G. Juppe, M. Alvarenga, and H. Hannaert. The Pyrolytic Decomposition of Terphenyls. Technical report, European Atomic Energy Community, 1964.
- [30] Warner B Kaufman and Leonard K Tower. Compatibility of Sodium and Lithium in Superalloy Heat Pipes. Technical report, AERO PROPULSION LABORATORY AIR FORCE WRIGHT AERONAUTICAL LABORATORES AIR FORCE SYSTEMS COMMAND WRIGHT-PATTERSON AIR FORCE BASE, 1985. URL http://oai.dtic.mil/oai/oai?verb=getRecord&metadataPrefix=html&identifier=ADA170601.
- [31] D. D Kenney and Jr. Feldman, K. T. Heat pipe life tests at temperatures up to 400 C. In 13th Intersociety Energy Conversion Engineering Conference, San Diego, 1978.
- [32] Deepak Kunzru, Yatish T Shah, and Edward B Stuart. Thermal Cracking of n-Nonane. Industrial & Engineering Chemistry Process Design and Development, 11(4):605–612, 1972. ISSN 0196-4305. doi: 10.1021/i260044a024. URL http://pubs.acs.org/doi/abs/10.1021/i260044a024.
- [33] Alexander Laskin, Carmen Tamburu, Faina Dubnikova, and Assa Lifshitz. Production of major reaction products in the initial steps of the thermal decomposition of naphthalene. Experimental shock-tube results and computer simulation. Proceedings of the Combustion Institute, 35(1):299–307, 2015. ISSN 15407489. doi: 10.1016/j.proci.2014.06.019. URL http://www.sciencedirect.com/science/article/pii/S1540748914001771.
- [34] E.W. Lemmon, M.L. Huber, and M.O. McLinden. *NIST Standard Reference Database 23: Reference Fluid Thermodynamic and Transport Properties REFPROP*. National Institute of Standards and Technology, Standard Reference Data Program, version 9.0 edition, 2010.
- [35] David R. Lide. *CRC Handbook of Chemistry and Physics*. CRC Press, 84 edition, 2003. URL http://oem.bmj.com/cgi/doi/10.1136/oem.53.7.504.
- [36] P. J. Linstrom and W. G. Mallard, editors. NIST Chemistry WebBook, NIST Standard Reference Database Number 69. National Institute of Standards and Technology, Gaithersburg MD, 20899, June 2005. URL http://webbook.nist.gov.
- [37] Ivan E. Locci, Angirasa Devarakonda, Evan Coplan, and Jami Olminsky. Analytical and Experimental Thermo-Chemical Compatibility Study of Potential Heat Pipe Materials. In 3rd International Energy Conversion Engineering Conference, number August, pages 1–8, Reston, Virigina, August 2005. American Institute of Aeronautics and Astronautics. ISBN 978-1-62410-062-8. doi: 10.2514/6.2005-5666. URL http://arc.aiaa.org/doi/pdf/10.2514/6.2005-5666.
- [38] Donald Mackay, Kuo-ching Ma, Sum Chi Lee, and Wan Ying Shiu. Handbook of Physical-Chemical Properties and Environmental Fate for Organic Chemicals, Second Edition, volume I-IV. CRC Press, Boca Raton, FL, 2 edition, March 2006. ISBN 978-1-56670-687-2. doi: 10.1201/9781420044393. URL http://www.crcnetbase.com/doi/book/10.1201/9781420044393.
- [39] Michael F. Modest. Radiative Heat Transfer. Academic Press, 2 edition, 2003.
- [40] W. MUENZEL. Compatibility tests of various heat pipe working fluids and structural materials at different temperatures. In 3rd International Heat Pipe Conference, Reston, Virigina, May 1978. American Institute of Aeronautics and Astronautics. doi: 10.2514/6.1978-398. URL http: //arc.aiaa.org/doi/abs/10.2514/6.1978-398.
- [41] Robert N. Pease and John M. Morton. Kinetics of Dissociation of Typical Hydrocarbon Vapors 1. Journal of the American Chemical Society, 55(8):3190–3200, August 1933. ISSN 0002-7863. doi: 10.1021/ja01335a021. URL http://pubs.acs.org/doi/abs/10.1021/ja01335a021.

[42] Bruce E. Poling, John M. Prausnitz, and John P. O'Connell. The Properties of Gases and Liquids. The McGraw-Hill Companies, Inc., 5 edition, February 2004. ISBN 0071499997. doi: 10.1300/J111v23n03_01. URL http://www.informaworld.com/openurl?genre=article&doi=10.1300/J111v23n03_01&magic=crossrefhttp://www.informaworld.com/openurl?genre=article&doi=10.1300/J111v23n03_01&magic=crossref||D404A21C5BB053405B1A640AFFD44AE3.

- [43] D.A. Reay, P.A. Kew, and R.J. McGlen. *Heat Pipes Theory, Design and Applications*. Butterworth-Heinemann, an imprint of Elsevier, Kidlington, Oxford, UK, 6th edition, 2014. ISBN 9780080982663. doi: 10.1016/B978-0-08-098266-3.00009-1. URL http://linkinghub.elsevier.com/retrieve/pii/B9780080982663000091.
- [44] Robert S Reid. Alkali Metal Heat Pipe Life Issues. pages 1–14, 2004.
- [45] John H. Rosenfeld, G. Yale Eastman, and James E. Lindemuth. Sulfur heat pipes for 600 K space heat rejection systems. In AIP Conference Proceedings, volume 246, pages 1170–1176. AIP, 1992. doi: 10.1063/1.41780. URL http://scitation.aip.org/content/aip/proceeding/aipcp/10.1063/1.41780.
- [46] John H. Rosenfeld, Donald M. Ernst, James E. Lindemuth, James L. Sanzi, Steven M. Geng, and Jon Zuo. An Overview of Long Duration Sodium Heat Pipe Tests. AIP Conference Proceedings, 699(1):140-147, 2004. ISSN 0094243X. doi: doi:http://dx.doi.org/10.1063/1.1649568. URL http://scitation.aip.org/content/aip/proceeding/aipcp/10.1063/1.1649568.
- [47] María Victoria Roux, Manuel Temprado, James S. Chickos, and Yatsuhisa Nagano. Critically evaluated thermochemical properties of polycyclic aromatic hydrocarbons. *Journal of Physical and Chemical Reference Data*, 37(4):1855–1996, 2008. ISSN 00472689. doi: 10.1063/1.2955570.
- [48] Elric W. Saaski and J.H. Hartl. Two-Phase Working Fluids for the Temperature Range 50 to 350°C. Technical report, Sigma Research, Inc., 1980.
- [49] Elric W. Saaski and Peter C. Owzarski. Two-Phase Working Fluids for the Temperature Range 50° to 350°C. Technical report, NASA Lewis Research Center, Cleveland, Ohio, 1977.
- [50] O Sanogo. Kinetic Studies of the Reaction of Tetraethoxysilane with Oxygen Atoms. Journal of The Electrochemical Society, 144(8):2919, 1997. ISSN 00134651. doi: 10.1149/1. 1837918. URL http://link.aip.org/link/?JES/144/2919/1http://dx.doi.org/10.1149/1.1837918http://jes.ecsdl.org/cgi/doi/10.1149/1.1837918.
- [51] Oumar Sanogo and Michael R. Zachariah. Étude de la décomposition thermique de l'octaméthylcyclosiloxane (D4) dans un réacteur à écoulement rapide. Comptes Rendus Chimie, 10(6):518-523, 2007. ISSN 16310748. doi: 10.1016/j.crci.2006.04.005. URL http://linkinghub.elsevier.com/retrieve/pii/S163107480700015X.
- [52] James M. Scarborough and Ronald B. Ingalls. Pyrolysis and high-temperature radiolysis of oterphenyl. The Journal of Physical Chemistry, 71(3):486–492, February 1967. ISSN 0022-3654. doi: 10.1021/j100862a005. URL http://pubs.acs.org/doi/abs/10.1021/j100862a005.
- [53] J. T. Sena and M.A. Merrigan. Niobium 1% zirconium/potassium and titanium/potassium life-test heat pipe design and testing. Technical report, Los Alamos National Lab, 1989.
- [54] Yatish T. Shah, Edward B. Stuart, and Kalapi D. Sheth. Coke Formation during Thermal Cracking of n-Octane. Industrial & Engineering Chemistry Process Design and Development, 15(4):518– 524, October 1976. ISSN 0196-4305. doi: 10.1021/i260060a007. URL http://pubs.acs. org/doi/abs/10.1021/i260060a007.
- [55] M. SZWARC. The C—H Bond Energy in Toluene and Xylenes. Nature, 160(4064):403-403, September 1947. ISSN 0028-0836. doi: 10.1038/160403a0. URL http://www.nature.com/doifinder/10.1038/160403a0.

[56] T.P. van der Stelt and P. Colonna. Experimental vapor pressures and thermodynamic models of perfluorocarbons PP80 and PP90. Fluid Phase Equilibria, 370:50-57, 2014. ISSN 03783812. doi: 10.1016/j.fluid.2014.02.027. URL http://www.sciencedirect.com/science/article/pii/S0378381214001228.

- [57] T.P. van der Stelt, E. Casati, N. Chan, and P. Colonna. Technical equation of state models for heat transfer fluids made of biphenyl and diphenyl ether and their mixtures. Fluid Phase Equilibria, 393:64–77, 2015. ISSN 03783812. doi: 10.1016/j.fluid.2015.02.025. URL http://linkinghub.elsevier.com/retrieve/pii/S037838121500093X.
- [58] N. B. Vargaftik, E. B. Gelman, V. F. Kozhevnikov, and S. P. Naursakov. Equation of state and critical point of cesium. *International Journal of Thermophysics*, 11(3):467–476, 1990. ISSN 0195928X. doi: 10.1007/BF00500839.
- [59] L. L. Vasil'ev, G M Volokhov, A S Gigevich, and M I Rabetskii. Heat pipes based on naphthalene. Journal of Engineering Physics, 54(6):623–626, June 1988. ISSN 0022-0841. doi: 10.1007/BF01102648. URL http://link.springer.com/10.1007/BF01102648.
- [60] Jason A. Widegren and Thomas J. Bruno. Thermal Decomposition Kinetics of Propylcyclohexane. Industrial & Engineering Chemistry Research, 48(2):654–659, January 2009. ISSN 0888-5885. doi: 10.1021/ie8008988. URL <GotoISI>://000248331200025http://pubs.acs.org/doi/abs/10.1021/ie8008988.
- [61] Carl L. Yaws. Transport properties of chemicals and hydrocarbons: viscosity, thermal conductivity, and diffusivity of C1 to C100 organics and Ac to Zr inorganic. William Andrew Inc., Norwich, NY, 2009. ISBN 9780815520399. doi: 10.1016/B978-0-8155-2039-9.50001-6. URL http://linkinghub.elsevier.com/retrieve/pii/B9780815520399500016.
- [62] Carl L. Yaws. The Yaws Handbook of Vapor Pressure Antoine Coefficients. Elsevier, 2 edition, 2015. ISBN 978-0-12-802999-2.
- [63] L.B. Yeatts, D.N. Hess, H.F. McDuffie, and W.T. Rainey. Kinetics of the thermal decomposition of biphenyl. Technical report, Oak Ridge National Laboratory, Oak Ridge, Tennessee, 1964.
- [64] Emily M Yoon, Leena Selvaraj, Semih Eser, and Michael M Coleman. High-Temperature Stabilizers for Jet Fuels and Similar Hydrocarbon Mixtures. 2. Kinetic Studies. Energy & Fuels, 10(3):812–815, January 1996. ISSN 0887-0624. doi: 10.1021/ef950229d. URL http://pubs.acs.org/doi/abs/10.1021/ef950229d.
- [65] Jian Yu and Semih Eser. Kinetics of Supercritical-Phase Thermal Decomposition of C 10 -C 14 Normal Alkanes and Their Mixtures. Industrial & Engineering Chemistry Research, 36(3): 585-591, 1997. ISSN 0888-5885. doi: 10.1021/ie9603934. URL http://pubs.acs.org/doi/abs/10.1021/ie9603934\$\backslash\$nfile:///C:/DocumentsandSettings/gfau/Bureau/ESA_2/biblio_esa_2/1-Pyrolysismechanism/Model/1997-KineticsofSupercritical-PhaseThermalDecompositionofC10-C14.pdf.

List of Symbols

Roman symbols

\boldsymbol{A}	area	[m ²]
\boldsymbol{A}	pre-exponential factor	[h ⁻¹]
а	activity coeficient	<u>-</u>
С	loss factor	<u>-</u>
c_p	specific heat capacity	$[kJ kg^{-1} K^{-1}]$
d	diameter	[m]
d_h	hydraulic diameter	[m]
Ε	activation energy	[kJ mol ⁻¹]
Ε	electromotive force	[V]
F	Faraday's constant	[C mol ⁻¹]
f	frequency	[Hz]
f_{f}	Moody friction factor	-
G	Gibbs free energy	[kJ mol ⁻¹]
g	gravitational acceleration	$[m s^{-2}]$
h	heat transfer coefficient	$[kW m^{-2} K^{-1}]$
I	current	[A]
I_{m}	moment of inertia	[kg m²]
K	resistance factor	-
k	reaction rate constant	[h ⁻¹]
L	latent heat of vaporisation	[kJ kg ⁻¹]
l	length	[m]
Μ	merit number	$[kW^4s^2/K^3]$
ṁ	mass flow	$[kg s^{-1}]$
n	number of electrons	-
N_{cl}	number of coil windings	-
P	power	[kW]
p	pressure	[MPa]
Q	heat flow	[kW]
q	heat flux	$[kW m^{-2}]$

R	gas constant	$[kJ K^{-1} mol^{-1}]$
R	resistance	[Ω]
r	radius	[m]
T	temperature	[K]
t	time	[h]
$t_{\mathtt{S}}$	thickness of side	[m]
v	velocity	$[m s^{-1}]$
w	width	[m]
x	mass fraction	-
у	height	[m]
Gree	ek symbols	
α	thermal expansion coefficient (solid)	$[m m^{-1} K^{-1}]$
β	thermal expansion coefficient	[K ⁻¹]
δ	penetration depth	[m]
ϵ	emissivity coefficient	-
ϵ_{r}	wall roughness	[m]
η	efficiency	-
γ	velocity ratio	-
λ	thermal conductivity	$[W m^{-1} K^{-1}]$
μ	dynamic viscosity	[Pas]
μ_{m}	relative magnetic permeability	-
ν	kinematic viscosity	$[m^2 s^{-1}]$
ω	rotational velocity	[rpm]
φ	fill factor	-
ρ	density	$[kg m^{-3}]$
$ ho_{e}$	electrical resistivity	$[\Omegam]$
σ	stress	[MPa]
σ	surface tension	$[N m^{-1}]$
$\sigma_{ extsf{SB}}$	Stefan-Boltzmann constant	$[kW m^{-2} K^{-4}]$
τ	torque	[N m]
ξ	space factor	-
Dim	ensionless numbers	
Fr	Froude number	$rac{\omega^2 r}{g}$
Gr	Grashof number	$\frac{g\beta\Delta Td^3}{v^2}$
		ν²

 $\frac{hd}{\lambda}$ Nu Nusselt number

 $\frac{c_p \mu}{\lambda}$ Pr Prandtl number $\frac{\rho v d}{\mu}$

Reynolds number Re

Sub- and superscripts

at standard conditions

 ∞ free stream

I liquid

adi adiabatic

axial ах

cl coil

condenser con

conv convective

critical С

eff effective

equivalent eq

evp evaporator

f film

i inner

m mist

o outer

rad radial

r reduced

sat at saturation

s surface

٧ vapor

θ tangential